The Flower Garden Banks *Siderastrea siderea* Coral as a Candidate Global Boundary Stratotype Section and Point for the Anthropocene Series

Kristine L. DeLong [a, b*], Kylie Palmer [a], Amy J. Wagner [c], Mudith M. Weerabaddana [d], Niall Slowey [e], Achim D. Herrmann [b, f], Nicolas Duprey [g], Alfredo Martinez-Garcia [g], Jonathan Jung [g], Irka Hajdas [h], Neil L. Rose [i], Sarah L. Roberts [i], Lucy R. Roberts[i], Andrew B. Cundy [j], Pawel Gaca [j], J. Andrew Milton [j], Handong Yang [i], Simon D. Turner [i], Chun-Yuan Huang [l], Chuan-Chou Shen [l], and Jens Zinke [k]
*Corresponding author

Affiliations

[a] Department of Geography and Anthropology, Louisiana State University, USA
[b] Coastal Studies Institute, Louisiana State University, USA
[c] Department of Geology, California State University, Sacramento, USA
[d] Department of Geosciences, University of Arizona, USA
[e] Department of Oceanography, Texas A&M University, College Station, USA
[f] Department of Geology and Geophysics, Louisiana State University, USA
[g] Climate Geochemistry Department, Max Planck Institute for Chemistry (Otto Hahn Institute), Germany
[h] ETH Zurich, Laboratory of Ion Beam Physics, Switzerland
[i] Environmental Change Research Centre, Department of Geography, University College London
[j] School of Ocean and Earth Science, National Oceanography Centre (Southampton), University of Southampton, UK
[k] School of Geography, Geology and the Environment, University of Leicester, UK
[l] High-precision Mass Spectrometry and Environment Change Laboratory and Research Center for Future Earth, Department of Geosciences, National Taiwan University, Taiwan, ROC

Keywords
Ba/Ca, carbon isotopes, mercury, nitrogen isotopes, oxygen isotopes, plutonium, radiocarbon, Sr/Ca

Abstract

The proposed Anthropocene Global Boundary Stratotype Section and Point (GSSP) candidate site of West Flower Garden Bank (27.8762ºN, 93.8147ºW) is an open ocean location in the Gulf of Mexico with a submerged coral reef and few direct human impacts. Corals contain highly accurate and precise (<±1 year) internal chronologies, similar to tree rings, and their exoskeletons are formed of aragonite and can be preserved in the rock record. Here we present results from a large *Siderastrea siderea* coral (core 05WFGB3; 1755–2005 CE) sampled with annual and monthly resolutions that show clear markers of global and regional human impacts. Atmospheric nuclear bomb testing by-products (^{14}C, $^{239+240}Pu$) have clear increases in this coral starting in 1957 for ^{14}C and the first increase in 1956 for $^{239+240}Pu$ (potential bases for the Anthropocene GSSP). Coral $\delta^{13}C$ declined especially after 1956 consistent with the Suess Effect resulting from the burning of fossil fuels. Coral skeletal $\delta^{15}N$ starts to increase in 1963 corresponding with the increase in agricultural fertilizers. Coral Hg concentrations (1933–1980) loosely track fluctuations in industrial pollution and coral Ba/Ca increases from 1965–1983 when offshore oil operations expand after 1947. Coral temperature proxies contain the 20th-century global warming trend whereas coral growth declines during this interval.

Introduction

The nuclear age first left its imprint on the Earth in World War II with the detonation of atomic bombs. In the following years, atmospheric nuclear weapons testing was conducted predominately in remote Pacific islands such as Bikini and Eniwetok atolls. Scientists found corals in these atolls contained radioactive bands that correlate to the weapons testing dates and

thus one could determine coral growth rates (Knutson et al., 1972). X-ray images (i.e. X-radiographs) of cross-sections cut from coral colonies also reveal high- and low-density bands within the coral skeleton, similar to tree rings, that correlated to radioactive bands and thus years of nuclear testing (Buddemeier et al., 1974; Knutson et al., 1972). Corals are colonial organisms with coral polyps living on top of their aragonite exoskeletons they deposit with varying skeletal density throughout the year as they grow. These annual density bands give scientists time markers for "reading" the environmental history contained in the coral's skeleton, similar to dendrochronology (Lough and Cantin, 2014). The ability to locate individual years in the coral skeleton allows researchers to correlate the coral's skeletal geochemical history to calendar dates with high accuracy. Furthermore, these nuclear weapons testing and the radioactive isotope "bomb spikes", which are present in coral skeletons, have been suggested as the global marker for the Anthropocene Global Boundary Stratotype Section and Point (GSSP) (Waters et al., 2015). The Anthropocene Working Group organized preparatory activities for formalizing the Anthropocene, including events leading to the submission of GSSP proposals, to facilitate a binding decision that the start of the Anthropocene is in the mid-20th century and should align with stratigraphic signals. These activities and proposals are detailed in the introductory article in this special issue (Waters, 2022).

This study will examine several radioactive isotopes and other potential Anthropocene markers in detail for a *Siderastrea siderea* coral located in West Flower Garden Bank (WFGB), one of two coral reefs within the Flower Garden Banks National Marine Sanctuary (FGBNMS) in the northern Gulf of Mexico (GoM). The tropical Atlantic coral species *S. siderea* is a particularly good species for archiving the past since it has a relatively slow growth rate (3–6 mm $year^{-1}$), which means an average-sized coral colony (1–2 m) is older (200–400 years) than

faster-growing coral species of the same size and therefore provides longer skeletal records. There is a broad scope of prior geochemical research with *S. siderea,* thus the reason we selected this species for the Anthropocene GSSP candidate; see the review on this species in the Supplemental Material.

The Flower Garden Banks (FGB) are located in the northern GoM at the edge of the wide-continental shelf about 185 km away from the Louisiana and Texas coastline and far from river runoff and coastal upwelling (Figure 1). FGBs' coral reefs are primarily comprised of large boulder-shaped corals and the reefs have ~50% live coral coverage (Schmahl et al., 2008), which is high for Atlantic coral reefs. Furthermore, FGB corals have so far been minimally affected by coral bleaching (Johnston et al., 2019), a condition caused by rising seawater temperatures threatening coral reefs worldwide, due to FGB's higher latitude (~28ºN), which is near the northernmost limits of coral reef-supporting conditions, and its deeper water depth (18–40 m) than most coral reefs. Fishing is restricted in the sanctuary boundaries to only conventional single hook and line gear. Divers are the typical visitors to FGBNMS and they travel there from April to July, before hurricane season peaks in August and September, and stay on live-aboard boats since the transit time is 10 to 12 hours. In the past 12 years (2009–2021), FGBNMS averaged about 800 divers per year, thus impacts from divers compared to other Atlantic coral reefs are minimal (personal communication Johnson, 2022).

The remote location of the FGBNMS means that these coral reefs are less vulnerable than coastal coral reefs to anthropogenic pollution from the land and are less disturbed by fishing and diving; one of the requirements for the Anthropocene GSSP (Waters, 2022). Furthermore, this means there is no local impact or signal in the coral's skeletal geochemistry, thus corals in FGBNMS are recording environmental histories that are regional or global rather than local. The

candidate site reported here is within the FGBNMS and is protected and actively managed by the National Oceanic Atmospheric Administration since 1992 with cooperation from fishermen, the oil industry, divers, and conservation groups. FGB has been studied since the 1930s with many books, papers, and annual scientific reports summarizing efforts published by FGBNMS. However, these coral reefs are not immune to anthropogenic influence. The formation of salt domes also creates space under the seabed in which oil and gas can collect. More than 9000 offshore platforms have operated in the northern GoM since 1982 (Figure 1a) and several offshore petroleum platforms have operated within 30 km of the FGB (Pulster et al., 2020), yet there have not been any documented changes in the health of the coral reef caused by oil operations (Office of National Marine Sanctuaries, 2008). Furthermore, FGBNMS was not impacted by the Deepwater Horizon oil spill in 2010, which is located ~540 km from FGBNMS (Figure 1a) (Johnston et al., 2021). The FGB coral reefs exist due to the rising salt domes and the salt domes themselves are indirectly a contributing reason to the predicted demise of coral reefs due to global warming (Dee et al., 2019; Frieler et al., 2012) by providing locations for crude oil to accumulate. Paradoxically, the FGB coral reefs are perhaps the healthiest in waters of the United States (US) and the Atlantic Ocean and are poised to survive longer than other coral reefs (Lawman et al., 2022), and thus another reason why we selected WFGB as a candidate site for the Anthropocene GSSP.

Materials and methods

Geographic settings of the core site

The GoM is a semi-enclosed basin located in the western Atlantic Ocean just northwest of the Caribbean Sea surrounded by the US, Mexico, and Cuba (Figure 1a). The gulf has an area of over 1,500,000 km^2 where one-third of that area is a broad gently sloping continental shelf

with a water depth of less than 200 m and also contains “salt domes” rising towards the ocean surface. Some of these submerged salt domes reach water shallow enough to have coral reefs form in the last 12,000 years after the Last Glacial Maximum when global sea level rose from the lowstand (Slowey et al., 2008).

Waters in the GoM are a mixture of riverine waters with warm and saltier waters from the Caribbean Sea, which is a mixture of North and South Atlantic waters (Wilson and Johns, 1997), brought into the gulf by the Loop Current through the Yucatan Channel and exiting through the Straits of Florida to ultimately form the Gulf Stream (Figure 1a) (Alvera-Azcrate et al., 2009). The northern extent of the Loop Current varies seasonally and sheds eddies that migrate and persist for many weeks (Alvera-Azcrate et al., 2009; Sturges and Evans, 1983). The surface water temperature in the northern gulf can reach 31ºC in the summer and cools to 18ºC in winter.

The primary freshwater source to the GoM is the Mississippi River, which accounts for 64% of the total freshwater discharge into the GoM (Darnell and Defenbaugh, 2015) and other notable rivers near FGBNMS are the Atchafalaya, Trinity, and Rio Grande (Figure 1a). Mississippi River discharge into the northern GoM contains immense amounts of nutrients that increase primary production in the ocean surface waters and lead to eutrophication that forms one of the largest hypoxic zones in the world along the Louisiana coast (Rabalais et al., 2002). This river water moves westward along the coast by seasonally varying cross-shelf currents (Zavala-Hidalgo et al., 2014).

Field collection of core, sampling, and core imagery

A team of divers from FGBNMS, Florida Keys National Marine Sanctuary, US Geological Survey, and Texas A&M University collected coral cores from WFGB in May 2005 under permit FGBNMS-2005-002. They used an underwater hydraulic drill system with a 4-inch

(101.6 mm) diameter diamond-tipped drill bit to vertically drill down from the top center of the coral colony. A 1.74 m-long cylindrical core (05WFGB3) was collected in five sections from a large boulder-shaped *S. siderea* coral colony (27.8762ºN, 93.8147ºW) at a water depth of 21.3 m. The coral colony is still on the reef and could be cored again with the proper permits and in cooperation with FGBNMS. The core 05WFGB3 is on loan from the FGBNMS and will ultimately be returned to them. Details on cutting the core, X-ray imaging, and preparations for extracting samples are detailed in the Supplemental Material.

Coral X-radiographs and scans were used to determine annual extension (one component of coral growth) per year, locate sampling paths, and assign years. A year was assigned to each density band couplet (light and dark) starting from the core top and counting down to the bottom of the core. The ruler tool in Adobe Photoshop was used to measure the distance from the top of successive high-density dark bands (~January) and distances were recorded in the measurement log. Three paths were measured for each slab and the results for each year were averaged together. The precision of this method is limited by the resolution of the X-radiographs, clarity of the density bands in the X-radiographs, and user experience; therefore, the precision for extension measurements was estimated by the standard error of the mean ($>\pm 0.174$ mm, 1σ).

Two sampling resolutions were used for geochemical analyses, annual for radiogenic isotopes, $\delta^{15}N$, and Hg, which require more mass, and monthly for trace elemental ratios and stable isotope ratios (Table 1). Annual coral samples were removed from coral slabs (slabs C and D) using X-radiographs to aid in cutting for each year starting in winter (assuming January) to the next year. For monthly samples, an micromill system was used to extract monthly samples (0.4 mm increment sample^{-1}) from the coral slab surface (DeLong et al., 2011; Weerabaddana et al., 2021), see Supplemental Material. Divots (1.5 mm deep) were made at every 12th sample,

which are visible in the coral scans and X-radiographs, as markers to assist in assigning time to the coral geochemistry.

Chronological controls

Chronologies for corals were determined by counting annual density band couplets from the top of the core when collected live and the collection date is known (May 2005 for core 05WFGB3) down core for each density band couplet. Two coral samples were dated with high precision ^{230}Th dating (<±1 year for corals <100 years old) (Shen et al., 2003; 2008) (Supplemental Figure 5). U-Th isotopic analysis was conducted in the High-Precision Mass Spectrometry and Environmental Change Laboratory at National Taiwan University with a Thermo Electron Neptune multi-collector inductively coupled plasma mass spectrometer (Cheng et al., 2013; Shen et al., 2012).

Time assignment for monthly data was performed with the ~monthly coral Sr/Ca using Analyseries software (Paillard et al., 1996) and then applied to the other geochemical series. Monthly Sr/Ca were aligned to a monthly sea surface temperature (SST) time series (ERSSTv3b for the 2º grid box centered on WFGB, 28ºN, 94ºW) (Smith et al., 2008) back to 1870 and then using a time series of repeating monthly SST climatology for the older coral sections. Coral Sr/Ca maxima were assigned to the coldest month each year and coral Sr/Ca minima to the warmest month each year. *S. siderea* can grow faster in summer when compared with winter; therefore, time assignment using only two tie-points per year may be biased towards the summer; therefore, mid-spring and mid-autumn tie points were used (DeLong et al., 2016). After time assignment, each time series was linearly interpolated to even monthly time intervals. The X-radiograph chronology was verified by matching the coral Sr/Ca annual cycles using the divots in the coral scans and X-radiographs.

Anthropocene proxies

Methods for radiogenic and stable isotopes and trace elements listed in Table 1 appear in Supplemental Material.

Numerical analysis

Means are reported with ±1 standard deviation. Correlation analysis is Pearson correlation using degrees of freedom. Significance of linear trends was assessed with the Mann-Kendall test (Greene et al., 2019). Change points (ischange.m in MATLAB) were detected for changes in linear slope, and/or means for a specified number of changes (Killick et al., 2012). Statistical tests assume a 5% significance level.

Results

Chronology

The entire core 05WFGB3 spans 1755–2005 as determined by counting annual density bands in the X-radiographs and annual cycles in monthly coral Sr/Ca and verified with two ^{230}Th dates (Supplemental Figure 5, Supplemental Table 2). There is no evidence of diagenesis in this coral core and we find no evidence of post-depositional alteration in the X-radiographs (Supplemental Figures 2–5). The core section containing 1932–2005 (05WFGB3-1), which is the interval of interest for the GSSP markers, is continuous and has no breaks except for ones that occurred in the laboratory for which there are no missing time (Supplemental Figures 2–5). The coral X-radiographs for the three slabs have clear annual density bands that correlate among the slabs and the years are easily marked. The monthly coral Sr/Ca and δ^{18}O variations co-vary with temperature records for FGB (see section Sr/Ca, Li/Ca, Li/Mg, and U/Ca; and Weerabaddana et al., 2021) further supporting the accurate to the year chronology assignment (1932–2005) for core section 05WFGB3-1. Further coral chronology results for the remainder of the core (1755–

1931) before the proposed Anthropocene base are located in Supplemental Material.

Calculation of growth rates

Measurements of the X-radiographs for each year resulted in an overall average annual linear extension of 5.99 (±0.61, 1σ) mm for 1928–2004, the interval for Anthropocene markers in this report (Figure 2). The maximum is 7.81 mm (1934) and the minimum is 3.58 mm (1932), the year of the break between core sections, which contributed to this low extension year. There is a significant decreasing trend (0.0092 mm $year^{-1}$) in coral annual extension during this interval resulting in a decrease in coral growth of 0.70 mm in 76 years. The minimum annual linear extension is greater than the threshold for growth-related effects for this species (<1.7 mm) for coral geochemical proxies (DeLong et al., 2016; Kuffner et al., 2017); therefore, there is no concern with growth-related effects for this coral's geochemistry.

Coral colonies do not grow at a constant rate but vary year-to-year and within the colony (Figure 2, Supplemental Figure 6) because the coral colony is dome-shaped and the coral grows vertically and horizontally at different rates. Boulder-shaped massive corals have internal centimeter-scale growth structures that can vary within the colony; however, *S. siderea* has relatively simple internal structures compared to other Atlantic massive coral species and thus has more internally reproducible geochemical records that result in robust geochemical time series (DeLong et al., 2011; 2016). Coral annual density couplets visible in X-radiographs provide highly accurate chronologies with continuous deposition of the coral skeleton with rare occurrences of missing and false years as are found in tree-ring chronologies (Black et al., 2019; DeLong et al., 2013).

Radioisotopes (and guidance for other proxies)

Radiocarbon – Core 05WFGB3 exhibits low (-50‰) $\Delta^{14}C$ from 1920 to 1957 followed by an

increase observed after 1957 (depth from core top to January 1957 = 284.1 mm) with the largest year-to-year increase occurring from 1961 to 1962 and increasing to a maximum in 1970 (depth = 207.2 mm) (Figure 2, Table 2, Supplemental Figure 7). For change point analysis (Killick et al., 2012), we tested 1 to 4 change points and found consistent results. We found this analysis is sensitive to the direction of the time series and results vary by 1 year; we used the earliest year for the proposed Anthropocene marker. The coral $\Delta^{14}C$ represents the transfer of the atmospheric $\Delta^{14}C$ signal to the surface ocean (i.e. the actual bomb peak observed in the atmosphere after 1954 in the northern hemisphere and 1955 in the southern hemisphere).

We compared core 05WFGB3 ^{14}C results to two *Orbicella faveolata* coral records (Wagner, 2011), one in the WFGB close to the coral where the core 05WFGB3 was extracted from and the other from Santiaguillo Reef offshore from Veracruz, Mexico in the southern GoM, both sampled with annual resolution (Figures 1a and 3). The Veracruz coral $\Delta^{14}C$ closely tracks the WFGB coral $\Delta^{14}C$ of the same species. There is a 4–7 year difference in the maximum $\Delta^{14}C$ peaks between the species and the maximum $\Delta^{14}C$ values differ by 11.8‰ with *S. siderea* having higher maximum values. The rapid increases or "bomb spikes" in all three of these coral $\Delta^{14}C$ records occur in the same years within the sampling uncertainty (±0.5 year), suggesting differences in coral species are not influencing these $\Delta^{14}C$ results.

The $\Delta^{14}C$ bomb peak in various parts of the world's oceans can have different shapes due to each part of the ocean having different patterns of mixing water. The radiocarbon bomb peak was used to untangle this information (Broecker and Peng, 1982). Surface ocean $\Delta^{14}C$ values are the result of equilibration with the atmosphere; however, upwelling, advection, and other mixing processes can influence oceanic $\Delta^{14}C$ (Mahadevan, 2001). In the northwestern GoM, weak springtime upwelling events (days–weeks) of waters as deep as 200 m can occur along the

continental shelf edge, where FGB is located, when the winds reverse in the spring (Murray et al., 1998; Teague et al., 2013). However, daily reef temperature measurements in FGB (Johnston et al., 2021) do not show evidence of cold water upwelling on the reef (the coldest daily temperature was 17.6ºC between 1986 and 2014). Furthermore, hermatypic (reef-building) corals generally cannot tolerate temperatures <17ºC, thus regular upwelling would impact the development of a coral reef in this location if it was occurring. These short-term upwelling events should not impact coral $\Delta^{14}C$ sampled with annual resolution (i.e. each sample represents the annual average $\Delta^{14}C$).

A comparison with an *O. faveolata* from the southern coast of Puerto Rico (Kilbourne et al., 2007) finds similar timing for the $\Delta^{14}C$ increases due to weapons testing (Figure 3). However, the WFGB $\Delta^{14}C$ record does not contain the $\Delta^{14}C$ depletion event between 1950 and 1953 seen in Puerto Rico and other Caribbean sites due to the mixing of low $\Delta^{14}C$ equatorial Atlantic surface waters in the Caribbean Sea (Kilbourne et al., 2007). This depletion event reduces the $\Delta^{14}C$ values for Puerto Rico creating a visual shift in the figure but the timing of the increase in $\Delta^{14}C$ is the same. The lack of this depletion event in the GoM coral $\Delta^{14}C$ records suggests that when the Caribbean waters reach the GoM this lower $\Delta^{14}C$ equatorial water has been mixed with other water and/or equilibrated with atmospheric ^{14}C sources; therefore, the GoM represents a more global signal.

Plutonium – The $^{239+240}Pu$ activities show marked increases in 1956 (depth from core top to January 1956 = 290.3 mm) and 1964 (depth = 240.0 mm) that follow periods of increased atmospheric thermonuclear weapons testing in the early 1950s and 1961–1963 (Figure 2, Table 3, Supplemental Figure 8). Plutonium was not detectable in pre-1950 samples. There is a decline in $^{239+240}Pu$ activities after 1964, with activities for coral samples dated to 1970, 1980, and 2000

being below detection limits. Unlike $\Delta^{14}C$, only 14 samples from the interval 1936–2000 were analyzed for $^{239+240}Pu$, and for 1950–1966 every other year was analyzed; therefore, it is possible greater $^{239+240}Pu$ peaks could have occurred in odd-numbered years that were not analyzed. This study also examined $^{239+240}Pu$ yearly from 1950–1959 in coral from Haiti (10LEO1) growing at the water surface (Supplemental Table 9) that has a peak in 1956.

Plutonium fallout from weapons testing has spread worldwide, mostly in the northern hemisphere, where more testing occurred, but was also affected by test location, wind and precipitation patterns, ocean currents, and water depth (Sanchez-Cabeza et al., 2021). A scaled comparison with other coral $^{239+240}Pu$ studies to highlight maximum values (Figure 4) shows the Pacific corals, especially those near the Pacific Proving Grounds testing sites (Enewetak and Bikini) have maximum $^{239+240}Pu$ values occurring before the Atlantic corals. Atlantic corals tend to record maximum $^{239+240}Pu$ activities in the early-mid 1960s following the 1963 global fallout maximum (Sanchez-Cabeza et al., 2021). The exception is the Haiti coral (10LEO1) that has a maximum in 1956. However, this is an artifact of the figure since we scaled by the maximum value for each core and Haiti did not have a sample measured between 1959 and 1970 and thus is missing the 1964 peak. The coral species may also play a role as the other Atlantic corals are *Orbicella sp.* and corals 05WFGB3 and 10LEO1 are *S. siderea*, both of which have higher $^{239+240}Pu$ activities than the *Orbicella* studies (Figure 4c). *S. siderea* is a coral with a dense skeleton and is relatively slow growing so it may take up and store Pu in its skeleton more readily than the less dense *Orbicella* corals.

Other artificial fallout radionuclides – No ^{137}Cs and ^{241}Am were detected in the core 05WFGB3 samples (Supplemental Results, Supplemental Table 4).

Novel materials

Spheroidal carbonaceous fly-ash particles (SCPs) – No SCPs were found in the 33 coral samples from core 05WFGB3 (Supplemental Results, Supplemental Figure 9, Supplemental Table 5).

Geochemical proxies for climate

Oxygen isotopes – The monthly-resolved coral $\delta^{18}O$ have clear seasonal cycles that significantly co-vary with temperature (Supplemental Figure 10, Supplemental Table 6) that were averaged annually (January–December) to assess trends. The annual average coral $\delta^{18}O$ record has a significant trend toward lower values for the interval from 1933 to 2005 indicating lower temperatures and/or saltier conditions similar to the interval from 1826 to 1890 (Figure 5a). Instrumental and other coral proxies reconstructions suggest the GoM is warming during the 20th century (Allard et al., 2016; DeLong et al., 2014; Flannery et al., 2017); therefore, we interpret this trend as the northern GoM is becoming saltier. Coral $\delta^{18}O$ is an important hydroclimate proxy that can provide insights into moisture flux from the ocean to the atmosphere and freshwater entering the ocean. Coral $\delta^{18}O$ by itself is not a marker for the Anthropocene but can inform us of the response of the climate system to anthropogenic forcing.

Sr/Ca, Li/Ca, Li/Mg, and U/Ca – We evaluated several coral temperature proxies from 1986 to 2005 and assessed the skill of the temperature reconstructions with reef temperature measurements from WFGB (Johnston et al., 2021) and OISST, a 1º gridded and interpolated data product that includes satellite-derived estimates of monthly SST for complete coverage (Reynolds et al., 2002). The monthly coral Sr/Ca, Li/Ca, Li/Mg, and U/Ca records have clear seasonal cycles that are significantly co-varying with temperature (Supplemental Figure 10, Supplemental Table 6). Coral Sr/Ca analyzed with ICP-OES has the highest correlation with reef temperature and OISST and is the best-performing coral temperature proxy (error of reconstruction =1.27ºC). Coral Sr/Ca analyzed with ICP-OES has a better analytical precision

than ICP-MS (Supplemental Table 1) likely due to isotopic interferences in the plasma. For the rest of the core 05WFGB3, we analyzed monthly Sr/Ca using ICP-OES and then determined annual averages (January–December) to assess long-term trends.

The annually-resolved coral Sr/Ca record has a significant linear decrease of 0.048 mmol mol^{-1}, equivalent to an increasing trend of 1.1ºC, for the interval from 1932 to 2005, similar to the global warming trend (Figures 2, 5c), using the coral Sr/Ca-SST calibration equation determined for this coral (Weerabaddana et al., 2021). The interval from 1940 to 1970 has cooler SST with warmer SST after 1970. The interval from 1755 to 1880, part of the Little Ice Age, is cooler than 1880–2005 with the coldest decades occurring between 1810 and 1880 when explosive volcanic eruptions cool global temperatures. Like coral $\delta^{18}O$, coral Sr/Ca is an important climate proxy that provides insights into past temperature variability. It is not an Anthropocene marker in itself but indicates the climate response to anthropogenic forcing. Additionally, coral Sr/Ca is useful for confirming the annual density band chronology by determining if a year is present when a band is not clear in the X-radiograph and for assessing temporal overlaps in core breaks.

Organic matter proxies

Carbon isotopes – The annually-resolved coral $\delta^{13}C$ averages –1.43‰ in the 1800s with a significant decreasing trend starting in the interval between 1906 and 1913 (results of change point analysis varies based on the number of change points) that accelerates from 2000 to 2005 to an average value of –3.14‰ (Figures 2, 5b). This trend is called the "Suess Effect" (Keeling, 1979) to describe the addition of CO_2 to the atmosphere from burning fossil fuels with lower $\delta^{13}C$ values compared to preindustrial levels. A comparison with atmospheric $\delta^{13}C$ measurements in Hawaii (1980–2005) (Keeling et al., 2001) finds a decrease of 0.67‰ while

coral $\delta^{13}C$ declines by 1.12‰ for the same time interval, thus the coral 05WFGB3 is capturing global trends in $\delta^{13}C$ and CO_2 but with a higher rate of decline. A comparison with Atlantic coral and sclerosponge $\delta^{13}C$ records (1800–2000) finds similar trends with more rapid decreases in the oceans due to a greater amount of CO_2 in the surface oceans and that the rate of decline is accelerating at the end of the 20th century (Swart et al., 2010). This new coral $\delta^{13}C$ record extended to 2005 confirms further acceleration. There are slightly different $\delta^{13}C$ timings in trends for South Pacific coral $\delta^{13}C$ records, but the overall trends are similar (Dassié et al., 2013).

Coral skeleton nitrogen isotopes (CS-$\delta^{15}N$) – The annually-resolved CS-$\delta^{15}N$ record for core 05WFGB3 contains stable values from 1928 to 1962 centered at 5.1 ± 0.15‰ followed by a significant increasing trend starting in 1963 (0.13‰ decade^{-1} for 1963–2005) (Figure 2, Table 4, Supplemental Figure 11). The CS-$\delta^{15}N$ is a robust indicator of the sources of nitrogen present in the surrounding environment (Duprey et al., 2020; 2017; Erler et al., 2015; Wang et al., 2016; 2018).

With values ranging from 4.8 to 6.0‰, the 05WFGB3 CS-$\delta^{15}N$ record is well-constrained by two end-members: the SubTropical Underwater (STUW) and the Mississippi and Atchafalaya River System (MARS) (see Supplemental Results for the definitions of the end-members). Changes in the CS-$\delta^{15}N$ can be interpreted as a change in the respective contribution of the STUW and the MARS to the GoM. The increase in CS-$\delta^{15}N$ values observed from the 1960s onward points toward a greater contribution of MARS-derived nitrogen to WFGB. Indeed, the coral record tracks remarkably the nitrogen load within the Mississippi River Basin (Figure 6) that almost doubles from the pre-1960s to 2000s with a ~0.7‰ increase during the same period. This interpretation is consistent with the increase in bulk $\delta^{15}N$ observed in the GoM for the 20th century in sediment cores (Rosenbauer et al., 2009) and deep-sea coral records (Prouty et al.,

2014) that is attributed to increased nutrient loading from the MARS. See additional CS-$\delta^{15}N$ results in the Supplemental Materials.

Inorganic geochemical signals

Lead-210 activity – The low total ^{210}Pb activities from the core 05WFGB3 and the disequilibrium give ^{210}Pb high uncertainties (Supplemental Table 7) and are not deemed an Anthropocene marker for this coral, see Supplemental Results.

Mercury – Mercury concentrations in the samples from the core 05WFGB3 are low and vary from 0.38 to 1.34 ng g^{-1} with a lower value in 1945 at the end of World War II that increases until 1980 when the lowest Hg value occurs (Figure 2, Supplemental Figure 12, Supplemental Table 8). The topmost sample (2005) includes residues from the coral tissue layer and thus this higher value represents the uptake of Hg by the living coral that is not incorporated into the coral skeleton. A study of *Porites astreoides* found that 96% of Hg is taken up by living tissue and only 4% was found in the coral skeleton (Bastidas and Garcîa, 2004).

The Hg concentration in core 05WFGB3 is lower by an order of magnitude than that found in *S. siderea* corals near industrial sites in Central America (Guzman and Garcìa, 2002) suggesting locations near pollution sources increase coral skeletal Hg concentration. Similar results were found in Bermuda for *Diploria labyrinthiformis* corals sampled near a landfill versus a nearby open bay (Prouty et al., 2013) with the WFGB coral having similar Hg concentrations as the corals near that landfill (Figure 7). A 200-year-long record of coral Hg from the South China Sea (Sun et al., 2016) has a lower baseline Hg concentration than core 05WFGB3 with a similar maximum Hg concentration; however, these two records are not co-varying. That study found increases in coral Hg are associated with Chinese wars. Core 05WFGB3 shows some co-variance with US apparent consumption and global production of Hg

(Kelly et al., 2014) (Figure 7b). The US and other countries enacted pollution regulations in the 1960s and 1970s thus contributing to the reduction in Hg production and consumption and possibly the reduced Hg levels seen in the coral samples for 1980, 1990, and 2000. The results suggest core 05WFGB3 may be recording the US and global Hg fluctuations within the resolution of these records yet further analysis, preferably annually, would help further resolve the coral Hg signal.

Barium – The monthly-resolved coral Ba/Ca record has clear seasonal cycles that do not significantly co-vary with temperature (Supplemental Figure 10). The coral Ba/Ca results presented here build upon the study of Weerabaddana et al. (2021) that revealed the seasonal cycle in monthly coral Ba/Ca is mostly driven by surface ocean productivity. Furthermore, that study found the GoM has some of the highest coral Ba/Ca values globally. The annually-averaged coral Ba/Ca contains a significant difference in mean coral Ba/Ca of 1.57 μmol mol^{-1} between 1933–1947 and 1948–2004, pre- and post-oil extraction operations in the GoM, respectively. There is a significant increasing trend from 1965 to 1983 (these years are change points along with 1947; Figure 2). Generally, coral Ba/Ca records upwelling or riverine sedimentation in the coastal environment (Alibert et al., 2003; Lea et al., 1989); however, WFGB is not close enough to a river source or upwelling that would influence coral Ba/Ca. However, the GoM is home to extensive ocean drilling operations that use barite ($BaSO_4$) as drilling muds and has many offshore oil platforms (Figure 1a) that discharge production waters that contain barite into the gulf (Bleiwas and Miller, 2015). The US barite production and consumption can be used as a proxy for barite input to the oceans (Kelly et al., 2014) since >90% of barite produced in the US are used for offshore oil drilling (Bleiwas and Miller, 2015) and the GoM is the primary oil field for the US. Barite production and consumption peaks in 1981 with a sharp

decline afterward with falling oil prices and coral Ba/Ca captures this peak in 1983 with a three-year delay due to barite production stockpiles taking time to be shipped to the offshore drilling platforms before being used as drilling mud (Weerabaddana et al., 2021).

Discussion

We propose the coral core 05WFGB3 as the Anthropocene GSSP and this discussion will address the requirements for a GSSP that applies to the Anthropocene (Head and Gibbard, 2015; Waters, 2022). The core 05WFGB3 provides a record of a primary Anthropocene marker, the $\Delta^{14}C$ bomb spike starting in 1957, and secondary markers in the 20th century, the $^{239+240}Pu$ bomb spikes in 1956 and 1964, that can be accurately dated to the year and correlated with global anthropogenic signals (Figure 2). The core 05WFGB3 is 1.74 m long and is comprised of primary aragonite with no signs of diagenesis, bioerosion, or disturbances in the core except for breaks that occur during coring or during cutting the core into slabs for X-radiographs and geochemical sampling (Supplemental Figures 1–5). The regular monthly coral Sr/Ca and Mg/Ca signals also support the pristine nature of this core since anomalies in these two elemental ratios can be the result of secondary aragonite or calcite precipitation (Quinn and Taylor, 2006; Sayani et al., 2011). *Siderastrea siderea* is a relatively slow-growing coral (~6 mm $year^{-1}$) when compared with other corals, yet its growth rate is more than sufficient to visually discern years in the density bands and for geochemical sampling on annual to weekly time scales. There is no distinct visible marker or litho-facies change for the year 1957 in the core 05WFGB3 but the year can be found by counting the annual density bands that are visible (wetting the surface helps to see the bands) but are easier to see in X-radiographs. Counting annual bands provides accurate dating and chronology control for corals similar to dendrochronology (Black et al., 2019). Furthermore, corals can be ^{230}Th-dated with accuracies better than ±1 year for corals <100 years

old when a single annual density band is dated (Shen et al., 2003; 2008). WFGB is an open ocean location managed and protected by the FGBNMS that is accessible by boat and to divers. FGBNMS also coordinates and compiles all research conducted in FGB in annual and other reports (Johnston et al., 2021).

Geochemical proxies are the primary markers used for chemostratigraphy in a coral skeleton such that researchers can examine how their variations are influenced by the evolution of global and regional anthropogenic activities (Figure 2). The fallout from atmospheric thermonuclear weapon testing is a significant, globally widespread, and abrupt signature that can be used as a global marker for the onset of human-dominated changes in the environment (Waters et al., 2015). However, the timing and amplitude of the bomb spikes in the surface ocean and thus corals can be affected by (1) location, (2) atmospheric distribution, (3) the rate of equilibration with the atmosphere, (4) the hydrographic regime of the location, (5) biological uptake of radioactive isotopes. The peak of thermonuclear testing occurred in 1951–1958 and 1961–1962 and declined after 1963 due to a Partial Test Ban Treaty and moratoriums when testing was mainly underground in the late 1960s (UNSCEAR, 2000).

Coral core 05WFGB3 contains the radiocarbon "bomb spike" with an increase starting in 1957 then a peak acceleration in 1962 and reaching a maximum in 1970 (Figure 2). Radiocarbon enters the ocean through gas exchange with the atmosphere with an equilibration time of 7–10 years (Broecker and Peng, 1982; Mahadevan, 2001). The bomb $\Delta^{14}C$ maximum in core 05WFGB3 exhibits this expected delay with respect to the atmosphere and the initial increase and acceleration is within the testing dates. The GoM corals do not contain the ^{14}C water mixing signal seen in the $\Delta^{14}C$ in corals from the Cariaco Basin and south of Puerto Rico from equatorial waters with ^{14}C depleted water (Figure 3) (Kilbourne et al., 2007; Wagner et al., 2009; Wagner

2011). Previous GoM coral $\Delta^{14}C$ studies found the source waters that feed the GoM and the air-sea exchange of CO_2 in the gulf are close to the global average (Wagner 2011, Wagner et al., 2009). Therefore, the $\Delta^{14}C$ in core 05WFGB3 is representative of a more global radiocarbon bomb spike than locations with upwelling and mixing water masses that contain ^{14}C-depleted water or locations near the weapons testing sites.

Plutonium-239 is a significant component of the radioactive fallout from thermonuclear weapons testing with a half-life of 24,110 years that will be detectable for ~100,000 years (Hancock et al., 2014) whereas ^{14}C is detectable for ~55,000 years (Hajdas et al., 2021). The coral $^{239+240}Pu$ record has two clearly marked "bomb spikes" in 1956 and 1964. These spikes are synchronous (±1–2 years) with other tropical Atlantic corals but occur after the bomb spikes in Pacific corals located closer to the testing sites (Sanchez-Cabeza et al., 2021) (Figures 2, 4) suggesting the WFGB coral is recording wind distributed ^{239}Pu thus a more global bomb spike (Waters et al., 2018). Since the WFGB coral and Haiti microatoll coral are synchronous for the 1956 spike, this suggests water depth and oceans currents are not a factor for these coral $^{239+240}Pu$ records; however, there are differences in the magnitude of $^{239+240}Pu$ activities for the Atlantic corals (Figure 4) suggesting a possible biological effect that could be contributing to the coral $^{239+240}Pu$ activities. Another consideration when comparing the $\Delta^{14}C$ and $^{239+240}Pu$ records in core 05WFGB3 is analytical precision and detection limits where the plutonium analysis was not different from the background for several samples analyzed for this study (Supplemental Figure 8) whereas the $\Delta^{14}C$ spike is much greater than analytical precision. Other radioactive isotopes investigated in this study were not detectable in corals possibly due to oceanic or biological processes.

At the same time as nuclear testing was occurring, pollution from industry, fossil fuel

burning, and other human activities was rapidly increasing and these proxies can serve as auxiliary Anthropocene markers. The decreasing trend since the 1800s in coral $\delta^{13}C$ due to fossil fuel burning has been studied in corals since 1978 (Swart et al., 2010). The decreasing trend in $\delta^{13}C$ is accelerating especially after the year 2000 and is almost in sync with atmospheric $\delta^{13}C$ due to the oceans up taking atmospheric CO_2 (Figure 5b) The $\delta^{13}C$ Suess effect is captured in many carbon-based archives that could also be used as chemostratigraphic tool. Parallel to the increasing fossil fuel burning is the addition of greenhouse gases in the atmosphere that is driving temperatures higher. The WFGB coral Sr/Ca is recording these temperature changes in the ocean (Figures 2, 5b) and contains the global warming trend. However, the timing of the warming trend does vary by location and is not globally synchronous to a year or even a decade (Abram et al., 2016; Consortium, 2013) but could serve as marker in a wide array of archives with resolutions that are not always annual. Mercury levels in the environment have tripled since the pre-industrial interval with an increase after World War II (Horowitz et al., 2014). The WFGB coral Hg record captures this variability (Figure 2) and fluctuates with Hg consumption and production (Kelly et al., 2014) (Figure 7b). Oil extraction operations using barite as a drilling mud have increased seawater Ba concentration in the GoM (Carriquiry and Horta-Puga, 2010; Deslarzes et al., 1995; Weerabaddana et al., 2021). The increase in mean coral Ba/Ca after 1965 represents the increase in global oil and gas demand after World War II (Figure 2). The coral Ba/Ca record is an indicator of the onset of anthropogenic activities in the GoM yet its scope remains regional and precludes its uses as an Anthropocene marker.

The GoM is intimately linked to North America via the Mississippi River and other rivers that bring anthropogenic pollutants from land to the ocean (mercury and nitrogen). The CS-$\delta^{15}N$ record in core 05WFGB3 provides an invaluable perspective on the alteration of the marine

nitrogen cycle in the GoM due to recent anthropogenic activities. A significant increase in CS-$\delta^{15}N$ is observed after 1963. Transforming forests to agricultural lands and grasslands in the era of "rapid acceleration" accompanied by the massive use of artificial fertilizer during the Green Revolution starting in the 1960s (Ruddiman et al., 2015) to meet the world's food supply needs has remarkably changed the ocean nitrogen cycle by the increased nutrient loading from agricultural systems. Exposed soil is prone to erosion and nutrient leaching that ended up in the oceans through river runoff is revealed in our coral record (Figures 2, 6). Although this record is surely a robust indicator of the onset of the anthropogenic footprint on the GoM and North America, its scope remains regional and precludes its use as an Anthropocene marker.

Conclusions

Corals are a unique archive presented here as a candidate for the Anthropocene GSSP. Corals are simultaneously recording the changes that we humans are making to our planet while also on the verge of becoming extinct themselves. Predictions for corals and coral reefs are that they could be dead by 2030 in some locations and by 2100 for most reefs. Hopefully, a few corals in places of refugia may survive, such as Flower Garden Banks. As the scientific community debates the Anthropocene, the GSSP site, and the year for the start of the Anthropocene, corals will ultimately become the recorder of their last years, passively archiving the changes in their environment, chronologize their stressors, the pollutants, and damage done to these otherwise multi-centenarians living organisms that are now doomed by humans to become a part of the rock record and no longer a part of the living planet Earth.

Acknowledgements

Analysis of the West Flower Garden Bank core was facilitated by the collaborative research project between KLD and the Anthropocene Working Group (AWG) to ratify the

stratigraphic Anthropocene. The AWG isco-ordinating the assessment of candidate GSSP sites in collaboration with the Haus der Kulturen der Welt (HKW, Berlin) in the framework of its long-term project Anthropocene Curriculum. The Anthropocene Curriculum is an international project for experimental forms of Anthropocene research and education developed by HKW and the Max Planck Institute for the History of Science (MPIWG, Berlin) since 2013. We are deeply grateful to the Flower Garden Banks National Marine Sanctuary for their assistance and access to coral and data resources. Corals were collected under permit FGBNMS-2005-002. We thank Ginesse Listi of the LSU FACES Laboratory for their assistance with the coral X-radiographs. Fred Taylor and Jud Partin at the University of Texas Institute for Geophysics for assisting with core slabbing. Chris Maupin and Brendan Roake at Texas A&M University for providing δ18O and δ13C analyses. We thank LSU PAST laboratory students Gilman Ouellette, Jacob Warner, Deborah Loke, Ashley Pomes, Othalia Roberts, Kendall Brome, and lab coordinator Sarah Crabtree for their efforts during this project. Coral data associated with this article are provided in a Supplemental Excel file. The authors are not aware of any affiliations, memberships, funding, or financial holdings that might be perceived as affecting the objectivity of this research.

Funding

The author(s) disclosed receipt of the following financial support for the research, authorship, and/or publication of this article: We would like to thank our funding source the Haus der Kulturen der Welt in support of the Anthropocene Working Group and this project. Additional support for this research is from the Department of the Interior South Central Climate Adaptation Science Center Cooperative Agreement G19AC00086 and the National Science Foundation award NSF-2102931 to KLD. Coral 230Th dating was supported by grants from the

Science Vanguard Research Program of the Ministry of Science and Technology (MOST) (110-2123-M-002-009), the National Taiwan University (110L8907 to C.-C.S.), and the Higher Education Sprout Project of the Ministry of Education (110L901001 and 110L8907) to CCS.

Supplemental material

Supplemental material for this article is available online.

Figures

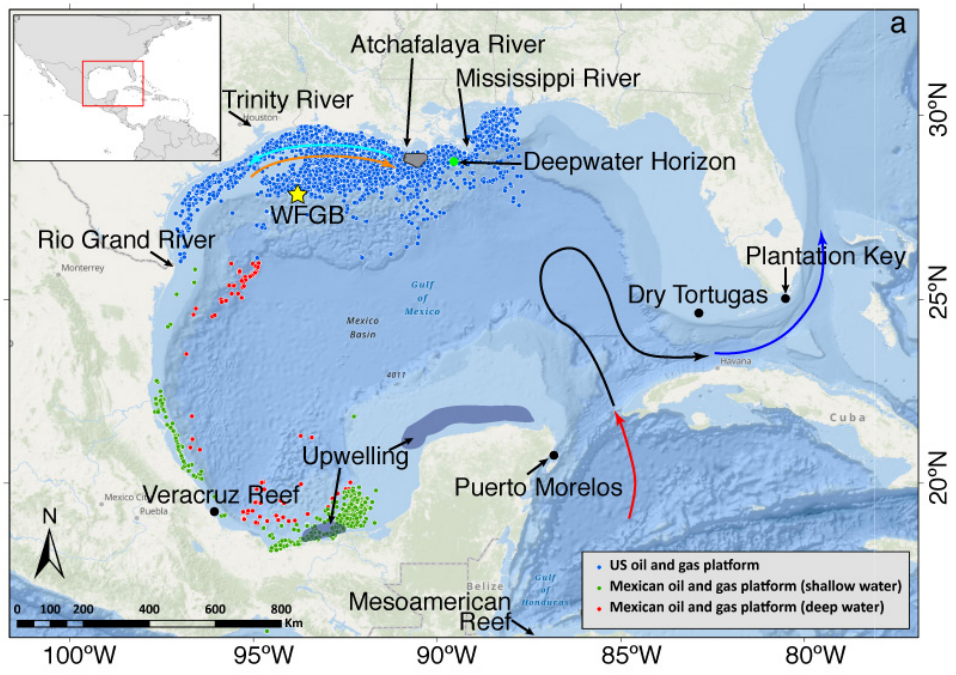
a
Atchafalaya River
Mississippi River
Trinity River
Deepwater Horizon
WFGB
Rio Grand River
Plantation Key
Dry Tortugas
Upwelling
Veracruz Reef
Puerto Morelos
Mesoamerican Reef
US oil and gas platform
Mexican oil and gas platform (shallow water)
Mexican oil and gas platform (deep water)
N
0 100 200 400 600 800 Km
100°W
95°W
90°W
85°W
80°W
30°N
25°N
20°N

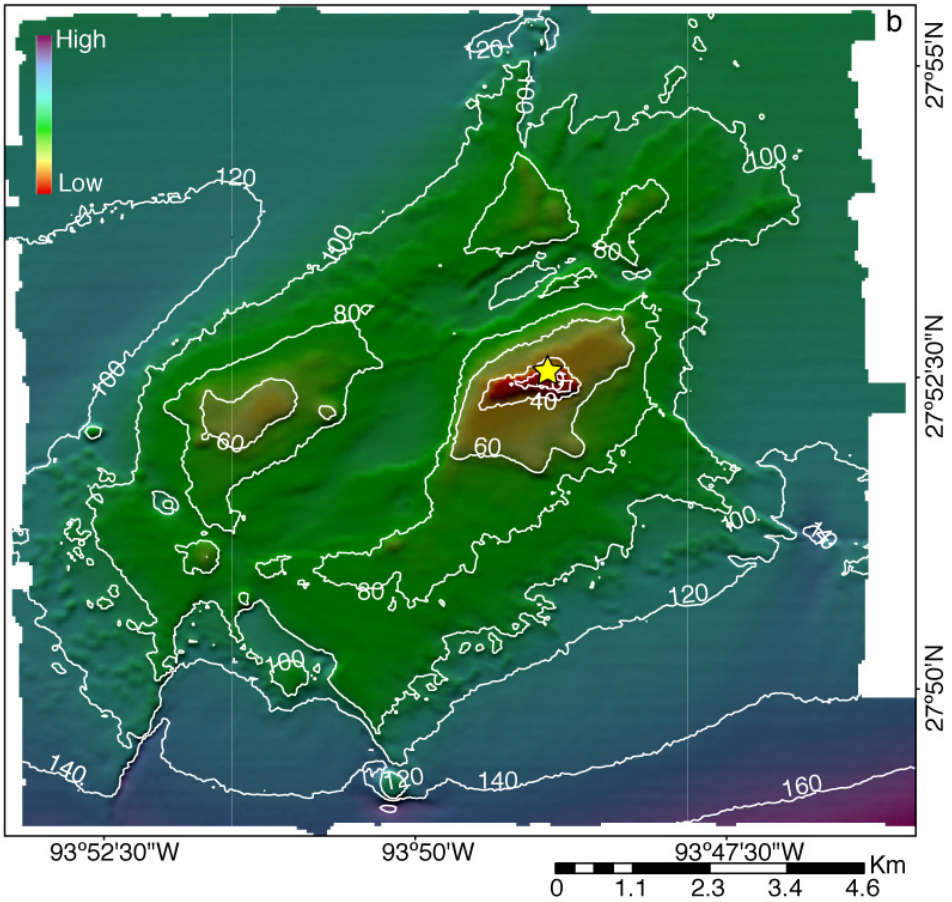
b
High
Low
120
100
80
60
40
93°52'30"W
93°50'W
93°47'30"W
27°55'N
27°52'30"N
27°50'N
0 1.1 2.3 3.4 4.6 Km

Figure 1. The location of West Flower Garden Bank (WFGB) (yellow ★) in the GoM of the western Atlantic Ocean. (a) Bathymetry map of the GoM and its location with respect to North America (inset). Curved arrows are the approximate locations of the predominant currents, the Caribbean Current entering the GoM (red line), the Loop Current (black line) that leaves the gulf becoming the Florida Current (blue line). Seasonal northern GoM coastal currents (winter cyan arrow and summer orange arrow) transport the Mississippi and Atchafalaya Rivers' discharge along the coastline. The approximate seasonal upwelling zones are dark blue areas. Locations of the United States' (US) (www.boem.gov) and Mexico's (mapa.hidrocarburos.gob.mx) oil platforms are small circles. Locations of other relevant sites are marked (●). (b) Bathymetry map of WFGB (https://pubs.usgs.gov/of/2002/0411/data.html) noting the location of the *S. siderea* colony cored for this study (yellow ★).

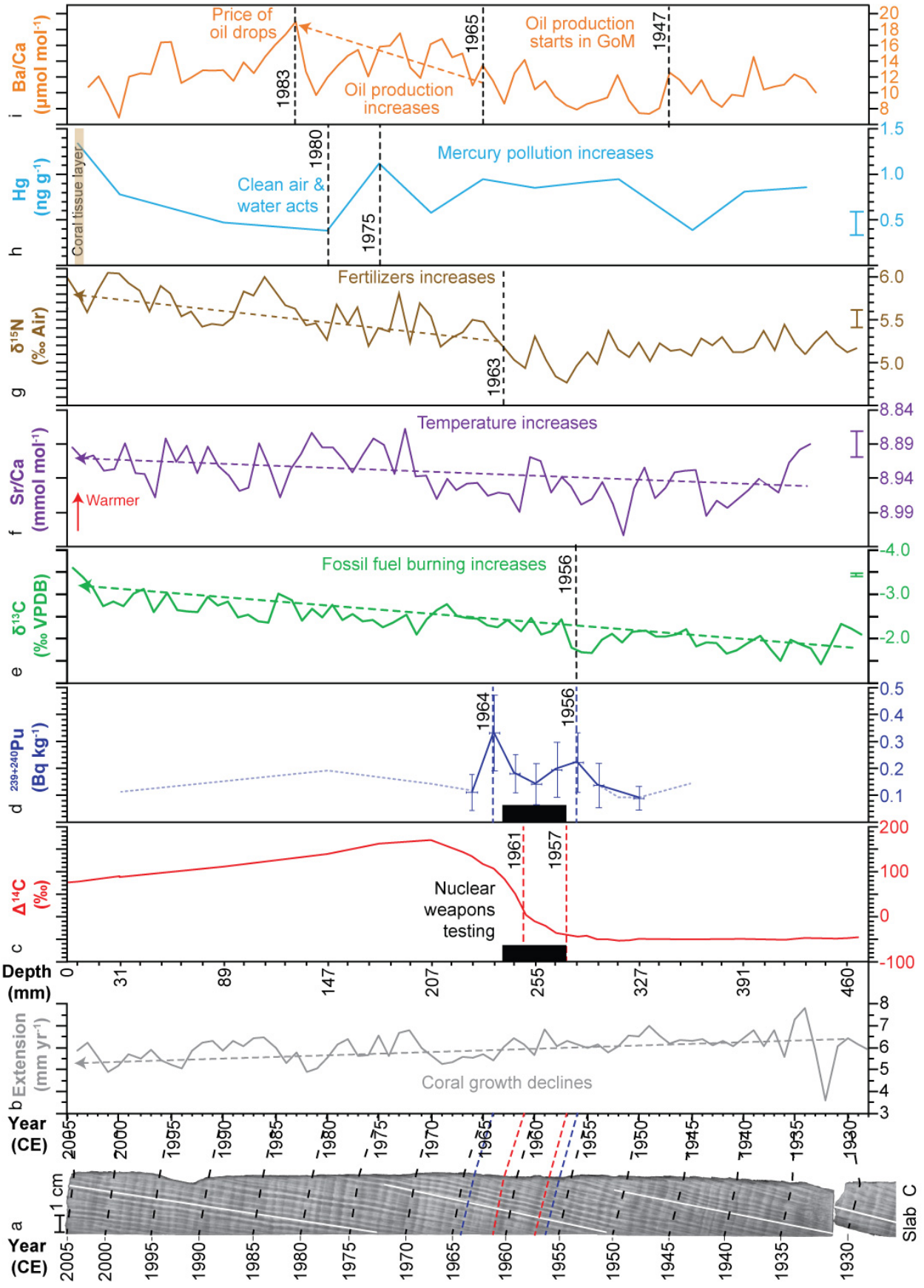
i Ba/Ca (µmol mol-1)
Price of oil drops
1983
Oil production increases
1965
Oil production starts in GoM
1947
h Hg (ng g-1)
Coral tissue layer
1980
Clean air & water acts
1975
Mercury pollution increases
g δ15N (‰ Air)
Fertilizers increases
1963
f Sr/Ca (mmol mol-1)
Temperature increases
Warmer
e δ13C (‰ VPDB)
Fossil fuel burning increases
1956
d 239+240Pu (Bq kg-1)
1964
1956
c Δ14C (‰)
1961
1957
Nuclear weapons testing
Depth (mm)
0
31
89
147
207
255
327
391
460
b Extension (mm yr-1)
Coral growth declines
Year (CE)
a
1 cm
Slab C
Year (CE)

Figure 2. Composite of annually-resolved proxies from core 05WFGB3: (a) X-radiograph of slab C with examples of counting path (white lines) and every 5 years noted (labels on ~January) connected to (b) years in the coral annual extension (black dashed lines). Years for the proposed base of the Anthropocene markers are noted as red dashed lines in (a, c) and secondary marker with blue dashed lines in (a, d) with blue dotted line is limit of detection values (sample activity is less than this value) rather than actual measured activity. (b) Annual extension was determined from coral growth direction noted as white lines in (a). Depth from core top for (c–i) is aligned with extension (b) and years (a) with depth noted for January of each year or the base of the annual sample for the annually-sampled proxies (c-d, g-h) and the annual average from monthly samples (e, f, i). Black boxes span 1957–1963, the period of extensive atmospheric thermonuclear weapons testing (c, d). Linear trends (dashed lines with arrowheads) are significant (1%). Error bars represent analytical precision (1σ) and if not plotted analytical precision is smaller than the line weight. Dating uncertainties for each proxy are given in Table 1.

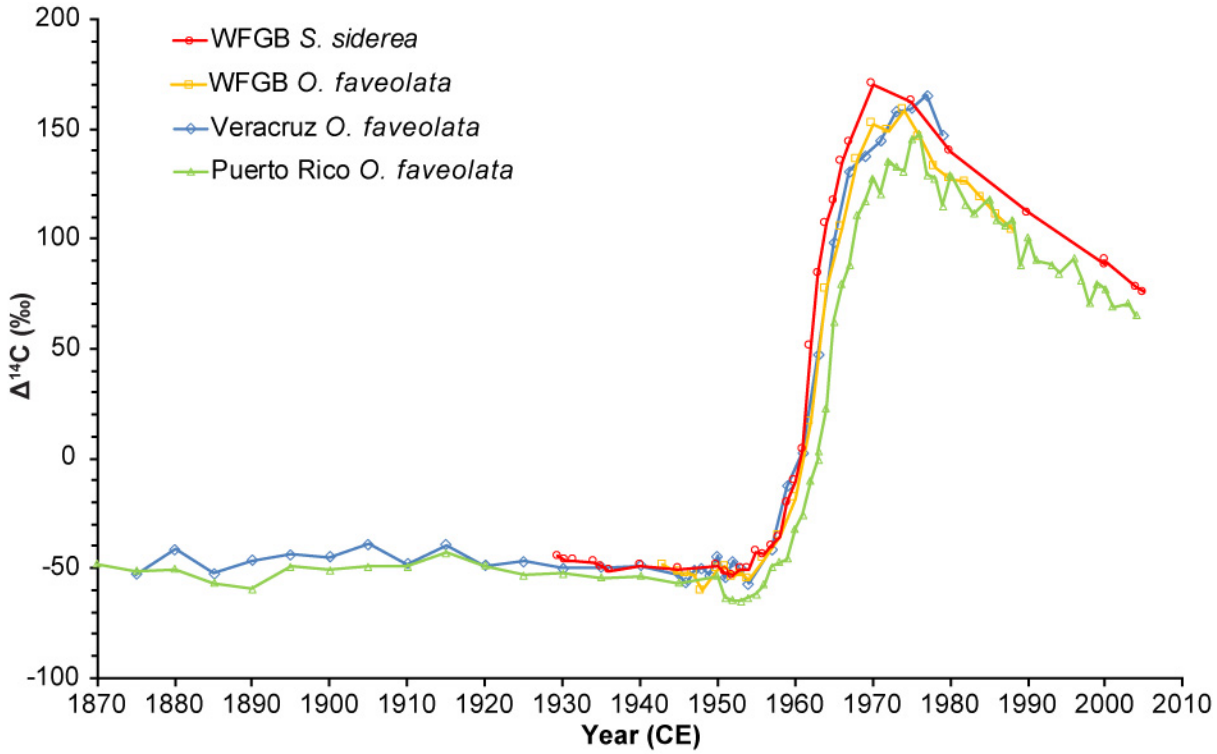

Figure 3. Coral core 05WFGB3 $\Delta^{14}C$ values compared with select corals from the tropical Atlantic Ocean (Kilbourne et al., 2007; Wagner, 2011). Coral $\Delta^{14}C$ records were not adjusted for the Suess Effect. Dating and $\Delta^{14}C$ uncertainties (2–3‰) are about the size of the hollow circle (Table 1).

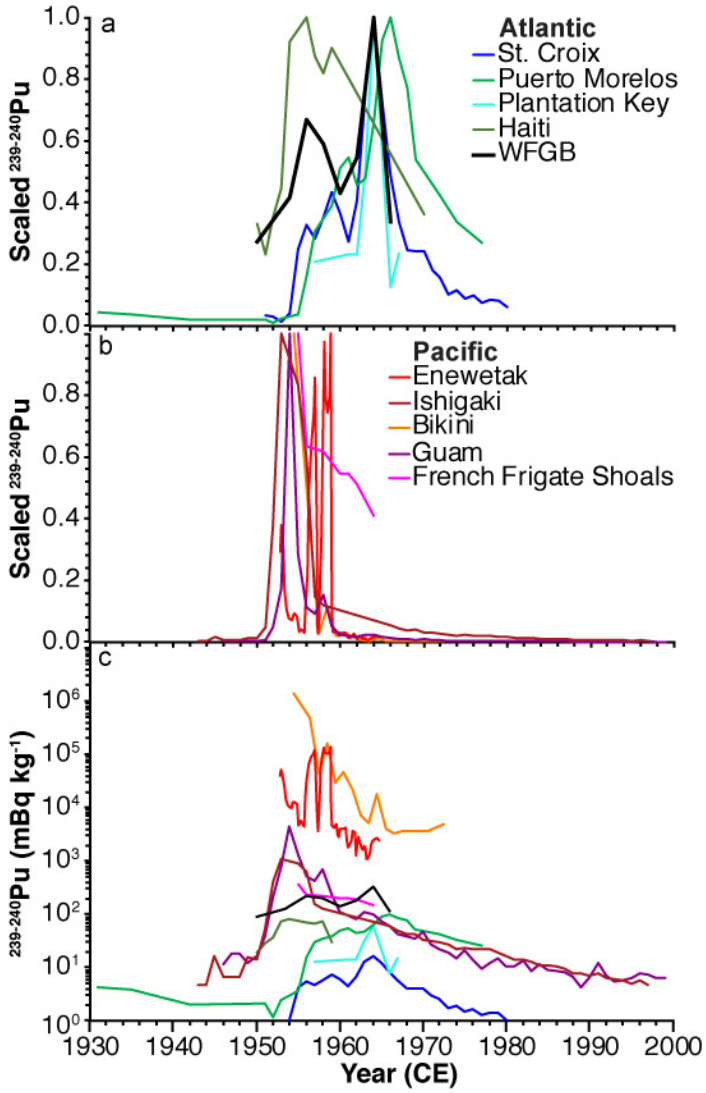

Figure 4. Summary of coral $^{239+240}$Pu studies. (a, b) Plutonium is scaled by the maximum activity of each record and is unitless; modified from Sanchez-Cabeza et al. (2021). Pacific sites (a) are warm colors and Atlantic sites (b) are cool colors. (c) Plutonium activities for each record not scaled using the same color labels as in (a, b). Sites are Bikini (Noshkin et al., 1975), Enewetak (Froehlich et al., 2017), Guam (Lindahl et al., 2011), Ishigaki (Lindahl et al., 2012), Hawaii (Buesseler, 1997), Croix (Benninger and Dodge, 1986), Plantation Key (Purdy and Druffel, 1989), Morelos (Sanchez-Cabeza et al., 2021), Haiti (10LEO1; Supplemental Table 9), and WFGB (this study).

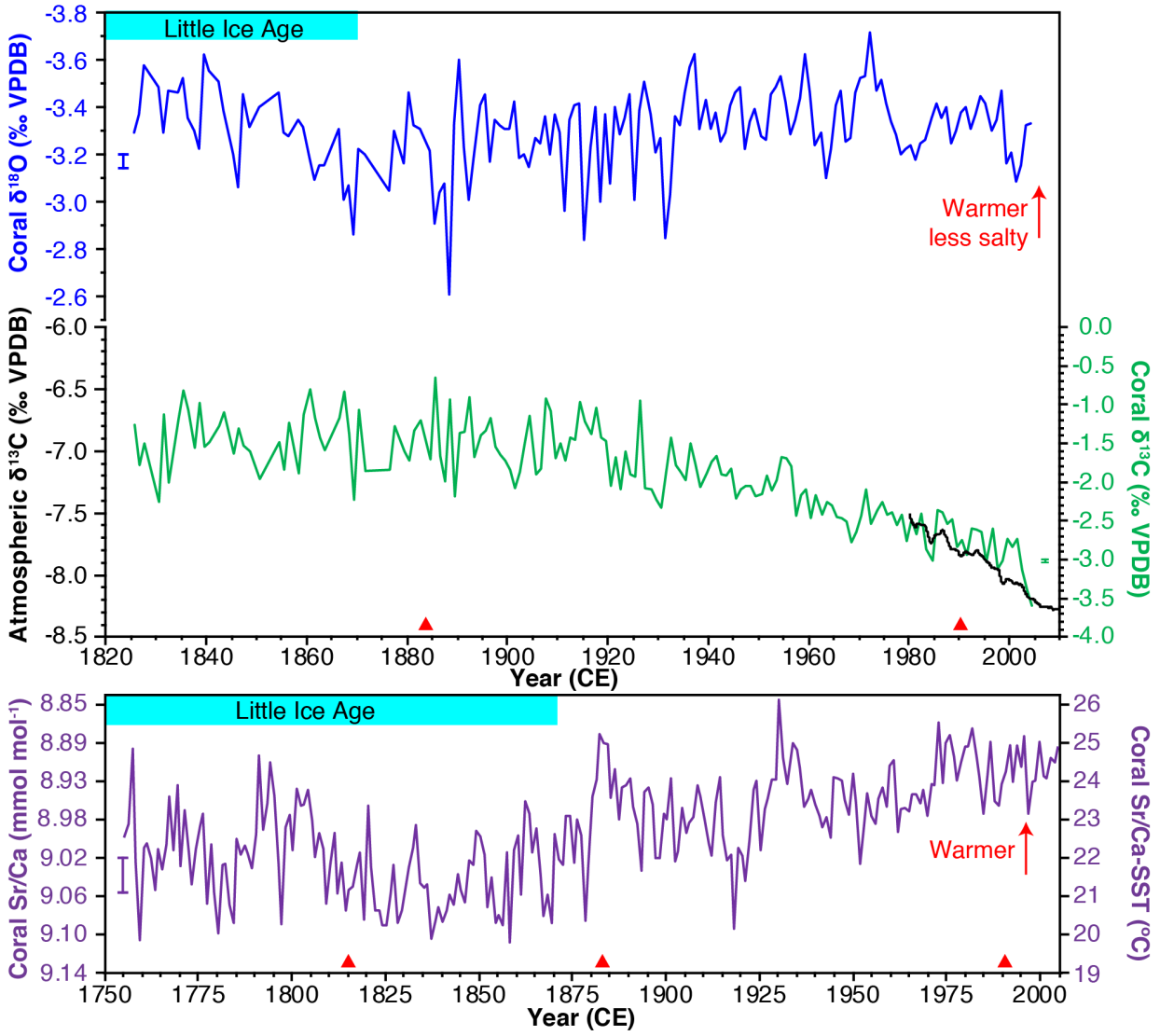

Figure 5. Annual average coral environmental markers from core 05WFGB3 for coral (a) $\delta^{18}O$, (b) $\delta^{13}C$, and (c) Sr/Ca. Monthly coral $\delta^{18}O$ and $\delta^{13}C$ values were averaged in the interval from 1932–2005 and annual maximum and minimum $\delta^{18}O$ and $\delta^{13}C$ values were averaged in the interval from 1826–1932. Monthly coral Sr/Ca variations were annually-averaged in the interval from 1755–2005. (b) Atmospheric $\delta^{13}C$ is from Mauna Loa, Hawaii is shown with the quasi-regular seasonal cycle removed (Keeling et al., 2001). (c) Coral Sr/Ca was converted to SST using the coral Sr/Ca-SST equation for this coral (Weerabaddana et al., 2021). Coral $\delta^{18}O$ and Sr/Ca are scaled to the same temperature range and plotted so that warmer values are up. Error

bars (1σ) are analytical precision determined for monthly samples. For Sr/Ca precision, PL precision is plotted (Supplemental Table 1).

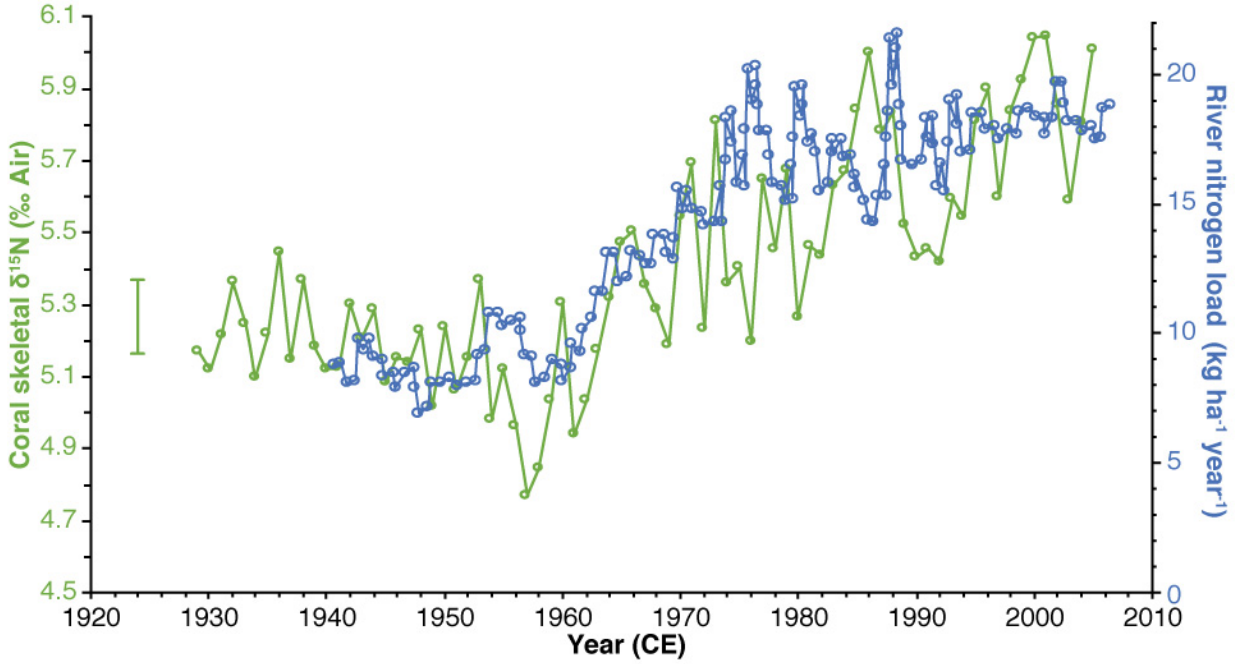

Figure 6. Comparison of CS-$\delta^{15}N$ and Mississippi River Basin nitrogen load (David et al., 2010). Error bar is analytical precision (1σ) and years are assessed to be accurate.

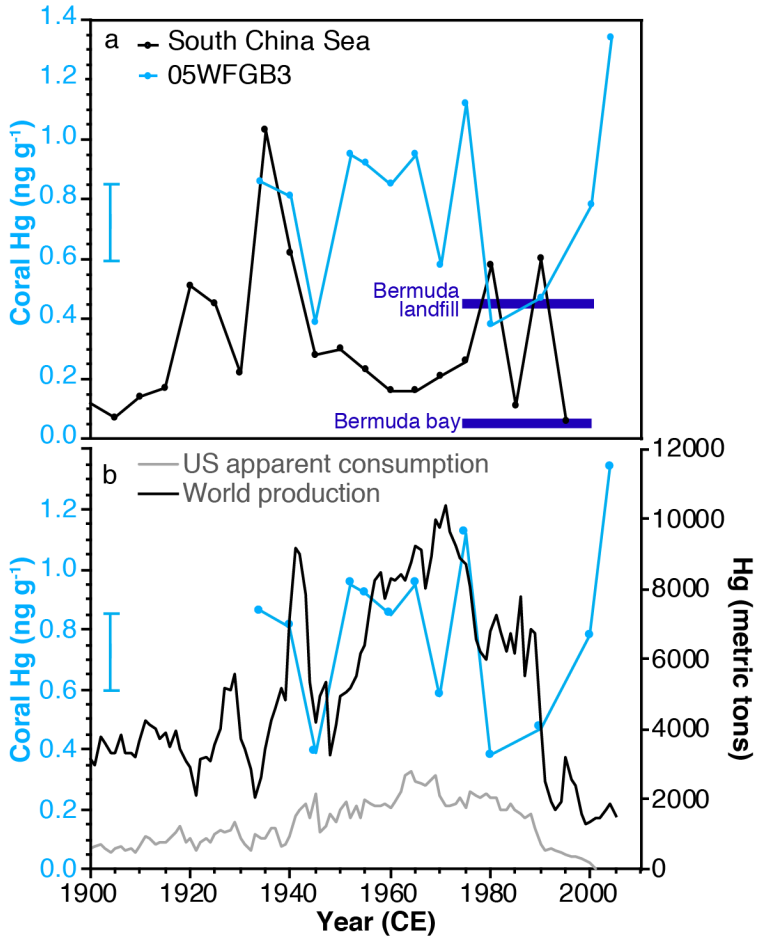

Figure 7. (a) Comparison of coral Hg skeletal concentrations with core 05WFGB3. Two coral Hg averages (1974–1994; dark blue squares) from Bermuda show differences between a relatively open ocean location and a coral growing near a landfill (Prouty et al., 2013). The South China Sea record has samples spanning 5-years and is plotted in the center of each 5-year interval (Sun et al., 2016). (b) US apparent consumption and world production of Hg (Kelly et al., 2014) compared with coral 05WFGB3 Hg concentration. WFGB samples are from one year but analyzed ~5-year intervals (Supplemental Table 8). Error bar is analytical precision (1σ) and years are assessed to be accurate.

Tables

Table 1. Sample details for geochemical analysis.

Analysis type	**Mass (mg)**	**Resolution**	**Interval** [a]	**Slab** [b]	**Date uncertainty** [c]
Radiocarbon (^{14}C) [a]	160–480	Annual	1929–2005	C	±0.1–0.2 year
Radiogenic isotopes [a]	520–980	Annual	1929–2005	C	±0.1–0.2 year
^{137}Cs, ^{210}Pb, ^{241}Am, $^{239\text{-}240}Pu$					
SCP's	570–1460	Annual	1929–2005	C	±0.1–0.2 year
Pollution metal (Hg) [a]	~500	Annual	1929–2005	C	±0.1–0.2 year
Coral skeletal-$\delta^{15}N$ [d]	8	Annual	1929–2005	D	±0.1–0.2 year
$\delta^{18}O$, $\delta^{13}C$	0.04–0.08	Monthly	1933–2005	A	±1–2 months
		2/year	1932–1755	A	±1–2 months
Trace elements					
Sr/Ca, Mg/Ca, Ba/Ca	0.063–0.210	Monthly	1755–2005	A	±1–2 months
Li/Ca, Li/Mg, U/Ca	0.063–0.210	Monthly	1981–2005	A	±1–2 months

[a] All years were not analyzed.

[b] See Supplemental Figure 1 for core cutting and slabbing plan.

[c] Estimated sample date uncertainty. Years were cut from the coral for ~January to December.

[d] Annual samples were cut consecutively for $\delta^{15}N$.

Table 2. Radiocarbon measurements for core 05WFGB3 carbonate analysis.

Sample [a] depth (mm)	Sample Code [b]	ETH-	^{14}C age (BP) [c]	±1σ	$F^{14}C$[d]	±1σ	$\delta^{13}C$ [e] (‰ VPDB)	±1σ	C (mg)
0.0–3.4	05WFG-3 Year: 2005	ETH-117559	-643	21	1.083	0.0029	-3.4	1.0	0.96
3.4–9.4	05WFG-3 Year: 2004	ETH-117560	-654	22	1.085	0.0029	-2.4	1.0	0.95
26.1–31.2	05WFG-3 Year: 2000	ETH-117561	-745	22	1.097	0.0030	1.2	1.0	0.56
26.1–31.2	05WFG-3 Year: 2000	ETH-117561	-732	22	1.095	0.0030	-3.2	1.0	0.95
82.7–88.5	05WFG-3 Year: 1990	ETH-117562	-889	21	1.117	0.0030	-4.8	1.0	0.86
141.0–146.6	05WFG-3 Year: 1980	ETH-117563	-1079	21	1.144	0.0030	-4.1	1.0	0.96
170.9–177.4	05WFG-3 Year: 1975	ETH-117564	-1235	21	1.166	0.0031	-3.7	1.0	0.96
202.2–207.2	05WFG-3 Year: 1970	ETH-117565	-1283	21	1.173	0.0031	-2.9	1.0	0.95
217.8–223.7	05WFG-3 Year: 1967	ETH-117566	-1096	22	1.146	0.0031	-2.8	1.0	0.95
223.7–229.1	05WFG-3 Year: 1966	ETH-117567	-1033	21	1.137	0.0030	-4.1	1.0	0.96
229.1–234.9	05WFG-3 Year: 1965	ETH-117568	-905	22	1.119	0.0030	-3.4	1.0	0.96
234.9–240.0	05WFG-3 Year: 1964	ETH-117569	-832	22	1.109	0.0030	-2.3	1.0	0.96
240.0–245.9	05WFG-3 Year: 1963	ETH-117570	-661	22	1.086	0.0029	-2.1	1.0	0.95
245.9–252.6	05WFG-3 Year: 1962	ETH-117571	-416	22	1.053	0.0029	-2.1	1.0	0.96
252.6–259.1	05WFG-3 Year: 1961	ETH-117572	-39	22	1.005	0.0027	-2.4	1.0	0.96
259.1–254.7	05WFG-3 Year: 1960	ETH-117573	72	22	0.991	0.0027	-2.7	1.0	0.96
264.7–271.7	05WFG-3 Year: 1959	ETH-117574	152	22	0.981	0.0027	-2.2	1.0	0.96
271.7–277.9	05WFG-3 Year: 1958	ETH-117575	282	22	0.965	0.0026	-3.2	1.0	0.90
277.9–284.1	05WFG-3 Year: 1957	ETH-117576	319	22	0.961	0.0026	-2.5	1.0	0.92
284.1–290.3	05WFG-3 Year: 1956	ETH-117577	352	22	0.957	0.0026	-2.9	1.0	0.95
290.3–296.6	05WFG-3 Year: 1955	ETH-117578	349	22	0.958	0.0026	-2.2	1.0	0.96
269.6–302.0	05WFG-3 Year: 1954	ETH-117579	414	22	0.950	0.0026	-3.0	1.0	0.95
302.0–307.7	05WFG-3 Year: 1953	ETH-117580	411	22	0.950	0.0025	-3.9	1.0	0.95
307.7–313.8	05WFG-3 Year: 1952	ETH-117581	440	22	0.947	0.0026	-2.1	1.0	0.95
313.8–320.3	05WFG-3 Year: 1951	ETH-117582	432	22	0.948	0.0026	-1.9	1.0	0.95
320.3–326.9	05WFG-3 Year: 1950	ETH-117583	401	22	0.951	0.0026	-2.1	1.0	0.96
353.9–360.4	05WFG-3 Year: 1945	ETH-117584	419	22	0.949	0.0026	-1.5	1.0	0.95
384.6–391.1	05WFG-3 Year: 1940	ETH-117585	411	22	0.950	0.0026	-2.1	1.0	0.96
410.8–416.0	05WFG-3 Year: 1936	ETH-117586	438	22	0.947	0.0026	-1.9	1.0	0.95
416.0–423.4	05WFG-3 Year: 1935	ETH-117587	418	22	0.949	0.0026	-2.3	1.0	0.95
423.4–431.1	05WFG-3 Year: 1934	ETH-117588	400	22	0.951	0.0026	-2.6	1.0	0.95
447.0–453.7	05WFG-3 Year: 1930 (1931)	ETH-117589	405	22	0.951	0.0026	-2.1	1.0	0.95
453.7–460.0	05WFG-3 Year: 1929 (1930)	ETH-117590	402	22	0.951	0.0026	-2.3	1.0	0.96
460.0–465.7	05WFG-3 Year: 1928 (1929)	ETH-117591	389	22	0.953	0.0026	-0.8	1.0	0.96

[a] Depth range for each ^{14}C annual sample starting from top of coral core (05WFGB3 Slab C) measured on X-radiographs.

[b] Years in parentheses are the actual years determined by counting coral Sr/Ca cycles, annual density bands and ^{230}Th dating. The dates were adjusted between core section 3-1 and 3-2 after samples for radiocarbon were cut. Years were cut from the coral for ~January to December for each year (Table 1). The depth is given as the top of each sample.

[c] BP = Before Present (before 1950 CE)

[d] $F^{14}C$ is fraction modern determined as exp(-^{14}C age/8033) (Reimer et al., 2004). If $F^{14}C$ >1, the sample indicates presence of bomb peak ^{14}C (post 1950 CE).

[e] $\delta^{13}C$ is a value measured on graphite and might include additional fractionation.

Table 3. $^{239+240}$Pu for core 05WFGB3.

Sample depth [a] (mm)	**Sample year [b]**	**$^{239+240}$Pu (Bq kg^{-1})**	**± [c] k=2**
26.1 – 31.2	2000	0.108	
141.0 – 146.6	1980	0.188	
202.2 – 207.2	1970	0.138	
223.7 – 229.1	1966	0.114	0.068
234.9 – 240.0	1964	0.336	0.141
245.9 – 252.6	1962	0.184	0.072
259.1 – 264.7	1960	0.145	0.077
271.7 – 277.9	1958	0.198	0.103
284.1 – 290.3	1956	0.225	0.112
296.6 – 302.0	1954	0.140	0.083
307.7 –313.8	1952	0.088	
320.3 – 326.9	1950	0.092	0.044
353.9 – 360.4	1945	0.139	
410.8 – 416.0	1936	0.085	

[a] Depth range for each annual sample starting from top of coral core (05WFGB3 Slab C) measured on X-radiographs.

[b] Each sample represents one year of coral growth for ~January to December (Table 1).

[c] Data points with no error bars indicate limit of detection values (i.e., sample activity is less than this value) rather than actual measured activity.

Table 4. Nitrogen isotope ratios for core 05WFGB3.

Sample	Sample depth (mm) [a]	Year [b]	N content (nmol mg^{-1})	δ^{15}N ‰ Air
GB05	0.0 – 3.6	2005	1.31	6.01
GB04	3.6 – 9.7	2004	1.38	5.81
GB03	9.7 – 16.1	2003	1.56	5.59
GB02	16.1 – 21.5	2002	1.50	5.85
GB01	21.5 – 26.8	2001	1.37	6.04
GB00	26.8 – 32.3	2000	1.49	6.04
GB99	32.3 – 38.0	1999	1.46	5.92
GB98	38.0 – 43.1	1998	1.43	5.84
GB97	43.1 – 49.2	1997	1.66	5.60
GB96	49.2 – 54.5	1996	1.69	5.90
GB95	54.5 – 59.9	1995	1.42	5.81
GB94	59.9 – 64.9	1994	1.60	5.54
GB93	64.9 – 70.9	1993	1.47	5.59
GB92	70.9 – 76.7	1992	1.43	5.42
GB91	76.7 – 83.4	1991	1.59	5.45
GB90	83.4 – 88.9	1990	1.44	5.43
GB89	88.9 – 95.6	1989	1.50	5.52
GB88	95.6 – 102.0	1988	1.65	5.83
GB87	102.0 – 108.4	1987	1.65	5.78
GB86	108.4 – 114.7	1986	1.47	6.00
GB85	114.7 – 120.5	1985	1.61	5.84
GB84	120.5 – 125.9	1984	1.72	5.67
GB83	125.9 – 131.7	1983	1.56	5.63
GB82	131.7 – 136.8	1982	1.39	5.44
GB81	136.8 – 142.2	1981	1.60	5.46
GB80	142.2 – 147.8	1980	1.82	5.26
GB79	147.8 – 153.7	1979	1.62	5.68
GB78	153.7 – 160.0	1978	1.51	5.46
GB77	160.0 – 165.3	1977	1.25	5.65
GB76	165.3 – 170.9	1976	1.51	5.20
GB75	170.9 – 177.7	1975	1.64	5.40
GB74	177.7 – 183.7	1974	1.79	5.36
GB73	183.7 – 190.5	1973	1.27	5.81
GB72	190.5 – 197.4	1972	1.43	5.23
GB71	197.4 – 203.4	1971	1.49	5.69
GB70	203.4 – 208.8	1970	1.45	5.54
GB69	208.8 – 214.2	1969	1.35	5.19
GB68	214.2 – 219.3	1968	1.52	5.29
GB67	219.3 – 224.4	1967	1.25	5.36
GB66	224.4 – 230.2	1966	1.38	5.50
GB65	230.2 – 236.2	1965	1.53	5.47
GB64	236.2 – 242.0	1964	1.44	5.32
GB63	242.0 – 248.0	1963	1.46	5.17
GB62	248.0 – 254.1	1962	1.34	5.04
GB61	254.1 – 260.0	1961	1.63	4.94
GB60	260.0 – 266.2	1960	1.90	5.31
GB59	266.2 – 272.4	1959	1.49	5.04
GB58	272.4 – 278.4	1958	1.27	4.84
GB57	278.4 – 284.7	1957	1.53	4.77
GB56	284.7 – 291.3	1956	1.59	4.96
GB55	291.3 – 297.2	1955	1.59	5.12
GB54	297.2 – 303.6	1954	1.47	4.98
GB53	303.6 – 309.3	1953	1.42	5.37
GB52	309.3 – 315.2	1952	1.26	5.15
GB51	315.2 – 321.2	1951	1.24	5.06
GB50	321.2 – 327.8	1950	1.33	5.24
GB49	327.8 – 334.7	1949	1.60	5.02
GB48	334.7 – 341.4	1948	1.62	5.23
GB47	341.4 – 347.8	1947	1.55	5.14
GB46	347.8 – 354.1	1946	1.41	5.15
GB45	354.1 – 360.3	1945	1.70	5.08
GB44	360.3 – 367.0	1944	1.53	5.29
GB43	367.0 – 373.2	1943	1.68	5.21
GB42	373.2 – 379.2	1942	1.83	5.30
GB41	379.2 – 385.4	1941	1.68	5.13
GB40	385.4 – 391.9	1940	1.81	5.12
GB39	391.9 – 398.6	1939	1.62	5.18
GB38	398.6 – 404.6	1938	1.48	5.37
GB37	404.6 – 411.1	1937	1.51	5.15
GB36	411.1 – 417.1	1936	1.35	5.45
GB35	417.1 – 423.9	1935	1.59	5.22
GB34	423.9 – 431.4	1934	1.65	5.10
GB33	431.4 – 434.4	1933	1.56	4.88
GB32	434.4 – 437.5	1932.5	1.37	5.25
GB31	437.5 – 441.0	1932	1.61	5.36
GB30	441.0 – 447.3	1931	1.85	5.22
GB29	447.3 – 453.7	1930	1.76	5.12
GB28	453.7 – 459.9	1929	1.80	5.17

[a] Depth range for each annual sample starting from top of coral core (05WFGB3 Slab D) measured on X-radiographs.
[b] Each sample represents one year of coral growth for ~January to December (Table 1). The dates for samples GB32 to GB28 were adjusted between core section 3-1 and 3-2 after samples were cut for analysis.

References

Abram NJ, McGregor HV, Tierney JE, et al. (2016) Early onset of industrial-era warming across the oceans and continents. *Nature* 536(7617):411-418.

Alibert C, Kinsley L, Fallon SJ, et al. (2003) Source of trace element variability in Great Barrier Reef corals affected by the Burdekin flood plumes. *Geochimica et Cosmochimica Acta* 67(2):231.

Allard J, Clarke III J and Keim B (2016) Spatial and temporal patterns of in situ sea surface temperatures within the Gulf of Mexico from 1901-2010. *American Journal of Climate Change* 5:314-343.

Alvera-Azcrate A, Barth A and Weisberg RH (2009) The surface circulation of the Caribbean Sea and the Gulf of Mexico as inferred from satellite altimetry. *Journal of Physical Oceanography* 39(3):640-657.

Bastidas C and Garcîa EM (2004) Sublethal effects of mercury and its distribution in the coral *Porites astreoides*. *Marine Ecology Progress Series* 267:133-143.

Benninger LK and Dodge RE (1986) Fallout plutonium and natural radionuclides in annual bands of the coral *Montastrea annularis*, St. Croix, U.S. Virgin Islands. *Geochimica et Cosmochimica Acta* 50(12):2785-2797.

Black B, A., Andersson C, Butler PG, et al. (2019) The revolution of crossdating in marine palaeoecology and palaeoclimatology. *Biology Letters* 15(1):20180665.

Bleiwas DI and Miller MM (2015) *Barite—A case study of import reliance on an essential material for oil and gas exploration and development drilling.* U.S. Geological Survey, Washington DC.

Broecker WS and Peng T-H (1982) *Tracers in the Sea.* Palisades, NY: Lamont-Doherty Geological Observatory, Columbia University.

Buddemeier RW, Maragos JE and Knutson DW (1974) Radiographic studies of reef coral exoskeletons: rates and patterns of coral growth. *Journal of Experimental Marine Biology and Ecology* 14(2):179-199.

Buesseler KO (1997) The isotopic signature of fallout plutonium in the North Pacific. *Journal of Environmental Radioactivity* 36(1):69-83.

Carriquiry JD and Horta-Puga G (2010) The Ba/Ca record of corals from the Southern Gulf of Mexico: Contributions from land-use changes, fluvial discharge and oil-drilling muds. *Marine Pollution Bulletin* 60(9):1625-1630.

Cheng H, Lawrence Edwards R, Shen C-C, et al. (2013) Improvements in ^{230}Th dating, ^{230}Th and ^{234}U half-life values, and U–Th isotopic measurements by multi-collector inductively coupled plasma mass spectrometry. *Earth and Planetary Science Letters* 371-372:82-91.

Consortium PK (2013) Continental-scale temperature variability during the past two millennia. *Nature Geosci* 6(5):339-346.

Darnell RM and Defenbaugh RE (2015) Gulf of Mexico: Environmental overview and history of environmental research. *American Zoologist* 30(1):3-6.

Dassié EP, Lemley GM and Linsley BK (2013) The Suess effect in Fiji coral δ^{13}C and its potential as a tracer of anthropogenic CO_2 uptake. *Palaeogeography, Palaeoclimatology, Palaeoecology* 370(0):30-40.

David MB, Drinkwater LE and McIsaac GF (2010) Sources of nitrate yields in the Mississippi River basin. *Journal of Environmental Quality* 39(5):1657-1667.

Dee SG, Torres MA, Martindale RC, et al. (2019) The future of reef ecosystems in the Gulf of Mexico: insights from coupled climate model simulations and ancient hot-house reefs. *Frontiers in Marine Science* 6:691. doi:10.3389/fmars.2019.00691.

DeLong KL, Flannery JA, Maupin CR, et al. (2011) A coral Sr/Ca calibration and replication study of two massive corals from the Gulf of Mexico. *Palaeogeography Palaeoclimatology Palaeoecology* 307(1-4):117-128.

DeLong KL, Flannery JA, Poore RZ, et al. (2014) A reconstruction of sea surface temperature variability in the southeastern Gulf of Mexico from 1734–2008 C.E. using cross-dated Sr/Ca records from the coral *Siderastrea siderea*. *Paleoceanography* 29(5):403-422.

DeLong KL, Maupin CR, Flannery JA, et al. (2016) Refining temperature reconstructions with the Atlantic coral *Siderastrea siderea*. *Palaeogeography, Palaeoclimatology, Palaeoecology* 462:1-15.

DeLong KL, Quinn TM, Taylor FW, et al. (2013) Improving coral-base paleoclimate reconstructions by replicating 350 years of coral Sr/Ca variations. *Palaeogeography Palaeoclimatology Palaeoecology* 373:6-24.

Deslarzes KJ, Boothe PN, Presely BJ, et al. (1995) Historical incorporation of barium in the reef bulding coral *Montastrea annularis* at the Flower Garden Banks, north-west Gulf of Mexico. *Marine Pollution Bulletin* 30(11):718-722.

Duprey NN, Wang TX, Kim T, et al. (2020) Megacity development and the demise of coastal coral communities: Evidence from coral skeleton $\delta^{15}N$ records in the Pearl River estuary. *Glob Chang Biol* 26(3):1338-1353.

Duprey NN, Wang XT, Thompson PD, et al. (2017) Life and death of a sewage treatment plant recorded in a coral skeleton $\delta^{15}N$ record. *Mar Pollut Bull* 120(1-2):109-116.

Erler D, Wang X, Sigman D, et al. (2015) Controls on the nitrogen isotopic composition of shallow water corals across a tropical reef flat transect. *Coral Reefs* 34(1):329-338.

Flannery JA, Richey JN, Thirumalai K, et al. (2017) Multi-species coral Sr/Ca based sea-surface temperature reconstruction using *Orbicella faveolata* and *Siderastrea siderea* from the Florida Straits. *Palaeogeography, Palaeoclimatology, Palaeoecology* 466:100-109.

Frieler K, Meinshausen M, Golly A, et al. (2013) Limiting global warming to 2°C is unlikely to save most coral reefs. *Nature Climate Change* 3(2):165-170.

Froehlich MB, Tims SG, Fallon SJ, et al. (2017) Nuclear weapons produced ^{236}U, ^{239}Pu and ^{240}Pu archived in a *Porites Lutea* coral from Enewetak Atoll. *J Environ Radioact* 178-179:349-353.

Greene CA, Thirumalai K, Kearney KA, et al. (2019) The climate data toolbox for MATLAB. *Geochemistry Geophysics Geosystems* 20(7):3774-3781.

Guzman HM and Garcìa EM (2002) Mercury levels in coral reefs along the Caribbean coast of Central America. *Marine Pollution Bulletin* 44(12):1415-1420.

Hajdas I, Ascough P, Garnett MH, et al. (2021) Radiocarbon dating. *Nature Reviews Methods Primers* 1(1):62.

Hancock Gary, J, Tims Stephen, G, Fifield, LK, Webster Ian, T (2014) The release and persistence of radioactive anthropogenic nuclides. Geological Society, London, Special

Publications, 395(1): 265-281, doi:10.1144/SP395.15.
Head MJ and Gibbard PL (2015) Formal subdivision of the Quaternary System/Period: past, present, and future. *Quaternary International* 383:4-35.
Horowitz HM, Jacob DJ, Amos HM, et al. (2014) Historical mercury releases from commercial products: global environmental implications. *Environmental Science & Technology* 48(17):10242-10250.
Johnston MA, Hickerson EL, Nuttall MF, et al. (2019) Coral bleaching and recovery from 2016 to 2017 at East and West Flower Garden Banks, Gulf of Mexico. *Coral Reefs* 38(4):787-799.
Johnston MA, O'Connell K, Blakeway RD, et al. (2021) Long-term monitoring at East and West Flower Garden Banks: 2019 Annual Report. National Marine Sanctuaries Conservation Series ONMS-21-02, Galveston, TX. U.S. Department of Commerce, National Oceanic and Atmospheric Administration, Flower Garden Banks National Marine Sanctuary.
Keeling CD (1979) The Suess effect: ^{13}Carbon-^{14}Carbon interrelations. *Environment International* 2(4): 229-300.
Keeling CD, Piper SC, Bacastow RB, et al. (2001) Exchanges of atmospheric CO_2 and $^{13}CO_2$ with the terrestrial biosphere and oceans from 1978 to 2000. I. Global aspects, SIO Reference Series, No. 01-06, Scripps Institution of Oceanography, San Diego.
Kelly TD, Matos GR, et al. (2014) Historical statistics for mineral and material commodities in the United States (2016 version), U.S. Geological Survey Data Series 140, Washington DC.
Kilbourne KH, Terrence MQ, Thomas PG, et al. (2007) Decadal- to interannual-scale source water variations in the Caribbean Sea recorded by Puerto Rican coral radiocarbon. *Climate Dynamics* 29(1):51-62.
Killick R, Fearnhead P and Eckley IA (2012) Optimal detection of changepoints with a linear computational cost. *Journal of the American Statistical Association* 107(500):1590-1598.
Knutson D, Buddemeier R and Smith S (1972) Coral chronometers: Seasonal growth bands in reef corals. *Science* 177(4045):270-272.
Kuffner IB, Roberts KE, Flannery JA, et al. (2017) Fidelity of the Sr/Ca proxy in recording ocean temperature in the western Atlantic coral *Siderastrea siderea*. *Geochemistry, Geophysics, Geosystems* 18(1):178-188.
Lawman AE, Dee SG, DeLong KL, et al. (2022) Rates of future climate change in the Gulf of Mexico and the Caribbean Sea: implications for coral reef rcosystems. *Journal of Geophysical Research: Biogeosciences* 127(9): e2022JG006999.
Lea DW, Shen GT and Boyle EA (1989) Coralline barium records temporal variability in equatorial Pacific upwelling. *Nature* 340(6232):373-376.
Lindahl P, Andersen MB, Keith-Roach M, et al. (2012) Spatial and temporal distribution of Pu in the Northwest Pacific Ocean using modern coral archives. *Environ Int* 40:196-201.
Lindahl P, Asami R, Iryu Y, et al. (2011) Sources of plutonium to the tropical Northwest Pacific Ocean (1943–1999) identified using a natural coral archive. *Geochimica et Cosmochimica Acta* 75(5):1346-1356.
Lough JM and Cantin NE (2014) Perspectives on massive coral growth rates in a changing ocean. *The Biological Bulletin* 226(3): 187-202.

Mahadevan A (2001) An analysis of bomb radiocarbon trends in the Pacific. *Marine Chemistry* 73(3):273-290.

Murray SP, Jarosz E and Weeks III ET (1998) An observational study of the Mississippi-Atchafalaya coastal plume: Final report. U.S. Department of the Interior, Minerals Management Service, Gulf of Mexico OCS Region New Orleans, LA.

Noshkin V, Wong K, Eagle R, et al. (1975) Transuranics and other radionuclides in Bikini Lagoon: concentration data retrieved from aged coral sections 1. *Limnology and Oceanography* 20(5):729-742.

Office of National Marine Sanctuaries (2008) Flower Garden Banks National Marine Sanctuary Condition Report 2008. U.S. Department of Commerce, National Oceanic and Atmospheric Administration, Office of National Marine Sanctuaries, Silver Spring, MD.

Paillard D, Labeyrie L and Yiou P (1996) Macintosh program performs time-series analysis. *EOS, Transactions American Geophysical Union* 77:379.

Prouty NG, Goodkin NF, Jones R, et al. (2013) Environmental assessment of metal exposure to corals living in Castle Harbour, Bermuda. *Marine Chemistry* 154:55-66.

Prouty NG, Roark EB, Koenig AE, et al. (2014) Deep-sea coral record of human impact on watershed quality in the Mississippi River Basin. *Global Biogeochemical Cycles* 28(1):29-43.

Pulster EL, Gracia A, Armenteros M, et al. (2020) A first comprehensive baseline of hydrocarbon pollution in Gulf of Mexico fishes. *Scientific Reports* 10(1):6437.

Purdy CB and Druffel ER (1989) Anomalous levels of ^{90}Sr and ^{239,240} Pu in Florida corals: Evidence of coastal processes. *Geochimica et Cosmochimica Acta* 53(6):1401-1410.

Quinn TM and Taylor FW (2006) SST artifacts in coral proxy records produced by early marine diagenesis in a modern coral from Rabaul, Papua New Guinea. *Geophysical Research Letters* 33:L04601.

Rabalais NN, Turner RE and Wiseman WJ (2002) Gulf of Mexico hypoxia, a.k.a "The Dead Zone". *Annu. Rev. Ecol. Syst.* 33(1):235-263.

Reimer PJ (2004) Discussion: Reporting and calibration of post-bomb ^{14}C Data. *Radiocarbon* 46(3):1299-1304. doi:10.1017/S0033822200033154.

Reynolds RW, Rayner NA, Smith TM, et al. (2002) An improved in situ and satellite SST analysis for climate. *Journal of Climate* 15(13):1609-1625.

Rosenbauer RJ, Swarzenski PW, Kendall C, et al. (2009) A carbon, nitrogen, and sulfur elemental and isotopic study in dated sediment cores from the Louisiana Shelf. *Geo-Marine Letters* 29(6):415-429.

Ruddiman WF, Ellis EC, Kaplan JO, et al. (2015) Defining the epoch we live in. *Science* 348(6230):38-39.

Sanchez-Cabeza J-A, Rico-Esenaro SD, Corcho-Alvarado JA, et al. (2021) Plutonium in coral archives: A good primary marker for an Anthropocene type section. *Science of The Total Environment* 771:145077.

Sayani HR, Cobb KM, Cohen AL, et al. (2011) Effects of diagenesis on paleoclimate reconstructions from modern and young fossil corals. *Geochimica et Cosmochimica Acta* 75(21):6361-6373.

Schmahl GP, Hickerson EL and Precht WF (2008) Biology and Ecology of Coral Reefs and

Coral Communities in the Flower Garden Banks Region, Northwestern Gulf of Mexico. In: Riegl, B.M., Dodge, R.E. (Eds.), *Coral Reefs of the USA.* Springer, Dordrecht, pp. 221-261.

Shen C-C, Cheng H, Edwards RL, et al. (2003) Measurement of attogram quantities of ^{231}Pa in dissolved and particulate fractions of seawater by isotope dilution thermal ionization mass spectroscopy. *Analytical Chemistry* 75(5):1075–1079.

Shen C-C, Li K-S, Sieh K, et al. (2008) Variation of initial ^{230}Th/^{232}Th and limits of high precision U–Th dating of shallow-water corals. *Geochimica et Cosmochimica Acta* 72(17):4201-4223.

Shen C-C, Wu C-C, Cheng H, et al. (2012) High-precision and high-resolution carbonate ^{230}Th dating by MC-ICP-MS with SEM protocols. *Geochimica et Cosmochimica Acta* 99(0):71-86.

Slowey NC, Holcombe T, Betts MP, et al. (2008) Habitat islands along the shelf edge of the Northwestern Gulf of Mexico. In: Ritchie KB and Keller BD (eds) *A Scientific Forum on the Gulf of Mexico: The Islands in the Stream Concept. Marine Sanctuaries Conservation Series NMSP-08-04.* U.S. Department of Commerce, National Oceanic and Atmospheric Administration, National Marine Sanctuary Program, Silver Spring, MD, pp. 22-27.

Smith TM, Reynolds RW, Peterson TC, et al. (2008) Improvements to NOAA's historical merged land–ocean surface temperature analysis (1880–2006). *Journal of Climate* 21(10):2283-2296.

Sturges W and Evans JC (1983) On the variability of the Loop Current in the Gulf of Mexico. *Journal of Marine Research* 41(4):639-653.

Sun R, Hintelmann H, Liu Y, et al. (2016) Two centuries of coral skeletons from the northern South China Sea record mercury emissions from modern Chinese wars. *Environmental Science & Technology* 50(11):5481-5488.

Swart PK, Greer L, Rosenheim BE, et al. (2010) The C-13 Suess effect in scleractinian corals mirror changes in the anthropogenic CO_2 inventory of the surface oceans. *Geophysical Research Letters* 37, L05604, doi:10.1029/2009gl041397.

Teague WJ, Wijesekera HW, Jarosz E, et al. (2013) Current and hydrographic conditions at the East Flower Garden Bank in 2011. *Continental Shelf Research* 63:43-58.

UNSCEAR (2000) *Sources and effects of ionizing radiation, 2000 report*. New York: United Nations.

Wagner AJ (2011) *Oxygen and Carbon Isotopes and Coral Growth in the Gulf of Mexico and Caribbean Sea as Environmental and Climate Indicators*. PhD Dissertation, Texas A&M University, College Station.

Wagner AJ, Guilderson TP, Slowey NC, et al. (2009) Pre-bomb surface water radiocarbon of the Gulf of Mexico and Caribbean as recorded in hermatypic corals. *Radiocarbon* 51(3): 947-954, doi:10.1017/S0033822200034020.

Wang XT, Cohen AL, Luu V, et al. (2018) Natural forcing of the North Atlantic nitrogen cycle in the Anthropocene. *Proc Natl Acad Sci U S A* 115(42):10606-10611.

Wang XT, Sigman DM, Cohen AL, et al. (2016) Influence of open ocean nitrogen supply on the skeletal δ^{15}N of modern shallow-water scleractinian corals. *Earth and Planetary Science Letters* 441:125-132.

Waters CN (2022) Candidate sites and other reference sections for the GlobalBoundary Stratotype Section and Point (GSSP) of the Anthropocene series. *The Anthropocene Review*. doi:10.1177/20530196221136422.

Waters CN, Syvitski JPM, Gałuszka A, et al. (2015) Can nuclear weapons fallout mark the beginning of the Anthropocene Epoch? *Bulletin of the Atomic Scientists* 71(3):46-57.

Waters CN, Zalasiewicz J, Summerhayes C, et al. (2018) Global Boundary Stratotype Section and Point (GSSP) for the Anthropocene Series: Where and how to look for potential candidates. *Earth-Science Reviews* 178:379-429.

Weerabaddana MM, DeLong KL, Wagner AJ, et al. (2021) Insights from barium variability in a *Siderastrea siderea* coral in the northwestern Gulf of Mexico. *Marine Pollution Bulletin* 173:112930.

Wilson WD and Johns WE (1997) Velocity structure and transport in the Windward Islands Passages. *Deep Sea Research Part I: Oceanographic Research Papers* 44(3): 487-520.

Zavala-Hidalgo J, Romero-Centeno R, Mateos-Jasso A, et al. (2014) The response of the Gulf of Mexico to wind and heat flux forcing: What has been learned in recent years? *Atmósfera* 27(3):317-334.

The Flower Garden Banks *Siderastrea siderea* Coral as a Candidate Global Boundary Stratotype Section and Point for the Anthropocene Series

Supplemental Material

Supplemental background

In the suite of coral species used for paleoenvironmental and paleoclimate reconstructions (mostly *Porites* sp. from the Indo-Pacific), the Atlantic species *S. siderea* is a relative newcomer but has quickly shown itself to be highly reproducible in its skeletal geochemistry ($\delta^{18}O$, Sr/Ca, Ba/Ca) within and among coral colonies and can produce robust climate and environmental reconstructions for the Atlantic Ocean with high fidelity (DeLong et al., 2011; 2014; 2016; Flannery et al., 2017; Guzman and Tudhope, 1998; Kuffner et al., 2017; Maupin et al., 2008; Reich et al., 2013; Weerabaddana et al., 2021). The geochemical proxies in *S. siderea* and other corals used for reconstructions include coral Sr/Ca for temperature (DeLong et al., 2011; 2014; 2016; Kuffner et al., 2017; Maupin et al., 2008) and coral $\delta^{18}O$ for temperature and hydroclimate (Guzman and Tudhope, 1998; Maupin et al., 2008; Pereira et al., 2022). Recently developed coral temperature proxies (Li/Ca, Li/Mg, Sr-U) and other temperature proxies (Mg/Ca, U/Ca) have not been assessed for *S. siderea* to the same degree as Sr/Ca (Alpert et al., 2017; Fowell et al., 2016). Coral skeletal $\delta^{15}N$ (CS-$\delta^{15}N$) has been used successfully to track the history of anthropogenic nitrogen discharge on coral reefs over the past decades (Duprey et al., 2020; 2017; Ren et al., 2017) with a single $\delta^{15}N$ study for *S. siderea* thus far (Moses and Swart, 2006). Other environmental markers (^{14}C, Pu, $\delta^{13}C$, Hg, etc.) have been studied in corals including *S. siderea* (see reviews of Saha et al., 2016; Thompson, 2021), particularly for *S. siderea* for heavy metals from pollution (Guzmán and Holst, 1993; Guzmán

and Jiménez, 1992), $\delta^{13}C$ for the Suess Effect (Guzman and Tudhope, 1998; Pereira et al., 2018), and Ba/Ca for upwelling and oil production pollution (Reuer et al., 2003; Weerabaddana et al., 2021). Studies examining *S. siderea* growth have found a reduction in coral skeletal density in the 20th century, possibly related to global warming or local impacts in the Florida Keys (Kuffner et al., 2013; 2015; Rippe et al., 2018).

Supplemental materials and methods

Field collection of core, sampling, and core imagery

The core was transported back to Texas A&M University in 2005. The core was slabbed with a lapidary saw into ~8 mm thick slabs along the principal growth axis of extending corallites to clearly image the internal density bands and for microsampling the slab for geochemical analyses. The optimal microsampling path for this coral species is along the synapticulothecal walls that should run parallel to the slab surface when correctly slabbed (DeLong et al., 2016). Core 05WFGB3 was cut into quarter sections in 2015 (Supplemental Figure 1). The top core slab (05WFGB3-1A) was transported to the PAST Laboratory at Louisiana State University (LSU) in April 2015 by Amy Wagner and the remaining core slabs (A) and quarter sections 2 and 3 to LSU in 2021. The other core half (H2) remains at Texas A&M University with Niall Slowey. Cores are named by the two-digit year they were collected (05), the 4-letter site abbreviation (WFGB), and the number it was assigned during collection, usually the order of collection, (3) for the core name 05WFGB3. Each core section is given a number (05WFGB3-1 to 05WFB3-5). A letter was added for each core section for clarity since coral slabs tend to break with handling and microsampling followed by a number if the core section broke again (05WFGB3-1-A1 and 05WFGB3-1-A2). Additional slabs were cut and labeled as core slabs as Slab 1, Slab 2, etc. (05WFGB3-1A1-Slab2) for cutting annual samples

for this study. In the LSU PAST laboratory, the slabs were cleaned with a Branson 400 sonifier digital ultrasonic cell disruptor using deionized water to remove organic matter, dust, and saw cuttings.

Digital X-radiographs of the coral slabs and quarter sections (Supplemental Figures 1–4) were made at the LSU Forensic Anthropology and Computer Enhancement Services Laboratory with an exposure of 48 kV for 0.4 seconds with a lead scale bar and density step wedge (giant clam) and then processed by an Agfa DX-D 40G digital processor that provides 7086 pixels m^{-1} DICOM images at true size (or 0.0014 mm $pixel^{-1}$). Coral slabs were scanned before and after sampling on an Epson Expression 10000 XL high-resolution scanner at 47,244 pixel m^{-1} and then merged with X-radiographs in Adobe Photoshop (Supplemental Figure 2).

Annual coral samples were removed from coral slabs (slabs C and D) using X-radiographs to aid in cutting for each year starting in winter (assuming January) to the next year. Annual coral samples were cut using a Dremel 200 handheld tool with a 0.635-mm thick Dremel wheel blade (No. 409). For consecutive sample years (e.g., 1967–1950), each year was cut as precisely as possible following the X-radiograph. It is important to acknowledge the sample loss from the 0.635-mm blade estimates as ~1 to 2 months per cut or ~2 to 4 months for consecutive samples. For sample years that were not consecutive (e.g., 1990, 1980), samples were cut a little larger (~1 to 1.2 years) to account for loss due to cutting. After cutting, coral pieces were cleaned for ~30 minutes in a sonicator in deionized water to remove cuttings and then dried at 50ºC for ~30 minutes. The mass for each coral sample was recorded and provided to each laboratory.

An automated triaxial micromill system (Taig Micromill with SuperCAM software from Supertech and Associates, Phoenix, Arizona) in the PAST Laboratory was used to extract monthly microsamples (0.4 mm sample resolution) from the coral slab surface. The

microsampling path creates a continuous trench on the coral slab surface using a box (0.4 mm × 0.4 mm) milling path to a depth of 1.0 mm and a 1.0 mm diameter dental drill bit extracting >500 μg of coral powder (DeLong et al., 2011; Weerabaddana et al., 2021). Sampling paths were shifted when the path was no longer optimal due to corallites not being parallel to the slab surface or when the synapticulothecal wall structure was discontinuous or to avoid the columella (DeLong et al., 2016). New paths overlap by at least by one year with the previous path. Months with more than one measurement were averaged together in building the final time series for each proxy. All time-assigned coral proxies and path sample depth data were compiled in Microsoft Excel.

Calculation of growth rates

Coral 05WFGB3 was cut into multiple slabs for all the analyses presented here (Supplemental Figure 1). The average for the three slabs was used as an estimate of overall coral extension (Figure 2, Supplemental Figure 6, Supplemental Table 3). The first year, 2005, is incomplete since the coral was collected in May 2005 and is excluded.

Anthropocene proxies

Radiocarbon – Annual coral samples were sent to ETH Zurich Laboratory of Ion Beam Physics for radiocarbon measurement. Coral samples (8–13 mg equivalent of ~1 mg carbon) were placed in 12 ml vials, flashed with helium and dissolved in 1 ml of concentrated phosphoric acid (85% H_3PO_4) using the Carbonate Handling system. The released CO_2 was transferred to a graphitization system, mixed with H_2, and heated to 580ºC, in the presence of Fe catalyst, for a reduction to C (Wacker et al., 2013). The mixed powder of graphite and Fe was then pressed into an Al cathode for the Accelerator Mass Spectrometer analysis of the carbon isotopes (^{12}C, ^{13}C, and ^{14}C) using the MICADAS system at the ETH facility (Synal et al., 2007). Samples of corals

were measured along with standards of known ^{14}C activity (HOx2) and blank samples made of marble (C-1, IAEA). The measured $^{14}C/^{12}C$ were normalized to the standard corrected for $\delta^{13}C$ and the background. The reported conventional units of $F^{14}C$ (fraction modern) were used to calculate the $\Delta^{14}C$ (Reimer, 2004; Stuiver and Polach, 1977).

Radiogenic isotopes – Pu-239+240 – $^{239+240}Pu$ was determined by alpha spectrometry at the University of Southampton GAU-Radioanalytical Laboratories, following sample dissolution with HCl, HF and HNO_3, radiochemical separation, and preparation of sources using electrodeposition from diluted HCl/oxalate solution. Prepared sources were counted using Alpha Octete spectrometers with PIPS detectors and spectra analyzed using Maestro 32 software. Samples were transferred into PTFE beakers, dissolved in 6M HCl, and spiked with Pu^{242} recovery tracer before evaporation to dryness. Residues were dissolved using concentrated HF solution (2x10 ml) and evaporated to dryness. Residues were re-dissolved in nitric acid and again evaporated to dryness (3x20 ml). Residues after nitric acid treatment were re-dissolved in 40 ml concentrated HCl and allowed to boil under cover for ~2 hours. After this ~2 g of boric acid was added and the samples were boiled again until complete boric acid dissolution (~2 hours).

Solutions were evaporated to dryness, re-dissolved in 30 ml 1M HNO_3 and boiled again under cover until a completely clear solution was obtained. 10 mg of Fe carrier was added and Pu was co-precipitated with $Fe(OH)_3$ using a concentrated ammonia solution. The obtained precipitates were dissolved in HCl and acid molarity was adjusted to 9M. Samples were then loaded onto anion exchange columns (1x5 cm), previously conditioned with 9M HCl. After the load solution had passed the columns, columns were washed with a further 30 ml of 9M HCl followed by 50 ml of 8M HNO_3 and again 10 ml of 9M HCl. Finally, Pu was eluted from the columns using 9M HCl/NH_4I solution into clean beakers.

Solutions were evaporated to dryness with 5 ml concentrated HNO_3 added to remove excess iodide. Finally, thin alpha-spectrometric sources were prepared using electrodeposition from diluted HCl/oxalate solution. The prepared sources were counted using Alpha Octete spectrometers with PIPS detectors and spectra analyzed using Maestro 32 software.

The alpha spectrometry method gives a total activity for the most abundant plutonium isotopes ^{239}Pu and ^{240}Pu ($^{239+240}$Pu), as these two isotopes cannot be distinguished using alpha spectrometry. ^{238}Pu was too low to be reliably measured. Annual samples were prepared using acid digestion with PIPs detectors. Extended count times (>1 week) were used to detect the low activities of $^{239+240}$Pu present in the coral samples. A second coral from Haiti (10LEO1) was also measured for $^{239+240}$Pu (Ouellette, 2017). This second coral was also screened via mass spectrometric methods, using a Thermo Scientific Neptune Plus MC-ICP-MS, after radiochemical re-purification of the Pu alpha spectrometry discs following Lokas et al. (2022) but measured activities (and isotopic ratios) were all close to or below instrument background.

Other radiogenic isotopes – Lead-210 (half-life is 22.3 years) is a naturally-produced radionuclide, derived from atmospheric fallout (termed unsupported ^{210}Pb). Cesium-137 (half-life is 30 years) and ^{241}Am are artificially produced radionuclides introduced by atmospheric fallout from thermonuclear weapons testing and nuclear reactor accidents. They have been extensively used in the dating of recent geological materials. Annual coral samples from core 05WFGB3-1 were analyzed for ^{210}Pb, ^{226}Ra, ^{137}Cs, and ^{241}Am by direct gamma assay in the Environmental Radiometric Facility at University College London using an ORTEC HPGe GWL series well-type coaxial low background intrinsic germanium detector. Lead-210 was determined via its gamma emissions at 46.5 keV, and ^{226}Ra by the 295 keV and 352 keV gamma rays emitted by its daughter isotope ^{214}Pb following three weeks of storage in sealed containers to

allow radioactive equilibration. Cesium-137 and ^{241}Am were measured by their emissions at 662 kev and 59.5 kev (Appleby et al., 1986). The absolute efficiencies of the detector were determined using calibrated sources and sediment samples of known activity. Corrections were made for the effect of self-absorption of low-energy gamma rays within the sample (Appleby et al., 1992).

Spheroidal carbonaceous fly-ash particles (SCPs) – The SCP extraction method developed for lake sediments (Rose, 1994) was adapted for coral material. Each annual coral sample was accurately weighed and then soaked in H_2O_2 overnight. Samples were centrifuged at 1500 rpm for 5 minutes and the supernatant was removed. This step was then repeated with distilled water. Samples were then subjected to sequential chemical attack by nitric, hydrofluoric, and hydrochloric acids to remove unwanted fractions of organic, siliceous, and carbonate and bicarbonates respectively. For each stage, acid was slowly added to prevent the loss of sample and then heated in a water bath at 80ºC for 2 hours. After each step, sample tubes were topped up with distilled water, centrifuged at 1500 rpm for 5 minutes and the supernatant pipetted off carefully to not disturb the sample pellet. The final HCl step was repeated until any precipitate formed in the HF stage had dissolved. The samples were then washed twice with distilled water and centrifuged as before. The sample residue was then transferred into labeled and weighed vials. A known fraction of this final suspension was evaporated onto a coverslip and mounted onto a microscope slide. The slides were scanned for SCPs on the coverslip using a light microscope at x400 magnification. The criteria for SCP identification under the light microscope followed Rose (2008). Analytical blanks were included and no SCPs were observed in these.

Stable isotopes ($\delta^{18}O$ and $\delta^{13}C$) – Aliquots of the monthly coral samples were analyzed at Texas A&M University in the Stable Isotope Geosciences Facility on a Thermo Scientific MAT 253

equipped with a Kiel IV device. Coral samples were dissolved in phosphoric acid at 70ºC. Undersized (<1700 mV) samples that still achieve $\delta^{18}O$ uncertainty of ±0.08‰ (1σ) were quality controlled or rerun. Overall analytical precision is ±0.06‰ (1σ) for $\delta^{18}O$ and ±0.04‰ (1σ) for $\delta^{13}C$ based on long-term replicate analyses of carbonate standards NBS-19 and IAEA-603 (6 samples day^{-1}). Isotopic values are reported in delta notation relative to Vienna PeeDee Belemnite (VPDB) isotopic standard. Monthly samples were analyzed for 1933–2005. For 1825–1932, the samples that were the seasonal maximum and minimum values in coral Sr/Ca were analyzed for isotopes since the seasonal cycles for Sr/Ca and $\delta^{18}O$ are in sync.

Trace elemental analysis (Ca, Sr, Mg, Li, U, and Ba) – Aliquots of the monthly coral samples were analyzed in the LSU PAST Laboratory using a PerkinElmer 8300 inductively coupled plasma optical emission spectrometer (ICP-OES) as described in Weerabaddana et al. (2021). Instrumental drift was corrected using the method of Schrag (1999) with an internal gravimetric standard (IGS) prepared by mixing ultrapure solution standards (Ca, Sr, Mg, and Ba) in proportion to mimic a coral. A laboratory standard (PL) of homogenized coral powder (*Porites lutea)* was dissolved in bulk and analyzed after every fifth sample. Highly accurate and precise values for Sr/Ca, Mg/Ca, and Ba/Ca for PL and IGS were determined by MC-ICP-MS in the HISPEC Laboratory at National Taiwan University (Lo et al., 2014). The international coral reference for trace elemental analysis JCp-1 (Hathorne et al., 2013; Okai et al., 2002) was analyzed once or twice per run. Analytical precision for trace elemental ratios are given in Supplemental Table 1.

Trace elemental analysis (Ca, Sr, Mg, Ba, Li, and U) – Analyses were performed in the LSU Department of Geology and Geophysics using a Thermo iCap Qc inductively coupled plasma mass spectrometer (ICP-MS) with the same sample preparation as the inductively coupled

plasma optical emission spectrometer (ICP-OES). The ICP-MS system was coupled to an ESI SC-DX2 autosampler equipped with a fast valve with SampleSense. Sample uptake and introduction were optimized to be less than 2 ml while providing a strong signal for all analytes. Isotopes of individual elements analyzed included ^{7}Li, ^{25}Mg, ^{26}Mg, ^{43}Ca, ^{84}Sr, ^{86}Sr, ^{87}Sr, ^{137}Ba, and ^{238}U. Signal strength was recorded in transient mode using Thermo Qtegra software (tQuant mode) during the analysis and data were reduced and quantified offline. WaveMetrics IgorPro v6.37 with Iolite v2.5 software was used for the initial data processing (Paton et al., 2011). Elemental concentrations were normalized by standard bracketing (Schrag, 1999) using an external gravimetric standard (IGS) as the bracketing standard similar to the ICP-OES method. The signal strength of ^{43}Ca of each analysis was used as the internal standard to normalize all elemental signal strengths to a stoichiometric Ca value of 38.5wt% of a coral. The external coral standard PL was analyzed after every fifth sample. JCp-1 was analyzed as a sample for an additional matrix-match reference at the beginning and end of each run. Analytical precisions are given in Supplemental Table 1.

Coral skeletal stable nitrogen isotopes (CS-$\delta^{15}N$) – Coral skeletal stable nitrogen isotopes were measured using the "denitrifier" method (Sigman et al., 2001) with the methodological updates (Wang et al., 2016; Weigand et al., 2016) at the Max-Planck-Institut for Chemistry (Mainz, Germany). Annual coral pieces were ground using an agate mortar and pestle and sieved to retain the fraction between 63 µm and 250 µm. Aliquots of 9 mg of coral powder were weighed into 4 ml borosilicate vials and cleaned for 24 hours with 13% reagent grade NaClO. The coral powder was then rinsed with deionized water four times and dried overnight at 60ºC. The next steps took place in a clean laboratory to avoid contamination. Aliquots of 8 mg of cleaned coral powder were weighted into combusted 4 ml borosilicate vials. Each coral sample was then dissolved

with 50 µl 4N HCl to remove the $CaCO_3$ matrix and release the skeletal organic matrix. The N-bearing compounds of the organic matrix were then oxidized to NO_3^- by using a buffered solution of peroxodisulfate at 121ºC for 65 minutes. Aliquots of the resulting nitrate solutions were inoculated into *Pseudomonas chlororaphis* cultures to quantitatively convert NO_3^- to N_2O. The N_2O derived from the coral samples was sent to a purpose-built inlet system, "the Sigbench" coupled to a Thermo Scientific MAT253 Plus isotope ratio mass spectrometer for CS-$\delta^{15}N$ analysis. Normalization to ‰ Air was made using international nitrate standards USGS34 and IAEA-NO_3. International amino-acid standards USGS40 and USGS65 were used alongside in-house coral standards (Leichliter et al., 2021) to ensure full conversion of the samples and to rule out any contamination during the analytical process. Analytical error (1σ) on the coral standard is typically <0.2‰ Air.

Inorganic geochemical signals (Mercury) – Coral samples (~1 year per sample) were analyzed for mercury concentration in the Environmental Change Research Centre at the University College London. Samples were digested with 7 ml Aqua Regia at 100ºC on a hotplate for 2 hours in rigorously acid-leached 50 ml polypropylene digestion tubes. Four standard reference materials of stream sediment GBW07305 (certified Hg value is 100 ng g^{-1}; our measured mean value is 101.6 ng g^{-1} ±2.3 ng g^{-1} (1σ; n=4) and six sample blanks were digested with the samples. Digested solutions were analyzed for Hg using cold vapor-atomic fluorescence spectrometry (CV-AFS; PSA 10.035 Millennium Merlin 163 Mercury Analyzer) following reduction with $SnCl_2$. Standard solutions and quality control blanks were measured in every five samples to monitor measurement stability. As most coral samples used for the digestion were 0.5 g or slightly more with coral Hg concentrations <1.4 ng g^{-1}, we assumed that 0.5 g dry weights for each sample representing the used reagents (7 ml) were used for the blank digestions. The

reagent blanks mean Hg concentration is 0.53 ng l^{-1} ±0.13 ng g^{-1} (1σ; n=6) and we use this blank standard deviation for reporting analytical precision. The detection limit is 4.32 ng l^{-1} for regent blank measurements.

Supplemental results

Chronology

The entire coral core 05WFGB3 spans 1755–2005 CE as determined by counting annual density bands in the X-radiographs and annual cycles in coral Sr/Ca as well as verified with two ^{230}Th dates (Supplemental Figure 5). There is no evidence of a growth hiatus in the core 05WFGB3 (Figure 2, Supplemental Figures 2–5). However, coring requires breaking the coral core inside the colony once the core barrel is full, therefore, the core 05WFGB3 is in five sections. There is a possibility to have missing material in core breaks due to abrasion during coring. The break between core sections 05WFGB3-1 and 05WFGB3-2 is minimal (Supplemental Figures 3–4); however, a small gap appears between the slabs from these sections (Supplemental Figure 5). We found by matching up core halves there is little missing core in this break. Additionally, we found for the quarter sections there is a slight rotation of the orientation of first core half cuts for these core sections so that the alignment is not tight between the core slabs. However, the density banding patterns are easily matched between these core sections. We confirm the age for core section 05WFGB3-2 with ^{230}Th dating with a sample that spans years 1921–1925 (Supplemental Figure 5), or an average of 1923 that resulted in a ^{230}Th date of 1921.9 ±2.4 (2σ) or a 95% confidence interval of 1919.5–1924.3 (Supplemental Table 2). If one year is missing between 05WFGB3-1 and 05WFGB3-2, the ^{230}Th sample would be years 1920–1924 or an average of 1922, which is also within the ^{30}Th dating confidence interval. Therefore, we assume there is no missing year between core sections 05WFGB3-1 and 05WFGB3-2, but it is

possible 1–3 months could be missing. For core sections 05WFGB3-2 and 05WFGB3-3 (Supplemental Figure 5), the coral's growth direction in the slab is slightly off the vertical and the paths are overlapping, which allows for the assessment of missing years between these core sections (DeLong et al., 2016; DeLong et al., 2013). These sections of the core are continuous and there are no missing years.

There is a break between core sections 05WFGB3-3 and 05WFGB3-4 where the core sections are also slightly rotated and the overlapping paths appear to be three years (Supplemental Figure 5). The remaining older core sections (05WFGB3-4 and 05WFGB3-5) contain overlapping years and we find no evidence of missing years in those sections. The sample dated from the bottom of the core spans five years (1762–1768) or an of 1765 (Supplemental Figure 5). The ^{230}Th date is 1756.7 ±2.7 (2σ) or a confidence interval of 1754.0–1759.4 (Supplemental Table 2); these dates differ by ~8.3 years. This would mean ~3.3 cm of coral missing from the break between core sections 05WFGB3-3 and 05WFGB3-4. Examination of the X-radiographs of the core halves show a clear connection between core sections with some evidence of grinding (Supplemental Figures 3–4) but we do not believe 3.3 cm of the core is missing. Removing the overlap in coral Sr/Ca between these sections would shift all the dates below the top of 05WFGB3-4 by three years and give a bottom date of 1752 and the ^{230}Th sample the years 1759–1765 (average 1762), which is closer to the ^{230}Th date by 5.3 years. ^{230}Th dating with a coral sample representing a single year could help improve the accuracy for ^{230}Th dating. We acknowledge the accuracy of years before 1821 CE could be 0 to 8.3 years.

Radioisotopes (and guidance for other proxies)

Other artificial fallout radionuclides – No ^{137}Cs and ^{241}Am were detected in the core 05WFGB3 samples (Supplemental Table 4). This may be due to the coral sample size not being large

enough or that these radioisotopes were not taken up by this coral living in deeper water. A literature search on Web of Science and Google found no studies measuring ^{137}Cs and ^{241}Am in coral skeletons, but they have been found in coral soils in Bikini and the Marshall Islands (Robison et al., 2000).

Novel materials

Fly-ash (SCPs) – No SCPs were found in the 33 coral samples from core 05WFGB3 (Supplemental Figure 9, Supplemental Table 5). The lack of SCPs in this coral may be due to its water depth (21.3 m), which is a deeper coral reef, and/or the coral's location in an open ocean location over 180 km from the nearest coastline and fossil fuel combustion sources. Furthermore, this does not mean corals do not ingest SCPs but the SCPs were not incorporated into the coral skeleton at least in the sample amounts investigated here. Corals actively transport ions to the calcifying fluid and thus may exclude SCPs at the calcification site. Corals are different from marine sediment records since coral skeletal material is biologically-mediated aragonite deposition. Other studies have found that coral skeletal material can contain dark bands from sedimentation events (Prouty et al., 2014) and thus a coral closer to a point source for SCPs may incorporate these particles in their skeletons. Wind direction may also play a role in SCP reaching FGB since the dominate wind direction is onshore.

Organic matter proxies

Coral skeleton nitrogen isotopes – Natural and Anthropogenic isotopic end-members in the Gulf of Mexico (GoM): Identifying the possible isotopic end-members in the system is thus key to interpret the CS-δ^{15}N record. In the GoM, the main source of nitrate is located in the thermocline (100–200 m) and is composed of the SubTropical Underwater (STUW) that is characterized by a nitrate concentration ([NO_3]) of 2.2 ±2.1 µM and a δ^{15}N-NO_3 of 3.5 ±1.1‰ (Howe et al., 2020).

The thermocline nitrate originates from the deeper, nutrient-rich Antarctic Intermediate Water (AAIW; $[NO_3]$=29.9 ±1.2µM; $\delta^{15}N\text{-}NO_3$=5.4 ±0.1‰). The low $\delta^{15}N\text{-}NO_3$ of the STUW results from the supply of remineralized organic matter deriving from N-fixation. Fixed-N is typically assumed to be close to -1‰ (Montoya et al., 2002; Sigman et al., 2009), causing the $\delta^{15}N\text{-}NO_3$ of the STUW to be lower than the AAIW. The second most important source of nitrogen to the GoM is the Mississippi and Atchafalaya River System (MARS) with an annual flux of $6.8.10^{13}$ mmol N m^{-2} y^{-1} characterized by $[NO_3]$ >10 µM and $\delta^{15}N\text{-}NO_3$ between 6 to 8‰ (Goolsby and Battaglin, 2001).

The mechanisms at play behind the increased nutrient loading in the MARS after 1960 could involve various, non-exclusive, processes such as an increase in the nitrogen fertilizer consumption (David et al., 2010), but also a change in the Mississippi River discharge rates. The Mississippi River discharge rate has increased after 1958 and is not explained by precipitation and climate change alone (Raymond et al., 2008; Schilling et al., 2010). Anthropogenic activities, mainly land-use change as a result of rapidly expanding agricultural practices in the Mississippi River Basin, have increased baseflow of the river due to shifts in perennial vegetation to seasonal crop cultivation (Zhang and Schilling, 2006). A notable increase in river discharge after the 1950 is associated with rapid increase (343%) in soybean and maize cultivation in the upper Mississippi River Basin (Donner, 2003). The increase in nitrogen-based fertilizer use with increasing crop cultivations coupled with river discharge during this same time interval have likely resulted in increased nitrogen content in the GoM.

The influence of anoxic water masses located along the northern coastline of the GoM, the “dead zone” (Rabalais et al., 2002) (Figure 1a), to the WFGB reef remains unclear. Indeed, this water mass is located in between the shoreline and the WFGB reef (~300 km; Figure 1a),

possibly altering the isotopic composition of the MARS-N as the nitrogen is transferred along the land-sea continuum. Anoxic water is typically associated with increased denitrification (Sigman and Fripiat, 2019) that could significantly alter the isotopic ratio of the oceanic N-pool. Whereas water-column denitrification is associated with strong isotopic effect (ε = 15–25‰), leading to a significant enrichment of the nitrate pool with ^{15}N, benthic denitrification has almost no isotopic effect, leaving the isotopic signature of the source-N unchanged. The 80-yearlong CS-$\delta^{15}N$ record does not contain values above 6‰, well below the values found in areas experiencing water column denitrification (>10‰), suggesting that benthic denitrification is the main process in the GoM. This agrees with nitrate isotopes (N and O) depth profiles for the GoM that failed to identify ^{15}N-enriched-NO_3 in the surface waters close to the MARS (Howe et al., 2020). As such, the 05WFGB3 CS-$\delta^{15}N$ record is possibly a direct record of the MARS-N and $\delta^{15}N$ discharge with time. We will explore the coral $\delta^{15}N$ record in more detail in a forthcoming paper.

Inorganic geochemical signals

Lead-210 activity – Total ^{210}Pb activities, supported ^{210}Pb activities, and unsupported ^{210}Pb activities, calculated by subtracting ^{226}Ra activity (as supported ^{210}Pb) from total ^{210}Pb activity, in coral core 05WFG3 are given in Supplemental Table 5. Unsupported ^{210}Pb activities are negative, suggesting disequilibrium between ^{226}Ra and supported ^{210}Pb in the coral samples. The oceanic flux of ^{222}Ra is only about 1% of the continental flux (Imboden and Stiller, 1982), suggesting most ^{222}Ra escaped from the seabed was captured by the seawater, and coral grows in the seawater above the seabed. These may cause radioactive disequilibrium in these coral samples. The study of Benninger and Dodge (Benninger and Dodge, 1986) also reported difficulties with the interpretation of ^{210}Pb due to not measuring ^{226}Ra. The low total ^{210}Pb activities from the core top and the disequilibrium give ^{210}Pb dating high uncertainties. Because

of the low ^{210}Pb activity, most of the samples were counted for 400 k to 500 k seconds for the coral samples, whereas "normal" sediment samples only need to be counted for about 80 k seconds. Lead-210 and $^{206/207}$Pb have been successfully measured in Atlantic corals (Dodge and Thomson, 1974; Kelly et al., 2009; Shen and Boyle, 1988) and these corals track the usage of gasoline with lead additives (Shen and Boyle, 1987). Deep-sea corals and sclerosponges have been dated using ^{210}Pb (Benavides and Druffel, 1986; Lazareth et al., 2000; Robinson et al., 2014; Rosenheim et al., 2005; Williams et al., 2007) with one study reporting sclerosponges incorporate more ^{210}Pb than corals.

Supplemental Figures

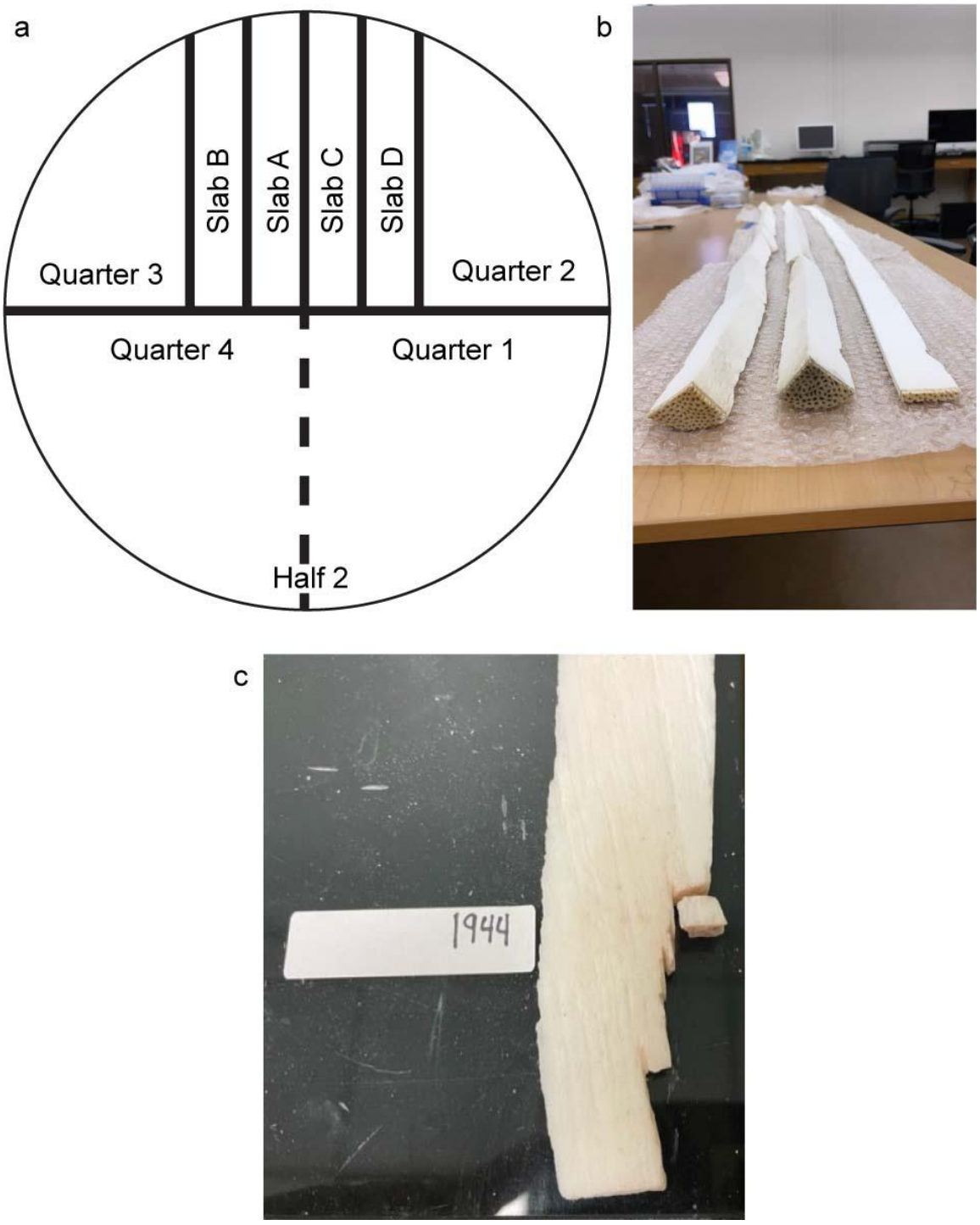

Supplemental Figure 1. Schematic of how the core 05WFGB3 was cut and slabbed for this study. (a) Core diagram is drawn to scale (1:1) and cut lines represent thickness of the saw blade (1.6 mm) and each slab is ~ 8 mm thick. (b) Photos of core Quarter Sections 2 and 3 and Slab C and (c) photo of cutting Slab D for annual sample for the year 1944.

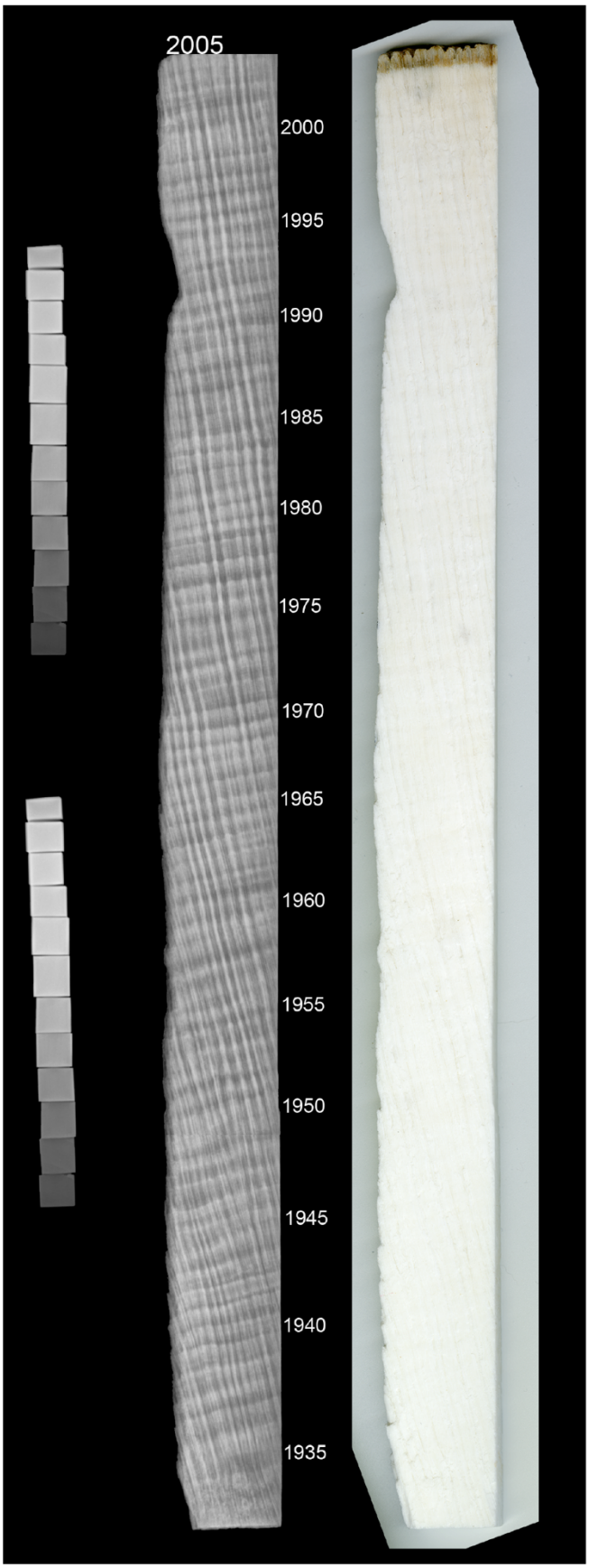

Supplemental Figure 2. Coral core 05WFGB3-1A1 Slab C compiled X-radiograph negatives and coral scan for 1932–2005. Every five years are noted from the core top collection year 2005. Annual samples (Table 1) were cut from each band on the right side of this image. Images are reduced 50% from true size.

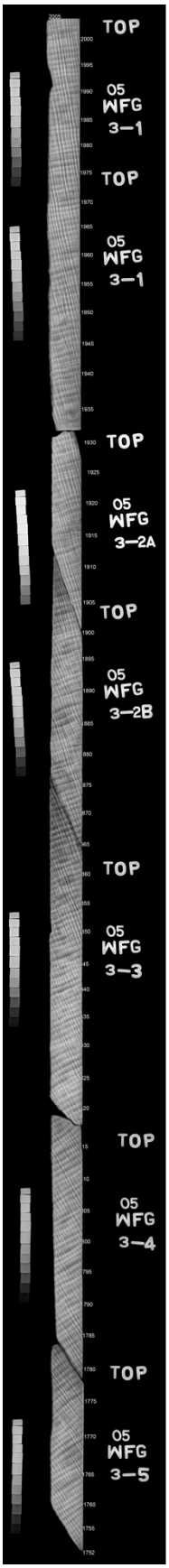

Supplemental Figure 3. Coral core 05WFGB3 Slab C compiled X-radiographs negatives.

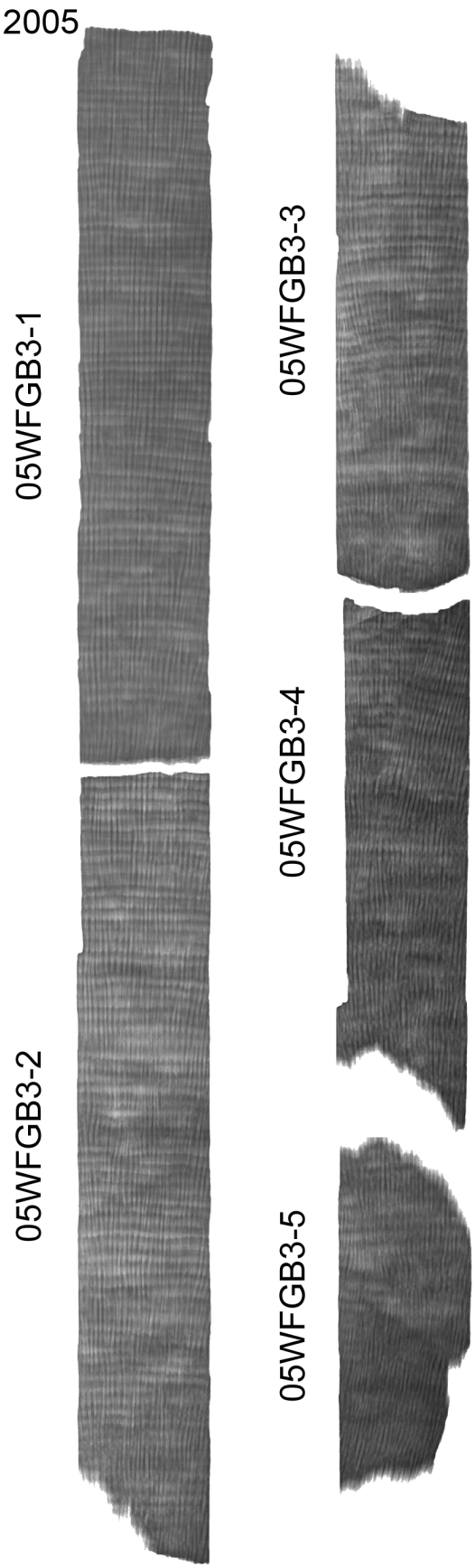

Supplemental Figure 4. Coral core 05WFGB3 halves compiled X-radiographs negatives.

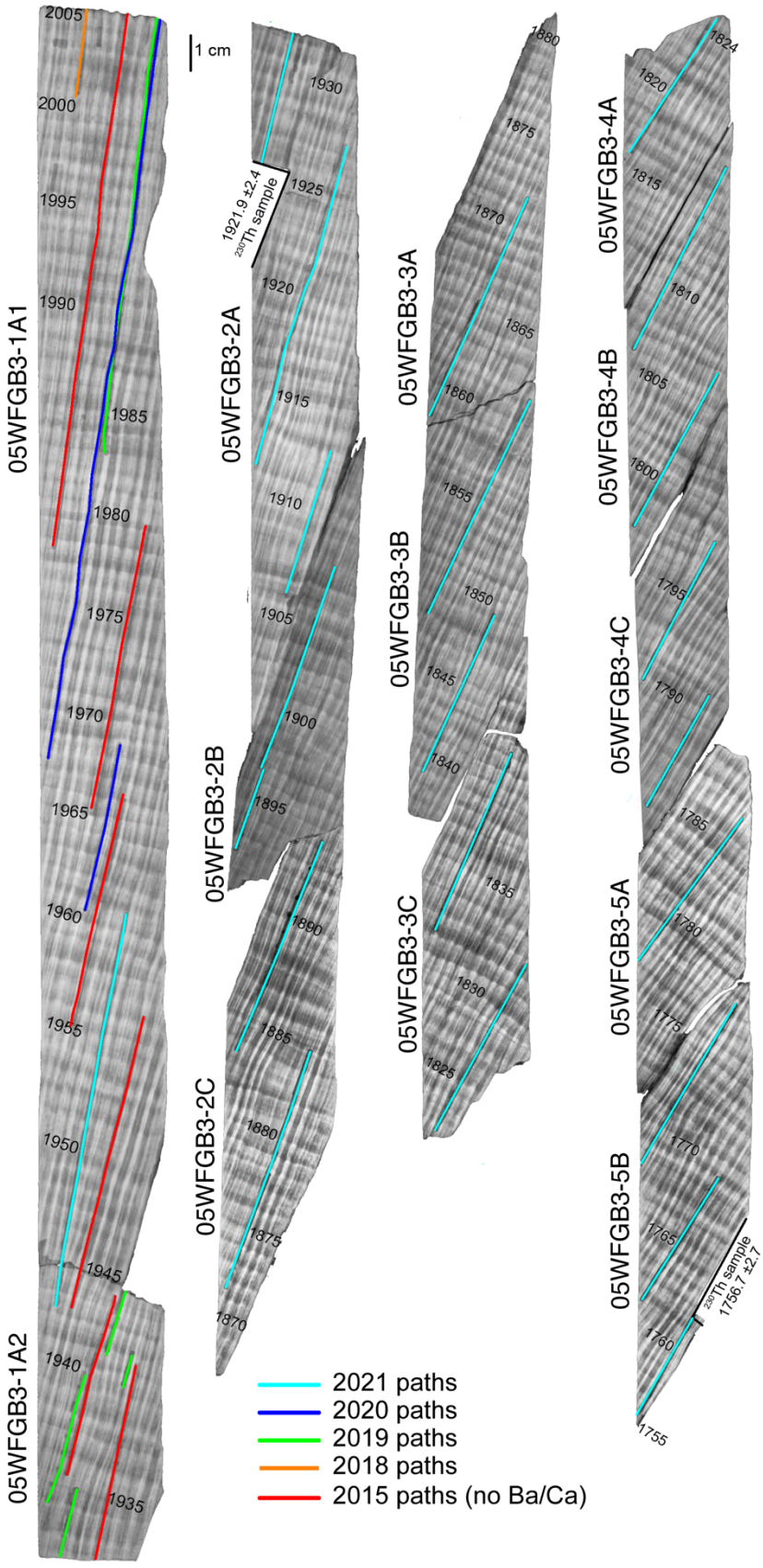

Supplemental Figure 5. X-radiograph negatives of core 05WFGB3 Slab A with years, sampling paths, core section names, and ^{230}Th dating samples noted. Core top is to the upper left and bottom to the lower right.

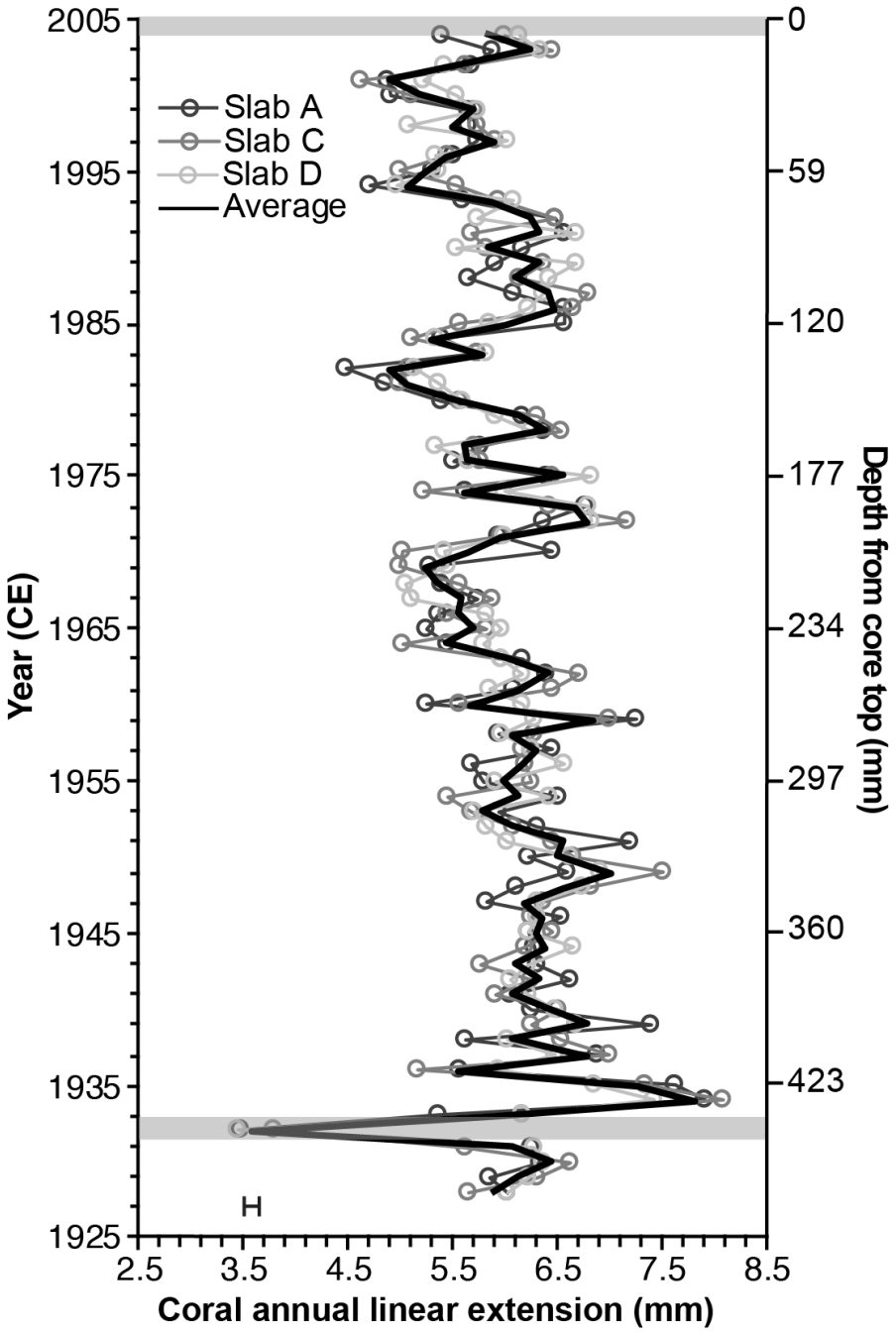

Supplemental Figure 6. Coral annual growth for core 05WFGB3 measured from X-radiographs. Depth is given as the distance from the core top to January for each year for each slab and this varies between slabs (depth from core top for slab C is shown). The depth measurements follow coral growth structures visible in X-radiographs and it is not a vertical measurement from the top of the core. The shaded areas in 2005 (when the core was collected in May 2005) and 1932 (break in core) are incomplete years. Error bar is standard error of the mean ±0.17 mm (1σ). Years are assessed to be accurate.

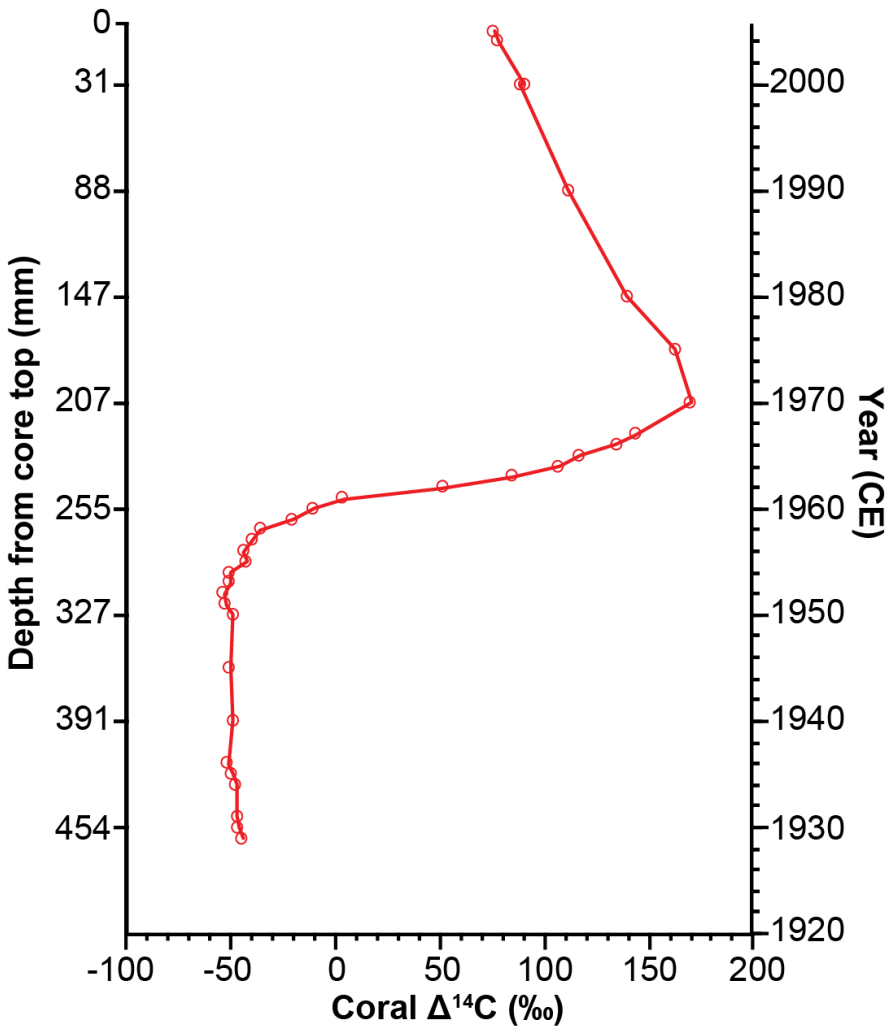

Supplemental Figure 7. Coral core 05WFGB3 $\Delta^{14}C$ results. $\Delta^{14}C$ determined as $F^{14}C*e^{((1950-year)/8267)}-1)*1000$ (Reimer, 2004). Depth is determined from top of core to each base of annual density band (~January) for the year of each ^{14}C coral sample. Dating and $\Delta^{14}C$ uncertainties (2–3‰) are about the size of the hollow circle (Table 1).

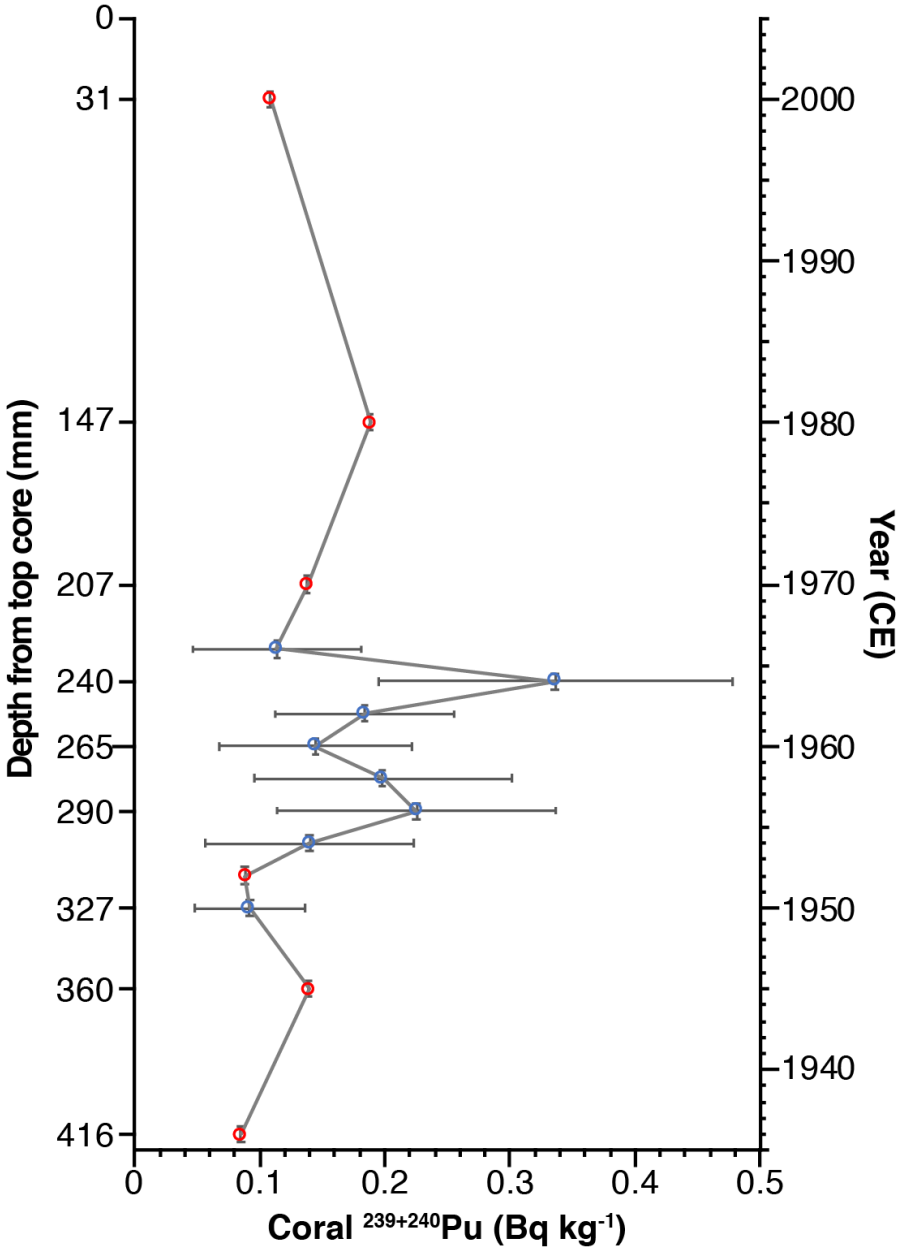

Supplemental Figure 8. Coral core 05WFGB3 $^{239+240}$Pu results. Data points marked as red indicate the limit of detection values (sample activity is less than this value) rather than actual measured activity. Depth is determined from top of core to each base of annual density band (~January) for the year of each Pu coral sample. Horizontal error bars are ±k=2, and vertical error bars are ±0.1–0.2 years for the estimated coral annual sample uncertainty (Table 1).

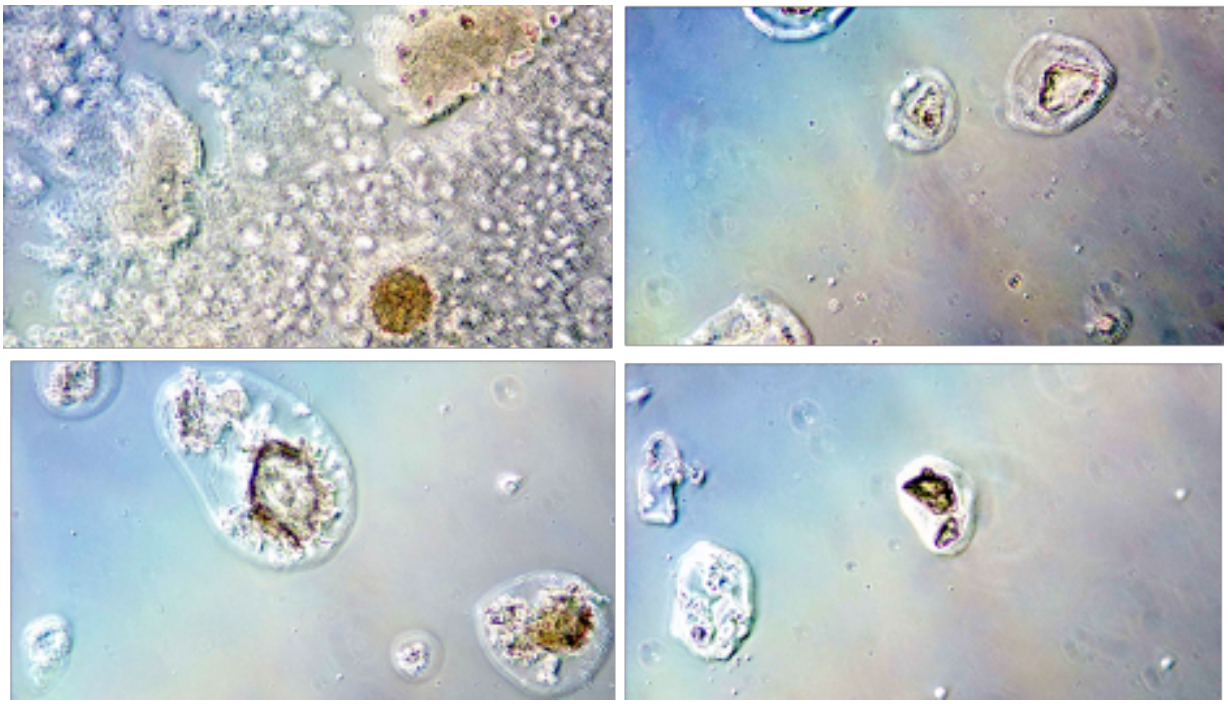

Supplemental Figure 9. A selection of light microscope images of samples analyzed for SCPs from the coral core 05WFGB3. Top row is samples from 2005 and 2000 and bottom row is samples from 1966 and 1957. No SCPs were found in the 33 coral samples examined (Supplemental Table 5).

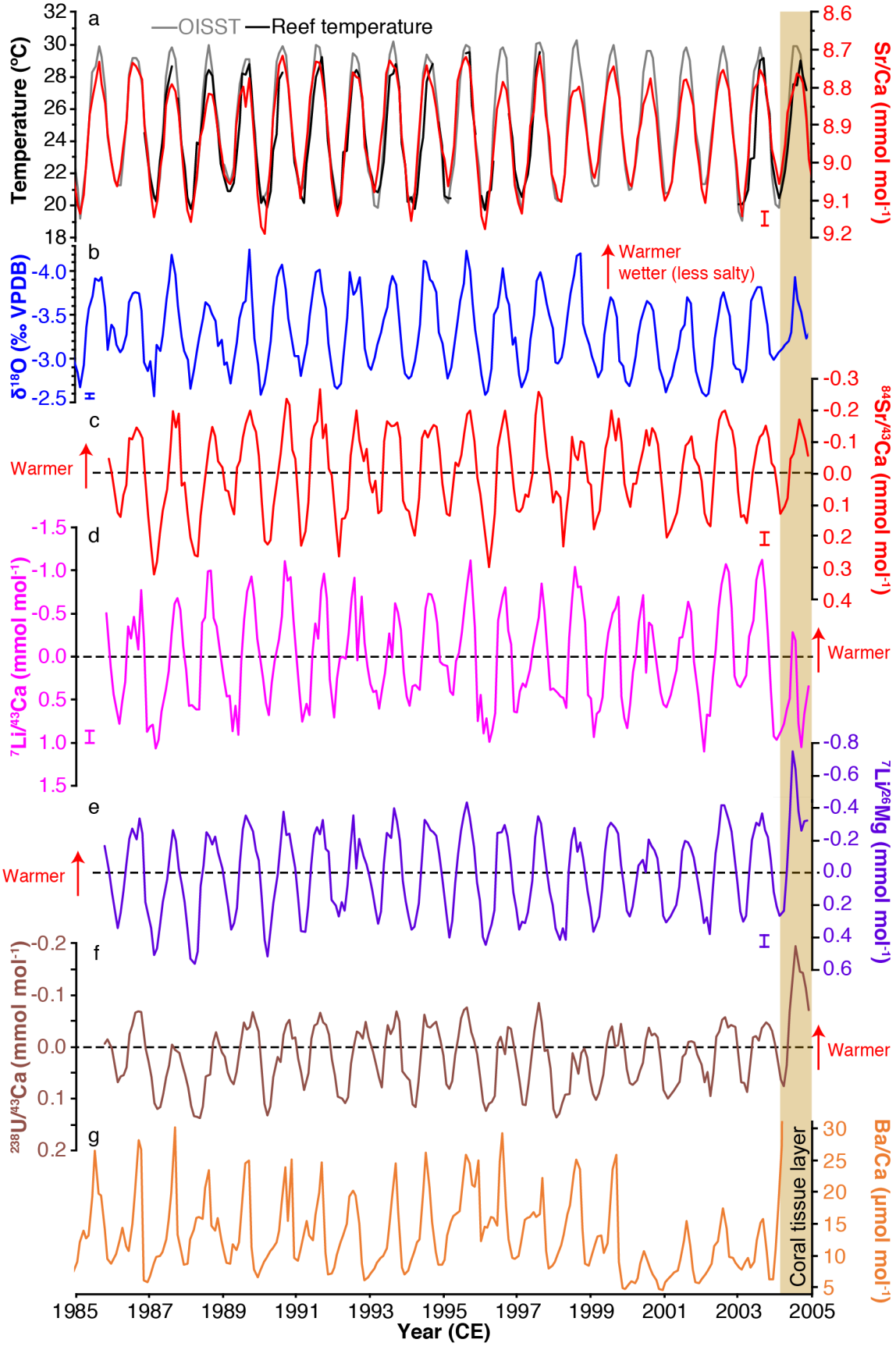
a
—OISST —Reef temperature
Temperature (°C)
Sr/Ca (mmol mol-1)
b
Warmer
wetter (less salty)
δ18O (‰ VPDB)
c
Warmer
84Sr/43Ca (mmol mol-1)
d
7Li/43Ca (mmol mol-1)
Warmer
e
Warmer
7Li/26Mg (mmol mol-1)
f
Warmer
238U/43Ca (mmol mol-1)
g
Coral tissue layer
Ba/Ca (µmol mol-1)
1985
1987
1989
1991
1993
1995
1997
1999
2001
2003
2005
Year (CE)

Supplemental Figure 10. Assessment of monthly coral trace metal ratios and $\delta^{18}O$ as temperature proxies for core 05WFGB3. (a) Coral Sr/Ca analyzed using ICP-OES is shown with OISSTv2 for the 1º grid centered on 27.5ºN, 93.5ºW (Reynolds et al., 2002) and WFGB reef temperature (Johnston et al., 2021). (b) Coral $\delta^{18}O$ analyzed using isotope ratio mass spectrometer. (c-f) Trace elemental ratios for given isotopes were analyzed using ICP-MS shown here with means removed for comparison. All temperature proxies are scaled to the same temperature range and plotted so that warmer values are up. (g) Monthly coral Ba/Ca determined using ICP-OES. Coral Ba/Ca is not a proxy for temperature and does not significantly correlate with either temperature record but is shown here with other monthly trace elements for comparison. The coral tissue layer is the beige area and has higher coral Li/Mg and Ba/Ca values. Error bars (1σ) are analytical precision determined using the internal coral standard PL (Supplemental Table 1) except for $\delta^{18}O$ (see Methods). Analytical precision is smaller than the line weight and scale bar for U/Ca and Ba/Ca and thus not plotted. Dating uncertainty for monthly samples is ±1–2 months (Table 1).

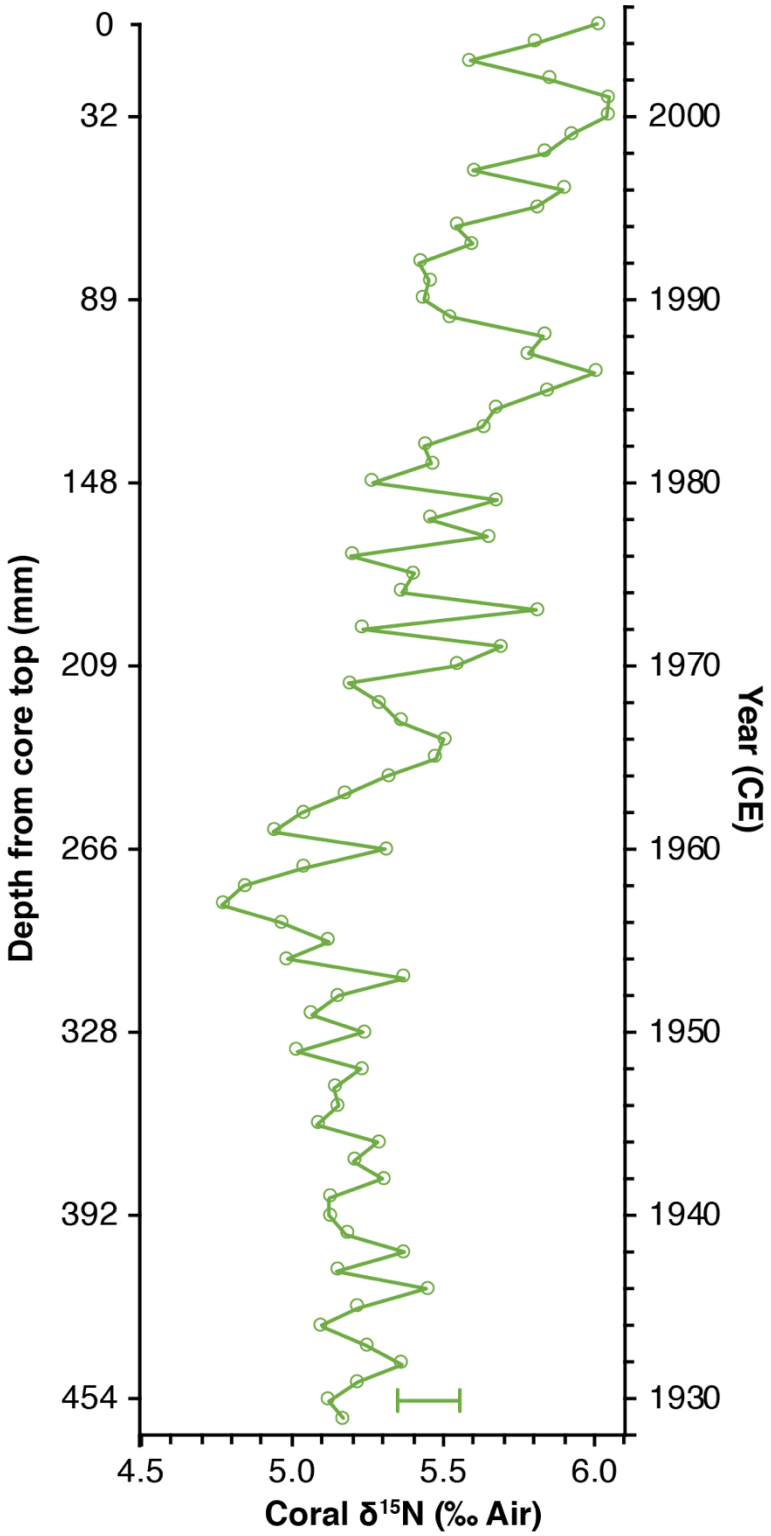

Supplemental Figure 11. Coral skeletal nitrogen isotope ratios for core 05WFGB3. Depth is determined from top of core to each base of annual density band (~January) for the year of each $\delta^{15}N$ coral sample. Each sample represents one year ±0.1–0.2 years (Table 1).Error bar is analytical precision (1σ) for $\delta^{15}N$.

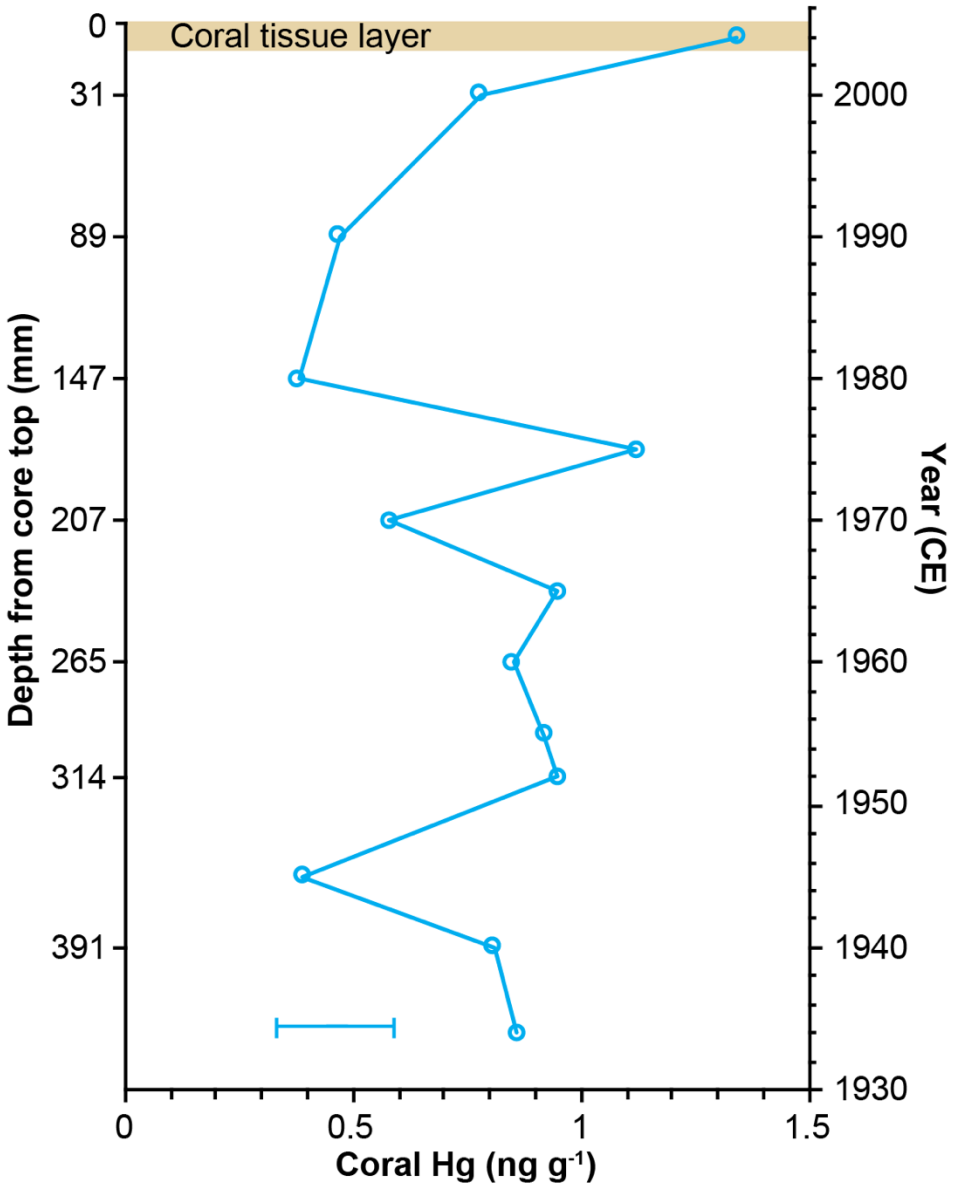

Supplemental Figure 12. Mercury concentration in coral core 05WFGB3. Depth is determined from top of core to each base of annual density band (~January) for the year of each Mg coral sample. Each sample represents one year ~±0.25 years (Table 1). Analytical precision is ±0.13 ng g^{-1} (1σ) determined by repeat reagent blank measurements (n=6).

Supplemental Tables

Supplemental Table 1. Analytical precision and accuracies for trace elemental ratio analyses.

ICP-OES [a]		**Sr/Ca (mmol mol^{-1})**			**Mg/Ca (mmol mol^{-1})**			**Ba/Ca (µmol mol^{-1})**		
Reference	Facility [b]	IGS	PL	JCp-1	IGS	PL	JCp-1	IGS	PL	JCp-1
Precision (1σ)	UMCES-CBL	±0.003	±0.015		±0.026	±0.069				
	USGS	±0.005	±0.011		±0.031	±0.072				
	LSU	±0.017	±0.038	±0.032	±0.048	±0.076	±0.050	±0.19	±0.21	±0.91
# of readings	UMCES-CBL	80	116		80	116				
	USGS	112	156		112	156				
	LSU	769	1279	92	139	246	13	115	221	13
ICP-MS [a]		**^{84}Sr/^{43}Ca (mmol mol^{-1})**			**^{26}Mg/^{43}Ca (mmol mol^{-1})**			**^{238}U/^{43}Ca (µmol mol^{-1})**		
Reference		IGS	PL	JCp-1	IGS	PL	JCp-1	IGS	PL	JCp-1
Precision (1σ)	LSU		±0.041	±0.034		±0.013	±0.007		±0.006	±0.010
# of readings	LSU		69	9		69	9		69	9
ICP-MS [a]		**^{7}Li/^{43}Ca (mmol mol^{-1})**			**^{7}Li/^{26}Mg (mmol mol^{-1})**					
Reference		IGS	PL	JCp-1	IGS	PL	JCp-1			
Precision (1σ)	LSU		±0.14	±0.16		±0.033	±0.041			
# of readings	LSU		69	9		69	9			

[a] ICP-MS labels include isotopes analyzed. Samples run on ICP-MS spans 1987–2005. Samples run on the ICP-OES span 1932–2005 except for Sr/Ca is for 1755–2005.

[b] UMCES-CBL is University of Maryland Center for Environmental Science Chesapeake Biological Laboratory and the samples analyzed span 1973–2005 for the 2015 paths in Supplemental Figure 5 and these data are included in Weerabaddana et al. (2021). USGS is United Stated Geological Survey in St. Petersburg, FL and the samples analyzed span 1932–1973 for 2015 paths in Supplemental Figure 5 and the laboratory method for this laboratory are reported by DeLong et al. (2016).

Supplemental Table 2. Uranium and thorium isotopic compositions and ^{230}Th ages for coral determined by MC-ICP-MS.

Sample ID	Weight (g)	^{238}U (ppb) [a]		^{232}Th (ppt)		δ^{234}U measured [a]		[^{230}Th/^{238}U] activity [c]		[^{230}Th/^{232}Th] (ppm) [d]		Age uncorrected		Age corrected [c,e]		$\delta^{234}U_{initial}$ corrected [b]		Year
WFGB 3-2 top	0.33396	2511.4	±2.2	430.6	±1.6	146.0	±1.7	0.001026	±0.000014	98.6	±1.4	97.7	±1.3	93.7	±2.4	146.0	±1.7	1921.9
WFGB 3-2 bottom	0.26605	2361.4	±2.2	335.9	±1.9	145.1	±1.7	0.002750	±0.000022	318.8	±3.1	262.2	±2.1	258.9	±2.7	145.2	±1.7	1756.7

Analytical errors are ±2σ of the mean.

[a] $[^{238}U] = [^{235}U] \times 137.77$ (±0.11‰) (Hiess et al., 2012); $\delta^{234}U = ([^{234}U/^{238}U]_{activity} - 1) \times 1000$.

[b] $\delta^{234}U_{initial}$ corrected was calculated based on ^{230}Th age (T), i.e., $\delta^{234}U_{initial} = \delta^{234}U_{measured} \times e^{\lambda 234 * T}$, and T is corrected age.

[c] $[^{230}Th/^{238}U]_{activity} = 1 - e^{-\lambda 230 T} + (\delta^{234}U_{measured}/1000)[l230/(\lambda_{230} - \lambda_{234})](1 - e^{-(\lambda 230 - \lambda 234)T})$, where *T* is the age. Decay constants are 9.1705 x 10^{-6} year^{-1} for ^{230}Th, 2.8221 x 10^{-6} year^{-1} for ^{234}U (Cheng et al., 2013), and 1.55125 x 10^{-10} year^{-1} for ^{238}U (Jaffey et al., 1971).

[d] The degree of detrital ^{230}Th contamination is indicated by the [^{230}Th/^{232}Th] atomic ratio instead of the activity ratio.

[e] Age corrections, relative to chemistry date on 11 March 2015 (2015.617), were calculated using an estimated atomic ^{230}Th/^{232}Th ratio of 4 ± 2 ppm (Shen et al., 2008).

Supplemental Table 3. Coral annual extension for coral core 05WFGB3.

Year	Slab A average (mm)	Slab C average (mm)	Slab D average (mm)	All slab average (mm)
2004	5.41	6.01	6.13	5.85
2003	5.87	6.46	6.35	6.23
2002	5.69	5.64	5.43	5.59
2001	4.89	4.61	5.23	4.91
2000	4.90	5.11	5.54	5.19
1999	5.65	5.71	5.74	5.70
1998	5.65	5.74	5.09	5.49
1997	5.74	5.92	6.04	5.90
1996	5.52	5.45	5.34	5.44
1995	5.32	4.99	5.38	5.23
1994	4.71	5.53	4.96	5.07
1993	5.61	5.93	6.08	5.87
1992	6.48	6.50	5.74	6.24
1991	6.58	5.70	6.70	6.32
1990	6.16	5.82	5.55	5.85
1989	5.93	6.37	6.68	6.32
1988	5.66	6.16	6.44	6.09
1987	6.09	6.80	6.38	6.42
1986	6.56	6.66	6.23	6.48
1985	6.57	5.56	5.86	6.00
1984	5.40	5.12	5.34	5.29
1983	5.74	5.75	5.83	5.77
1982	4.47	5.08	5.15	4.90
1981	4.85	4.98	5.36	5.06
1980	5.39	5.58	5.60	5.52
1979	6.17	6.31	5.90	6.13
1978	6.37	6.55	6.26	6.39
1977	5.78	5.70	5.33	5.60
1976	5.51	5.78	5.64	5.64
1975	6.41	6.47	6.82	6.57
1974	5.63	5.21	6.00	5.61
1973	6.76	6.41	6.79	6.66
1972	6.38	7.16	6.83	6.79
1971	5.93	5.97	6.01	5.97
1970	6.46	5.03	5.42	5.64
1969	5.29	5.00	5.45	5.25
1968	5.39	5.57	5.07	5.34
1967	5.74	5.90	5.10	5.58
1966	5.37	5.44	5.82	5.54
1965	5.27	5.83	5.97	5.69
1964	5.46	5.03	5.79	5.43
1963	6.16	5.96	5.96	6.03
1962	6.39	6.71	6.18	6.43
1961	6.08	6.45	5.86	6.13
1960	5.26	5.58	6.17	5.67
1959	7.25	7.00	6.28	6.84
1958	5.94	6.29	5.98	6.07
1957	6.46	6.16	6.27	6.30
1956	5.69	6.20	6.58	6.16
1955	5.81	6.27	5.91	5.99
1954	6.50	5.47	6.43	6.13
1953	5.93	5.69	5.72	5.78
1952	6.30	6.09	5.82	6.07
1951	7.20	6.46	6.01	6.56
1950	6.24	6.66	6.64	6.51
1949	6.61	7.52	6.91	7.01
1948	6.11	6.83	6.74	6.56
1947	5.82	6.38	6.33	6.17
1946	6.53	6.26	6.30	6.36
1945	6.22	6.47	6.22	6.30
1944	6.28	6.20	6.66	6.38
1943	6.33	5.78	6.23	6.11
1942	6.64	6.27	6.05	6.32
1941	6.06	5.93	6.21	6.07
1940	6.26	6.51	6.48	6.42
1939	7.40	6.27	6.68	6.78
1938	5.64	6.53	6.03	6.07
1937	6.88	6.99	6.49	6.78
1936	5.57	5.17	5.94	5.56
1935	7.63	7.35	6.85	7.28
1934	7.93	8.08	7.44	7.81
1933	5.37	6.16	6.17	5.90
1932 [a]	3.49	3.79	3.46	3.58
1931	6.25	5.64	6.30	6.06
1930	6.33	6.63	6.37	6.44
1929	5.86	6.31	6.23	6.14
1928	6.02	5.66	6.02	5.90

Extension was determined for ~January to January for each year.

[a] The break in core in 1932 (Supplemental Figure 5) made measuring extension for this year this incomplete.

Supplemental Table 4. Artificial fallout radionuclide concentrations for core 05WFGB3.

Sample depth [a] (mm)	Sample year [b]	^{137}Cs (Bq kg^{-1})	±	^{241}Am (Bq kg^{-1})	±
0.0 – 3.4	2005	0	0	0	0
26.1 – 31.2	2000	0	0	0	0
82.7 – 88.5	1990	0	0	0	0
223.7 – 229.1	1966	0	0	0	0
234.9 – 240.0	1964	0	0	0	0
240.0 – 245.9	1963	0	0	0	0
245.9 – 252.6	1962	0	0	0	0
313.8 – 320.3	1951	0	0	0	0
410.8 – 416.0	1935-1936	0	0	0	0

[a] Depth range for each annual sample starting from top of coral core (05WFGB3 Slab C) measured on X-radiographs.
[b] Each sample represents one year of coral growth for ~January to December (Table 1).

Supplemental Table 5. SCP counts for core 05WFGB3 by particle size and concentration.

Sample depth [a] (mm)	Sample year [b]	Total SCP count	SCP concentration (number l^{-1})
0.0 – 3.4	2005	0	0
3.4 – 9.4	2004	0	0
26.1 – 31.2	2000	0	0
82.7 – 88.5	1990	0	0
141.0 – 146.6	1980	0	0
170.9 – 177.4	1975	0	0
202.2 – 207.2	1970	0	0
217.8 – 223.7	1967	0	0
223.7 – 229.1	1966	0	0
229.1 – 234.9	1965	0	0
234.9 – 240.0	1964	0	0
240.0 – 245.9	1963	0	0
245.9 – 252.6	1962	0	0
252.6 – 259.1	1961	0	0
259.1 – 264.7	1960	0	0
264.7 – 271.7	1959	0	0
271.7 – 277.9	1958	0	0
277.9 – 284.1	1957	0	0
284.1 – 290.3	1956	0	0
290.3 – 269.6	1955	0	0
269.6 – 302.0	1954	0	0
302.0 – 307.7	1953	0	0
307.7 – 313.8	1952	0	0
313.8 – 320.3	1951	0	0
320.3 – 326.9	1950	0	0
353.9 – 360.4	1945	0	0
384.6 – 391.1	1940	0	0
410.8 – 416.0	1936	0	0
416.0 – 423.4	1935	0	0
423.4 – 431.4	1934	0	0
447.0 – 453.7	1931	0	0
453.7 – 460.0	1930	0	0
460.0 – 465.7	1929	0	0

[a] Depth range for each annual sample starting from top of coral core (05WFGB3 Slab C) measured on X-radiographs.

[b] Each sample represents one year of coral growth for ~January to December (Table 1).

Supplemental Table 6. Summary statistics for coral proxies for temperature.

	$^{7}Li/^{43}Ca$	$^{7}Li/^{26}Mg$	$^{26}Mg/^{43}Ca$	$^{84}Sr/^{43}Ca$	$^{238}U/^{43}Ca$	ICP-OES Sr/Ca	$\delta^{18}O$	Reef temp [a]	OISST [b]
$^{7}Li/^{43}Ca$		0.78	-0.35	0.74	0.50	0.74	0.79	-0.73	-0.79
$^{7}Li/^{26}Mg$			-0.84	0.89	0.87	0.89	0.80	-0.85	-0.89
$^{26}Mg/^{43}Ca$				-0.70	-0.88	-0.70	-0.53	0.65	0.67
$^{84}Sr/^{43}Ca$					0.85	0.88	0.78	-0.84	-0.87
$^{7}Li/^{43}Ca$						0.78	0.62	-0.73	-0.72
ICP-OES Sr/Ca							0.84	-0.89	-0.93
$\delta^{18}O$								-0.87	-0.89
Reef									0.95

Error (ºC) [c]							
Reef	2.25	1.60	1.67	2.31	1.27	2.38	
OISST	2.25	1.64	1.79	2.58	1.27	1.74	

Pearson correlations are significant (p=0.05) even when adjusted for degrees of freedom. Elemental isotope ratios were measured on ICP-MS unless otherwise noted.

[a] Reef temp is the temperature measured at WFGB at 20 m depth from 1987–2003 but is not continuous (n=138) (Johnston et al., 2021).

[b] OISST is the optimal interpolated SST version 2 for the 1º grid centered on 27.5ºN, 93.5ºW spanning 1987–2004 (n=216) (Reynolds et al., 2002).

[c] Error of reconstruction is determined for each temperature proxy as in previous studies (DeLong et al., 2013, 2016) to assess which temperature proxy skill in reconstructing temperature.

Supplemental Table 7. ^{210}Pb concentrations for core 05WFGB3.

Sample depth [a] (mm)	Sample year [b]	Total ($Bq\ kg^{-1}$)	±	^{226}Ra ($Bq\ kg^{-1}$)	±	Unsupported ($Bq\ kg^{-1}$)	±
0.0 – 3.4	2005	24.19	6	123.82	2.1	-99.63	6.36
26.1 – 31.2	2000	0	0	17.7	0.97	-17.7	0.97
82.7 – 88.5	1990	0.94	4.67	20.09	1.26	-19.15	4.84
223.7 – 229.1	1966	1.71	4.86	21.09	1.32	-19.38	5.04
234.9 – 240.0	1964	0	0	13.53	1.83	-13.53	1.83
240.0 – 245.9	1963	0	0	20.74	1.52	-20.74	1.52
245.9 – 252.6	1962	0	0	18.43	1.58	-18.43	1.58
313.8 – 320.3	1951	5.66	4.55	16.62	1.14	-10.95	4.69
416.0 – 423.4	1935-36	0	0	12.35	1.13	-12.35	1.13

[a] Depth range for each annual sample starting from top of coral core (05WFGB3 Slab C) measured on X-radiographs

[b] Each sample represents one year of coral growth for ~January to December (Table 1).

Supplemental Table 8. Mercury concentration for core 05WFGB3.

Sample depth [a] (mm)	Sample year [b]	Hg (ng g^{-1})
3.4 – 9.4	2004	1.34
26.1 – 31.2	2000	0.78
82.7 – 88.5	1990	0.47
141.0 – 146.6	1980	0.38
170.9 – 177.4	1975	1.12
202.2 – 207.2	1970	0.58
229.1 – 234.9	1965	0.95
259.1 – 264.7	1960	0.85
290.3 – 269.6	1955	0.92
307.7 – 313.8	1952	0.95
353.9 – 360.4	1945	0.39
384.6 – 391.1	1940	0.81
423.4 – 431.4	1934	0.86

[a] Depth range for each annual sample starting from top of coral core (05WFGB3 Slab C) measured on X-radiographs.
[b] Each sample represents one year of coral growth for ~January to December (Table 1).

Supplemental Table 9. $^{239+240}$Pu for coral core 10LEO1 from Haiti.

Year [a]	Actual dates from sample ID	$^{239-240}$Pu (Bq kg^{-1})	± k=2
1970		0.029	0.010
1959		0.073	0.028
1958		0.066	0.027
1957		0.071	0.022
1956		0.081	0.023
1954	1954–1955	0.075	0.021
1953		0.036	0.013
1952	~1952–1953	0.029	0.012
1951	~1951	0.019	0.011
1950	~1950–1949	0.027	0.011

[a] Each sample represents one year of coral growth for ~January to December unless otherwise noted.

Supplementary data

See provided Excel file.

Supplementary references

Alpert AE, Cohen AL, Oppo DW, et al. (2017) Twentieth century warming of the tropical Atlantic captured by Sr-U paleothermometry. *Paleoceanography* 32(2):146-160. doi:10.1002/2016PA002976.

Appleby PG, Nolan PJ, Gifford DW, et al. (1986) ^{210}Pb dating by low background gamma counting. *Hydrobiologia* 143(1):21-27. doi:10.1007/BF00026640.

Appleby PG, Richardson N and Nolan PJ (1992) Self-absorption corrections for well-type germanium detectors. *Nuclear Instruments and Methods in Physics Research Section B: Beam Interactions with Materials and Atoms* 71(2):228-233. doi:110.1016/0168-583X(92)95328-O.

Benavides LM and Druffel ERM (1986) Sclerosponge growth rate as determined by ^{210}Pb and Δ^{14}C chronologies. *Coral Reefs* 4(4):221-224.

Benninger LK and Dodge RE (1986) Fallout plutonium and natural radionuclides in annual bands of the coral *Montastrea annularis*, St. Croix, U.S. Virgin Islands. *Geochimica et Cosmochimica Acta* 50(12):2785-2797. doi:10.1016/0016-7037(86)90227-9.

Cheng H, Lawrence Edwards R, Shen C-C, et al. (2013) Improvements in ^{230}Th dating, ^{230}Th and ^{234}U half-life values, and U–Th isotopic measurements by multi-collector inductively coupled plasma mass spectrometry. *Earth and Planetary Science Letters* 371-372:82-91. doi:10.1016/j.epsl.2013.04.006.

David MB, Drinkwater LE and McIsaac GF (2010) Sources of nitrate yields in the Mississippi River basin. *Journal of Environmental Quality* 39(5): 1657-1667. doi:10.2134/jeq2010.0115.

DeLong KL, Flannery JA, Maupin CR, et al. (2011) A coral Sr/Ca calibration and replication study of two massive corals from the Gulf of Mexico. *Palaeogeography Palaeoclimatology Palaeoecology* 307(1-4):117-128. doi:10.1016/j.palaeo.2011.05.005.

DeLong KL, Flannery JA, Poore RZ, et al. (2014) A reconstruction of sea surface temperature variability in the southeastern Gulf of Mexico from 1734–2008 C.E. using cross-dated Sr/Ca records from the coral *Siderastrea siderea*. *Paleoceanography* 29(5):403–422. doi:10.1002/2013PA002524.

DeLong KL, Maupin CR, Flannery JA, et al. (2016) Refining temperature reconstructions with the Atlantic coral *Siderastrea siderea*. *Palaeogeography, Palaeoclimatology, Palaeoecology* 462:1-15. doi:10.1016/j.palaeo.2016.08.028.

DeLong KL, Quinn TM, Taylor FW, et al. (2013) Improving coral-base paleoclimate reconstructions by replicating 350 years of coral Sr/Ca variations. *Palaeogeography Palaeoclimatology Palaeoecology* 373:6-24. doi:10.1016/j.palaeo.2012.08.019.

Dodge RE and Thomson J (1974) The natural radiochemical and growth records in contemporary hermatypic corals from the Atlantic and Caribbean. *Earth and Planetary Science Letters* 23(3):313-322.

Donner S (2003) The impact of cropland cover on river nutrient levels in the Mississippi River Basin. *Global Ecology and Biogeography* 12(4):341-355. doi:10.1046/j.1466-822X.2003.00032.x.

Duprey NN, Wang TX, Kim T, et al. (2020) Megacity development and the demise of coastal coral communities: Evidence from coral skeleton $\delta^{15}N$ records in the Pearl River estuary. *Glob Chang Biol* 26(3):1338-1353. doi:10.1111/gcb.14923.

Duprey NN, Wang XT, Thompson PD, et al. (2017) Life and death of a sewage treatment plant recorded in a coral skeleton $\delta^{15}N$ record. *Mar Pollut Bull* 120(1-2):109-116. doi:10.1016/j.marpolbul.2017.04.023.

Flannery JA, Richey JN, Thirumalai K, et al. (2017) Multi-species coral Sr/Ca based sea-surface temperature reconstruction using *Orbicella faveolata* and *Siderastrea siderea* from the Florida Straits. *Palaeogeography, Palaeoclimatology, Palaeoecology* 466:100-109. doi:10.1016/j.palaeo.2016.10.022.

Fowell SE, Sandford K, Stewart JA, et al. (2016) Intrareef variations in Li/Mg and Sr/Ca sea surface temperature proxies in the Caribbean reef-building coral *Siderastrea siderea*. *Paleoceanography* 31(10):1315-1329. doi:10.1002/2016pa002968.

Goolsby DA and Battaglin WA (2001) Long-term changes in concentrations and flux of nitrogen in the Mississippi River Basin, USA. *Hydrological Processes* 15(7):1209-1226. doi:10.1002/hyp.210.

Guzman H and Tudhope A (1998) Seasonal variation in skeletal extension rate and stable isotopic ($^{13}C/^{12}C$ and $^{18}O/^{16}O$) composition in response to several environmental variables in the Caribbean reef coral *Siderastrea siderea*. *Marine Ecology Progress Series* 166:109-118. doi:10.3354/meps166109.

Guzmán HM and Holst I (1993) Effects of chronic oil-sediment pollution on the reproduction of the Caribbean reef coral *Siderastrea siderea*. *Marine Pollution Bulletin* 26:276-282.

Guzmán HM and Jiménez CE (1992) Contamination of coral reefs by heavy metals along the Caribbean coast of Central America (Costa Rica and Panama). *Marine Pollution Bulletin* 24(11):554-561. doi:10.1016/0025-326X(92)90708-E.

Hathorne EC, Gagnon A, Felis T, et al. (2013) Interlaboratory study for coral Sr/Ca and other element/Ca ratio measurements. *Geochemistry, Geophysics, Geosystems* 14(9):3730-3750. doi:10.1002/ggge.20230.

Hiess J, Condon DJ, McLean N, et al. (2012) $^{238}U/^{235}U$ Systematics in terrestrial uranium-bearing minerals. *Science* 335(6076):1610-1614. doi:10.1126/science.1215507.

Howe S, Miranda C, Hayes CT, et al. (2020) The dual isotopic composition of nitrate in the Gulf of Mexico and Florida Straits. *Journal of Geophysical Research: Oceans* 125(9). doi:10.1029/2020jc016047.

Imboden DM and Stiller M (1982) The influence of radon diffusion on the ^{210}Pb distribution in sediments. *Journal of Geophysical Research: Oceans* 87(C1):557-565. doi:10.1029/JC087iC01p00557.

Jaffey AH, Flynn KF, Glendenin LE, et al. (1971) Precision measurement of half-lives and specific activities of ^{235}U and ^{238}U. *Physical Review C* 4(5):1889-1906. doi:10.1103/PhysRevC.4.1889.

Johnston MA, O'Connell K, Blakeway RD, et al. (2021) Long-term monitoring at East and West Flower Garden Banks: 2019 Annual Report. National Marine Sanctuaries Conservation Series ONMS-21-02. Galveston, TX. U.S. Department of Commerce, National Oceanic and Atmospheric Administration, Flower Garden Banks National Marine Sanctuary.

Kelly AE, Reuer MK, Goodkin NF, et al. (2009) Lead concentrations and isotopes in corals and water near Bermuda, 1780–2000. *Earth and Planetary Science Letters* 283(1):93-100. doi:10.1016/j.epsl.2009.03.045.

Kuffner IB, Hickey TD and Morrison JM (2013) Calcification rates of the massive coral *Siderastrea siderea* and crustose coralline algae along the Florida Keys (USA) outer-reef tract. *Coral Reefs* 32(4):987-997. doi:10.1007/s00338-013-1047-8.

Kuffner IB, Lidz BH, Hudson JH, et al. (2015) A century of ocean warming on Florida Keys coral reefs: historic in situ observations. *Estuaries and Coasts* 38(3): 1085-1096. doi:10.1007/s12237-014-9875-5.

Kuffner IB, Roberts KE, Flannery JA, et al. (2017) Fidelity of the Sr/Ca proxy in recording ocean temperature in the western Atlantic coral *Siderastrea sidere*a. *Geochemistry, Geophysics, Geosystems* 18(1):178-188. doi:10.1002/2016GC006640.

Lazareth C, Willenz P, Navez J, et al. (2000) Sclerosponges as a new potential recorder of environmental changes: lead in *Ceratoporella nicholsoni. Geology* 28:515-518. doi:10.1130/0091-7613(2000)28<515:SAANPR>2.0.CO;2.

Leichliter JN, Lüdecke T, Foreman AD, et al. (2021) Nitrogen isotopes in tooth enamel record diet and trophic level enrichment: results from a controlled feeding experiment. *Chemical Geology* 563:120047. doi:10.1016/j.chemgeo.2020.120047.

Lo L, Shen C-C, Lu C-J, et al. (2014) Determination of element/Ca ratios in foraminifera and corals using cold- and hot-plasma techniques in inductively coupled plasma sector field mass spectrometry. *Journal of Asian Earth Sciences* 81:115-122. doi:0.1016/j.jseaes.2013.11.016.

Łokas E, Wachniew P, Baccolo G, et al. (2022) Unveiling the extreme environmental radioactivity of cryoconite from a Norwegian glacier. *Science of The Total Environment* 814:152656. doi:10.1016/j.scitotenv.2021.152656.

Maupin CR, Quinn TM and Halley RB (2008) Extracting a climate signal from the skeletal geochemistry of the Caribbean coral *Siderastrea siderea*. *Geochemistry Geophysics Geosystems* 9:Q12012. doi:10.1029/2008GC002106.

Montoya JP, Carpenter EJ and Capone DG (2002) Nitrogen fixation and nitrogen isotope abundances in zooplankton of the oligotrophic North Atlantic. *Limnology and Oceanography* 47(6):1617-1628. doi:10.4319/lo.2002.47.6.1617.

Moses C and Swart P (2006) Stable isotope and growth in corals from the island of Tobago: Not simply a record of the Orinoco. *Proceedings of 10th International Coral Reef Symposium* 10:580-587.

Okai T, Suzuki A, Kawahata H, et al. (2002) Preparation of a new geological survey of Japan geochemical reference material: coral JCp-1. *Geostandards and Geoanalytical Research* 26(1): 95-99.

Ouellette G (2017) Paleoenvironmental reconstructions using coral microatolls from the Gulf Of Gonâve, Haiti (Sp. *Siderastrea siderea*), PhD Dissertation, Louisiana State University.

Paton C, Hellstrom J, Paul B, et al. (2011) Iolite: Freeware for the visualisation and processing of mass spectrometric data. *Journal of Analytical Atomic Spectrometry* 26(12):2508-2518. doi:10.1039/C1JA10172B.

Pereira NS, Clarke LJ, Chiessi CM, et al. (2022) Mid to late 20th century freshening of the western tropical South Atlantic triggered by southward migration of the Intertropical Convergence Zone. *Palaeogeography, Palaeoclimatology, Palaeoecology*. doi:10.1016/j.palaeo.2022.111013.111013.

Pereira NS, Sial AN, Kilbourne KH, et al. (2018) Carbon stable isotope record in the coral species *Siderastrea stellata*: A link to the Suess Effect in the tropical South Atlantic Ocean. *Palaeogeography, Palaeoclimatology, Palaeoecology* 497:82-90. doi:10.1016/j.palaeo.2018.02.007.

Prouty NG, Storlazzi CD, McCutcheon AL, et al. (2014) Historic impact of watershed change and sedimentation to reefs along west-central Guam. *Coral Reefs* 33(3):733-749. doi:10.1007/s00338-014-1166-x.

Rabalais NN, Turner RE and Wiseman WJ (2002) Gulf of Mexico Hypoxia, a.k.a. "The Dead Zone". *Annu. Rev. Ecol. Syst.* 33(1):235-263. doi:10.1146/annurev.ecolsys.33.010802.150513.

Raymond PA, Oh N-H, Turner RE, et al. (2008) Anthropogenically enhanced fluxes of water and carbon from the Mississippi River. *Nature* 451(7177):449-452. doi:10.1038/nature06505.

Reich CD, Kuffner IB, Hickey TD, et al. (2013) Complexity of nearshore strontium-to-calcium ratio variability in a core sample of the massive coral *Siderastrea siderea* obtained in Coral Bay, St. John, U.S. Virgin Islands. U.S. Geological Survey Open-File Report 2013–1092. http://pubs.er.usgs.gov/publication/ofr20131092.

Reimer PJ (2004) Discussion: Reporting and calibration of post-bomb ^{14}C Data. *Radiocarbon* 46(3):1299-1304. doi:10.1017/S0033822200033154.

Ren H, Chen Y-C, Wang XT, et al. (2017) 21st-century rise in anthropogenic nitrogen deposition on a remote coral reef. *Science* 356(6339):749-752.

Reuer MK, Boyle EA and Cole JE (2003) A mid-twentieth century reduction in tropical upwelling inferred from coralline trace element proxies. *Earth and Planetary Science Letters* 210(3-4):437-452. doi:10.1016/S0012-821X(03)00162-6.

Reynolds RW, Rayner NA, Smith TM, et al. (2002) An improved in situ and satellite SST analysis for climate. *Journal of Climate* 15(13):1609-1625. doi:10.1175/1520-0442(2002)015<1609:AIISAS>2.0.CO;2.

Rippe JP, Baumann JH, De Leener DN, et al. (2018) Corals sustain growth but not skeletal density across the Florida Keys Reef Tract despite ongoing warming. *Global Change Biology* 24(11):5205-5217. doi:10.1111/gcb.14422.

Robinson LF, Adkins JF, Frank N, et al. (2014) The geochemistry of deep-sea coral skeletons: A review of vital effects and applications for palaeoceanography. *Deep Sea Research Part II: Topical Studies in Oceanography* 99:184-198. doi:10.1016/j.dsr2.2013.06.005.

Robison WL, Conrado CL, Hamilton TF, et al. (2000) The effect of carbonate soil on transport and dose estimates for long-lived radionuclides at a US Pacific Test Site. *Journal of Radioanalytical and Nuclear Chemistry* 243(2):459-465. doi:10.1023/a:1016090517426.

Rose NL (1994) A note on further refinements to a procedure for the extraction of carbonaceous fly-ash particles from sediments. *Journal of Paleolimnology* 11(2):201-204. doi:10.1007/BF00686866.

Rose NL (2008) Quality control in the analysis of lake sediments for spheroidal carbonaceous particles. *Limnology and Oceanography: Methods* 6(4):172-179. doi:10.4319/lom.2008.6.172.

Rosenheim BE, Swart PK and Thorrold SR (2005) Minor and trace elements in sclerosponge *Ceratoporella nicholsoni:* Biogenic aragonite near the inorganic endmember? *Palaeogeography, Palaeoclimatology, Palaeoecology* 228(1-2):109-129.

Saha N, Webb GE and Zhao J-X (2016) Coral skeletal geochemistry as a monitor of inshore water quality. *Science of The Total Environment* 566:652-684. doi:10.1016/j.scitotenv.2016.05.066.

Schilling KE, Chan K-S, Liu H, et al. (2010) Quantifying the effect of land use land cover change on increasing discharge in the Upper Mississippi River. *Journal of Hydrology* 387(3):343-345. doi:10.1016/j.jhydrol.2010.04.019.

Schrag DP (1999) Rapid analysis of high-precision Sr/Ca ratios in corals and other marine carbonates. *Paleoceanography* 14(2):97-102. doi:10.1029/1998PA900025.

Shen C-C, Li K-S, Sieh K, et al. (2008) Variation of initial $^{230}Th/^{232}Th$ and limits of high precision U–Th dating of shallow-water corals. *Geochimica et Cosmochimica Acta* 72(17):4201-4223. doi:10.1016/j.gca.2008.06.011.

Shen GT and Boyle EA (1987) Lead in corals: reconstruction of historical industrial fluxes to the surface ocean. *Earth and Planetary Science Letters* 82(3-4):289-304. doi:10.1016/0012-821x(87)90203-2.

Shen GT and Boyle EA (1988) Determination of lead, cadmium and other trace metals in annually-banded corals. *Chemical Geology* 67(1):47-62. doi:10.1016/0009-2541(88)90005-8.

Sigman DM, Casciotti KL, Andreani M, et al. (2001) A bacterial method for the nitrogen isotopic analysis of nitrate in seawater and freshwater. *Analytical Chemistry* 73(17): 4145-4153. doi:10.1021/ac010088e.

Sigman DM and Fripiat F (2019) Nitrogen isotopes in the ocean. *Encyclopedia of Ocean Sciences*. pp.263-278.

Sigman DM, Karsh KL and Casciotti KL (2009) Nitrogen isotopes in the ocean. In: Steele JH (ed) *Encyclopedia of Ocean Sciences (Second Edition)*. Oxford: Academic Press, pp.40-54.

Stuiver M and Polach HA (1977) Reporting of ^{14}C data. *Radiocarbon* 19(3):355–363. doi:0.1017/S0033822200003672.

Synal H-A, Stocker M and Suter M (2007) MICADAS: A new compact radiocarbon AMS system. *Nuclear Instruments and Methods in Physics Research Section B: Beam Interactions with Materials and Atoms* 259(1):7-13. doi:10.1016/j.nimb.2007.01.138.

Thompson DM (2021) Environmental records from coral skeletons: A decade of novel insights and innovation. *WIREs Climate Change* 13(1):e745. doi:10.1002/wcc.745.

Wacker L, Fülöp RH, Hajdas I, et al. (2013) A novel approach to process carbonate samples for radiocarbon measurements with helium carrier gas. *Nuclear Instruments and Methods in Physics Research Section B: Beam Interactions with Materials and Atoms* 294:214-217. doi:10.1016/j.nimb.2012.08.030.

Wang XT, Sigman DM, Cohen AL, et al. (2016) Influence of open ocean nitrogen supply on the skeletal δ15N of modern shallow-water scleractinian corals. *Earth and Planetary Science Letters* 441:125-132. doi:10.1016/j.epsl.2016.02.032.

Weerabaddana MM, DeLong KL, Wagner AJ, et al. (2021) Insights from barium variability in a *Siderastrea siderea* coral in the northwestern Gulf of Mexico. *Marine Pollution Bulletin* 173:112930. doi:10.1016/j.marpolbul.2021.112930.

Weigand MA, Foriel J, Barnett B, et al. (2016) Updates to instrumentation and protocols for isotopic analysis of nitrate by the denitrifier method. *Rapid Communications in Mass Spectrometry* 30(12):1365-1383. doi:10.1002/rcm.7570.

Williams B, Risk MJ, Ross SW, et al. (2007) Stable isotopes from deep-water antipatharians: 400-year records from the southeastern coast of the United States. *Bulletin of Marine Science* 81(3):437-447.

Zhang YK and Schilling KE (2006) Increasing streamflow and baseflow in Mississippi River since the 1940s: Effect of land use change. *Journal of Hydrology* 324(1):412-422. doi:10.1016/j.jhydrol.2005.09.033.